Alma Mater Studiorum – Università di Bologna

DOTTORATO DI RICERCA IN

MECCANICA E SCIENZE AVANZATE DELL'INGEGNERIA

Ciclo 33

Settore Concorsuale: 09/C2 – FISICA TECNICA E INGEGNERIA NUCLEARE

Settore Scientifico Disciplinare: ING/IND-18 – FISICA DEI REATTORI NUCLEARI

DEVELOPMENT AND OPTIMIZATION OF TECHNIQUES AND DESIGN PARAMETERS FOR THE ENGINEERING OF ATMOSPHERIC PRESSURE PLASMA DEVICES FOR BIOMEDICAL APPLICATIONS AND PLASMA MEDICINE

Presentata da: **Raluca Alina Bisag**

Coordinatore Dottorato

Marco Carricato

Supervisore

Vittorio Colombo

Co-supervisore

Matteo Gherardi

Esame finale anno 2021

"Non pretendiamo che le cose cambino, se continuiamo a fare le stesse cose. La crisi può essere una grande benedizione per le persone e le nazioni, perché la crisi porta progressi.

La creatività nasce dall'angoscia come il giorno nasce dalla notte oscura. È nella crisi che sorge l'inventiva le scoperte e le grandi strategie. Chi supera la crisi supera sé stesso senza essere superato. Chi attribuisce alla crisi i suoi fallimenti e disagi, inibisce il proprio talento e dà più valore ai problemi che alle soluzioni.

La vera crisi è l'incompetenza. Il più grande inconveniente delle persone e delle nazioni è la pigrizia nel cercare soluzioni e vie di uscita ai propri problemi. Senza crisi non ci sono sfide, senza sfide la vita è una routine, una lenta agonia. Senza crisi non c'è merito. È nella crisi che emerge il meglio di ognuno, perché senza crisi tutti i venti sono lievi brezze. Parlare di crisi significa incrementarla, e tacere nella crisi è esaltare il conformismo. Invece, lavoriamo duro. L'unico pericolo della crisi è la tragedia che può conseguire al non voler lottare per superarla."

"Let's not pretend that things will change if we keep doing the same things. A crisis can be a real blessing to any person, to any nation. For all crises bring progress.

Creativity is born from anguish, just like the day is born form the dark night. It's in crisis that inventiveness is born, as well as discoveries made and big strategies. He who overcomes crisis, overcomes himself, without getting overcome. He who blames his failure to a crisis neglects his own talent and is more interested in problems than in solutions. Incompetence is the true crisis. The greatest inconvenience of people and nations is the laziness with which they attempt to find the solutions to their problems.

There's no challenge without a crisis. Without challenges, life becomes a routine, a slow agony. There's no merit without crisis. It's in the crisis where we can show the very best in us. Without a crisis, any wind becomes a tender touch. To speak about a crisis is to promote it. Not to speak about it is to exalt conformism. Let us work hard instead. Let us stop, once and for all, the menacing crisis that represents the tragedy of not being willing to overcome it."

Albert Einstein

Table of contents

Abstract ***6***

Abbreviations ***8***

1 Design and characterization of a multiwire plasma source for the production of Plasma Activated Liquids (PALs) having anti-tumor effects ***9***

1.1 Introduction 10

1.1.1 CAP devices for the treatment of liquids *12*

1.1.2 Reaction pathways of biologically relevant RONS *14*

1.1.2.1 Hydrogen peroxide formation 15

1.1.2.2 Nitrites formation 16

1.1.3 The roles of RONS in antitumoral activity *16*

1.2 Materials and methods 19

1.2.1 Plasma device and electrical characterization *19*

1.2.2 Plasma treatment and quantitative measure of RONS *20*

1.2.3 Low-speed and high-speed filter imaging *22*

1.2.4 Optical absorption spectroscopy *23*

1.2.5 Cell lines and culture conditions *24*

1.2.6 Cell treatment and viability assay *24*

1.3 Results and discussion 25

1.3.1 Electrical characterization *25*

1.3.2 Chemical characterization of the treated liquid *27*

1.3.3 Evaluation of plasma discharge behavior and emission by means of low-speed and high-speed filter imaging *29*

1.3.4 Evaluation of RONS concentrations in gas phase *30*

1.3.5 Cell viability after PA-RL treatment *30*

1.4 Conclusions and future perspectives 33

1.5 References 34

1.6 Appendix 40

1.6.1 CAP prototypes for the treatment of a liquid substrate *40*

1.6.2 Plasma device and electrical characterization *41*

1.6.3 Chemical characterization of the treated liquid *42*

1.6.4 Biological results *43*

2 Design and realization of a Cold Atmospheric Plasma (CAP) device for dental applications ***45***

2.1 Introduction 46

2.1.1 Development and regulation of medical devices *49*

2.2 Materials and methods 52

2.2.1 Temperature measurements *52*

2.2.2 UV irradiance measurements and optical emission spectroscopy *53*

2.2.3 Leakage current measurements ... *53*
2.3 Results and discussion ... 55
2.3.1 First prototype ... *55*
2.3.2 Second prototype ... *58*
2.3.3 Third prototype ... *60*
2.3.4 AlmaMED: a tabletop device for dental applications ... *62*
2.3.5 Evaluation of temperature profile evolution ... *64*
2.3.6 Evaluation of the UV irradiance and the OES spectrum ... *65*
2.3.7 Leakage current measurements ... *66*
2.4 Conclusions and future perspectives ... 67
2.5 References ... 68
3 Design and realization of a Cold Atmospheric Plasma (CAP) device for the inactivation of airborne pathogens ... ***71***
3.1 Introduction ... 72
3.1.1 CAP devices for the treatment of airborne pathogens ... *75*
3.2 Materials and methods ... 77
3.2.1 Plasma device and electrical characterization ... *77*
3.2.2 Qualitative monitoring of aerosol behavior by means of low-speed imaging ... *78*
3.2.3 Optical Absorption Spectroscopy ... *79*
3.2.4 S. epidermidis culture condition and CAP treatment ... *80*
3.3 Results and discussion ... 81
3.3.1 Electrical characterization of the DBD plasma source ... *81*
1.3.2 Qualitative evaluation of the aerosol outgoing from the DBD plasma source ... *81*
1.3.3 Evaluation of RONS concentrations in gas phase ... *82*
3.3.4 CAP effect on bioaerosol containing S. epidermidis ... *83*
3.4 Conclusions and future perspectives ... 85
3.5 References ... 86
3.6 Appendix ... 90
3.6.1 First DBD prototype for the inactivation of airborne pathogens ... *90*
3.6.2 Second DBD prototype for the inactivation of airborne pathogens ... *91*
1.6.3 Biological experiments required to verify CAP anti-bacterial activity of the first prototype on bioaerosol containing S. epidermidis ... *91*
Acknowledgements ... ***94***

Abstract

In the last decades, the possibility to generate plasma at atmospheric pressure gave rise to a new emerging field called plasma medicine. It is an interdisciplinary research field which combines numerous sectors, among which: engineering, medicine, life science, clinical medicine, biology, biotechnology, chemistry, and physics. Plasma medicine deals with the application of cold atmospheric pressure plasmas (CAPs) or plasma-treated solutions (better known as plasma activated liquids – PALs) on or in the human body for therapeutic effects. Thanks to a blend of synergic biologically active agents (i.e., free radicals, electrons, ions, reactive species, UV radiation, and electrical field) and biocompatible temperatures (below 40°C), CAPs were successfully employed by several research groups in many different biomedical applications such as dentistry, dermatology, wound healing, cancer treatment, blood coagulation, etc.… For these purposes there were used different kinds of plasma sources which differ in principle of operation, geometry, or working gas; thus, a broad range of parameters could be controlled through the design of the plasma source to obtain the most suitable biological effect. Despite their effectiveness has been verified in the above-mentioned biomedical applications, over the years, researchers throughout the world described in their scientific works numerous plasma sources which are still laboratory devices not optimized for the specific application.

In this perspective, the aim of my Ph.D. project has been focused on the development and optimization of techniques and design parameters for the engineering of CAP sources for different biomedical applications and plasma medicine among which cancer treatment, dentistry and bioaerosol decontamination. For each of these applications, I started with the realization of laboratory devices necessary to assess their efficacy for the specific application. Subsequently, I focused my attention on the plasma source itself and I analyzed the advantages and the critical points to be avoided or implemented inside a new optimized device. I designed the plasma devices from an engineering point of view, and I have ensured that each single device so that it could be easily realized, assembled, and disassembled. At the same time, I designed the prototypes so that they could be used safely and with ease. Moreover, in all cases I tried to individuate the good equilibrium between geometry, materials to be used, and especially the technological process necessary for the realization of each component of the devices. I also had the opportunity to actively participate in the realization of the devices and this feature made me realize aspects which could be improved in the design phase. The challenging task of balancing the characteristics of each plasma source and the biological effects has been achieved thanks to a fruitful collaboration among researchers belonging to different research fields. While offering a unique opportunity of personal and scientific growth, the cooperation with different research groups has enabled a multidisciplinary view on results achieved and allow me to improve my research activity.

My dissertation is organized in three different sections reporting the results achieved during the three years of Ph.D. studies. The first chapter presents a multiwire device used for the first time to produce plasma-activated Ringer's Lactate (PA-RL) solution containing oxygen and nitrogen reactive species (RONS) having anticancer activity. The discharge electrical parameters and the behavior of the plasma streamers were investigated by means of electrical characterization and high-speed imaging, respectively. In addition, to correlate the liquid and the gas phase

chemistry were performed quantitative measurements of RONS concentrations in liquid and gas phase using commercial colorimetric assays and optical absorption spectroscopy (OAS). The above-mentioned activities were part of the UNIBO AlmaIDEA Grant Senior project entitled "Chemo-physical and biological mechanisms behind the anticancer activity of plasma activated liquids for the treatment of peritoneal carcinosis from primitive epithelial ovarian/tubular tumor", run under the supervision of Prof. Pierandrea De Iaco from the Department of Gynecology and Obstetrics, S. Orsola-Malpighi Hospital, Alma Mater Studiorum-Università di Bologna. The aim of this project was the development of a novel intraperitoneal therapy for Epithelial Ovarian Cancer (EOC) treatment using plasma activated liquids (PALs) on *in vitro* and *ex vivo* cells.

The second chapter presents all the steps that led me to the realization of a Plasma Gun (PG) device for dental applications expected to be translated into the clinical environment. I designed each plasma device according to the most important regulations for biomedical devices (i.e. ISO 14971 (Medical devices - Application of risk management to medical devices) and IEC 60601 (Medical electrical equipment – Part 1: General requirements for basic safety and essential performance) and subsequently I measured the temperature of the most thermally stressed element, the UV irradiation and the current flowing through a patient. The activities described in this chapter were carried out with the valuable support of Dr. Riccardo Tonini and the spin-off company AlmaPlasma s.rl..

Finally, the third chapter reports all the steps necessary for the design, realization, and optimization of a dielectric barrier discharge (DBD) source for the inactivation of bioaerosol. This topic is strongly related to the current COVID-19 pandemic and the object of all the activities was to set the foundation for the realization of a CAP system suitable for assisting the control of the spread of Sars-CoV-2 virus in indoor and poorly ventilated spaces. In this perspective were carried out electrical and gas phase characterizations whose results were compared with biological ones. These activities are part of "Project VIKI (Virus Killer) – Plasma inactivation device to contrast bioaerosol indoor transport" financed by 2014 – 2020 Emilia – Romagna Regional Operational Program of the European Regional Development Fund on industrial research and innovation projects for contrast solutions to the spread of COVID-19. Various research groups and companies participate to this project, among which the Research Group for Industrial Application of Plasmas (IAP group), Unit of Microbiology (The Great Romagna Hub Laboratory), AlmaPlasma s.rl. and Alintel s.rl.

Abbreviations

APPJ	Atmospheric pressure plasma jet
CAP	Cold atmospheric plasma
DBD	Dielectric barrier discharge
DBGD	Dielectric barrier grating discharge
EOC	Epithelial ovarian cancer
FIW	Ionization wavefronts
HIPEC	Intraperitoneal hyperthermic chemotherapy
OC	Ovarian cancer
PAL	Plasma activated liquid
NOS	Nitric oxide synthase
PAM	Plasma activated medium
PBS	Phosphate buffered solution
PG	Plasma Gun
PMMA	Polymethylmethacrylate
PA-RL	Plasma activated Ringer Lactate solutin
RONS	Reactive oxygen and nitrogen species
ROS	Reactive oxygen species
RNS	Reactive nitrogen species
SEM	Scanning Electron Microscope
SRB	Sulforhodamine B
WHO	World Health Organization

1

Design and characterization of a multiwire plasma source for the production of Plasma Activated Liquids (PALs) having anti-tumor effects

1.1 Introduction

Cancer represents a wide and heterogeneous group of diseases made up of over 100 different tumor types that cause abnormal cell division without any control. Of all the types of tumors, Epithelial Ovarian Cancer (EOC) is one of the most common among women; it is a lethal and a silent gynecological tumor that originates from the epithelium of the ovary, Fallopian tubes or the peritoneum.[1,2] In its early phase, due to the absence of symptoms, the signs are difficult to identify and they are often confused with less severe diseases; as a consequence, about 75% of affected women are diagnosed at advanced stages (III-IV) [1], with a survival rate of 29% within 5 years from diagnosis.[3,4] Moreover, as reported in Figure 1.1, a common complication consists in the diffusion of tumor nodules of variable sizes and consistencies from the ovary to peritoneal surfaces (carcinosis).[3] Since the 1980s, the available therapeutic options are cytoreductive surgery followed by intravenous platinum/taxane based chemotherapy. While the first procedure has become the gold standard for the removal of the tumoral masses of the abdominal cavity in case of ovarian cancer, the second one still presents significant drawbacks, since it involves the use of high volumes of toxic chemotherapeutic liquids which are introduce systemically, thus impacting not only the area of interest (peritoneum).[3,5] In this regard, further improvements are being sought to specifically target ovarian cancer cells within the peritoneal cavity, such as the intra-peritoneal administration of antineoplastic agents (i.e. cisplatin or paclitaxel). The advantage of this procedure, which is currently the gold standard for the treatment of ovarian cancer, is the reduction of the toxicity normally associated with intravenous therapy. More recently, to increase the sensitivity of cancer cells to direct contact with cytotoxic agents, a new treatment modality was developed: intraperitoneal hyperthermic chemotherapy (HIPEC), consisting in the administration of a heated (42°C) chemotherapeutic solution within the peritoneal cavity. This procedure was already known in the 1970s when B. P. Giovanella *et al*. studied the effect of supranormal temperatures upon healthy and neoplastic primary human cells collected directly from the operating room.[6] Nowadays, it is well known that high temperatures are able to damage cancer cells membrane and promotes cancer cells apoptosis.[7,8] Moreover, hyperthermia seems to increase the sensitivity to chemotherapeutic agents (in particular cisplatin), in both platinum-sensitive and platinum-resistant cells.[9] Despite the promising results of intraperitoneal chemotherapy administration, the critical point of this procedure consists in its low efficacy of targeting nodules smaller than few millimetres.

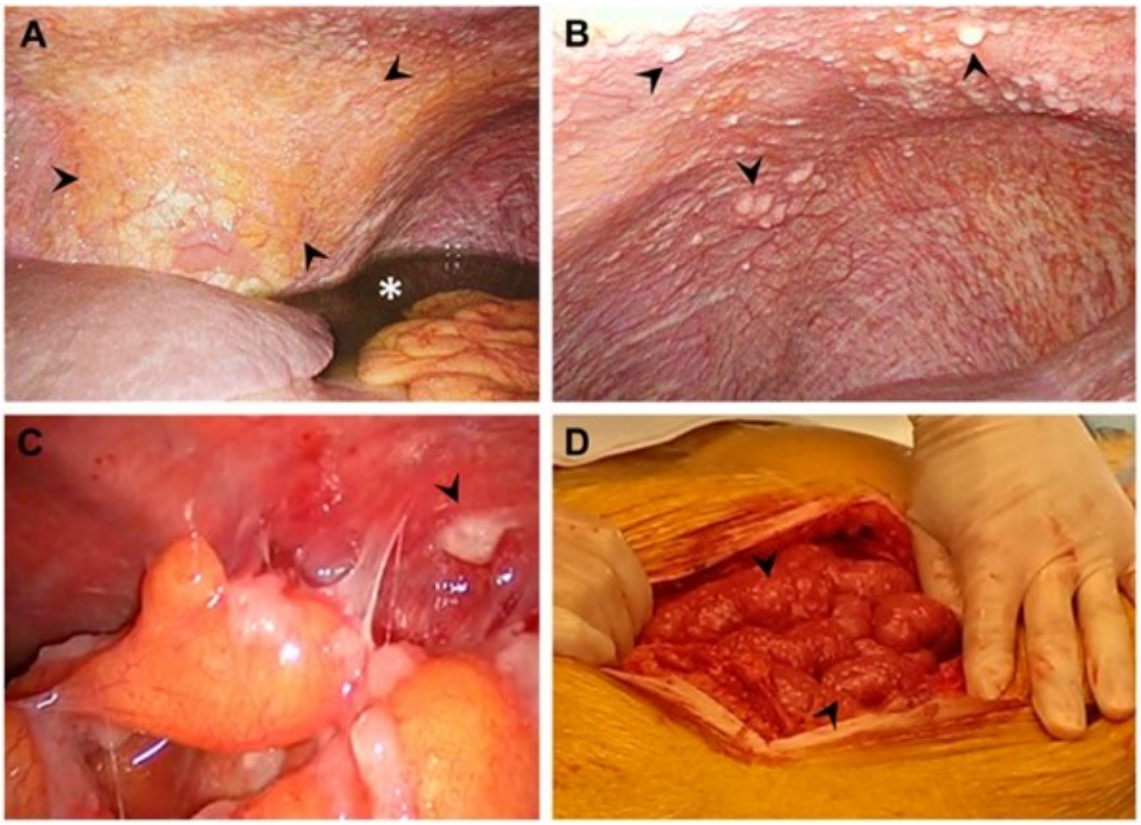

Figure 1.1 - Example of peritoneal carcinomatosis localized at the A-C) parietal and D) visceral peritoneum (arrows). The presence of peritoneal carcinomatosis is generally characterized also from the presence of ascites (asterisk), an abnormal buildup of liquids into the abdominal cavity. With permission from [2].

Since in the vast majority of patients these conventional therapies are not sufficient, innovative solutions have to be found. Recently, the use of plasma activated liquids (PALs) to deliver reactive oxygen and nitrogen species (RONS) to cancer tissues by washing the peritoneal cavities has been proposed as an alternative procedure having convenient analogies with the conventional intra-peritoneal chemotherapy procedures. Indeed it was demonstrated in *in vitro* and *in vivo* experiments that, depending on their RONS content, PALs might exert anticancer effects, even in a selective manner.[10–16] PALs are produced from the interaction between a gas phase plasma and an underlying liquid; when a sufficiently high voltage is applied to a gas, plasma filaments are generated, leading to the formation of free radicals, electrons, ions, reactive species and UV radiation that that can diffuse into the liquid surface. Subsequently gas phase species solvate into the liquid and give rise to additional reactions with the production of RONS like nitrites (NO_2^-), nitrates (NO_3^-), peroxynitrites ($ONOO^-$), ozone (O_3), hydroxyl radicals ($OH^\cdot$), hydrogen peroxide (H_2O_2), superoxide anion ($O_2^{\bullet-}$), nitric oxide ($NO^\bullet$), singlet oxygen ($^1O_2$), etc....[17] All these active agents are known for their importance in maintaining the cellular homeostasis.[18,19]

PAL turned out to be effective in terms of anti-tumor activity against EOC cells [11,14,20,21], but in certain cases they were produced from liquids (i.e. culture medium) whose safety for humans was not guaranteed.[13] In order to circumvent this problematic aspect, Tanaka *et al*. [12] first proposed the use of a Ringer Lactate (RL), a liquid commonly used in clinical practice, for the production of PAL; its simple composition (water, NaCl, KCl, $CaCl_2$ and lactate) makes it properly adoptable for the production of PAL, avoiding the possible influence of more organic medium components on the final biological effect.[22] It has been demonstrated that plasma-

activated Ringer's Lactate solutions (PA-RL) exhibit an anti-tumor effect in lung, mammary, ovarian cancer cells as well in glioblastoma *in vitro* [12,23,24], and in pancreatic and cervical cancer *in vivo*.[12,25] Several studies demonstrated that the effects of PA-RL may be ascribed to RONS, together with the activation of lactate.[12,24] All these results suggest that the use of PA-RL may represent a new potential therapeutic strategy for intraperitoneally disseminated cancers. Nonetheless, PA-RL selective cytotoxicity on EOC cells remains to be assessed. Indeed, the capability of an anti-neoplastic drug to act selectively against cancer cells is essential to preserve the healthy tissue counterpart.[20] This aspect is one of the most important for the application of PA-RL to ovarian cancer (OC) treatment.[23]

1.1.1 CAP devices for the treatment of liquids

In recent years, many research groups working on the topic of plasma medicine have dedicated enormous attention to the development of CAP sources for the treatment of biologically compatible liquids; these devices differ in terms of geometry and even in the discharge type. The most common sources recently reviewed by A. Khylyustova et al. [26], are the atmospheric pressure plasma jets (APPJs); as reported by X. Lu *et al*. [27], there are many types of APPJs with different configurations. Generally, the most commonly used for biomedical applications is named Plasma Gun, introduced for the first time by E. Robert *et al*. [28], and consists of a long (several centimeters) dielectric cylindrical tube of a few millimeters in diameter (used for the injection of plasma gas) equipped with an inner high voltage electrode and an outer ground electrode.[28–31] Although this device can be used for the treatment of different types of substrates, the contact area does not exceed a few mm^2; in the case of the treatment of liquid substrates, this results in limited volumes of the solutions to be treated (a few milliliters).[32–37] More recently, to overcome the problems related to the small dimensions of the plasma plume and consequently the surface of interaction with the underlying solution, T. H. Chung *et al*. [38] developed a multijet device connected to a primary APPJ which is able to increase the treatment surface. In addition to APPJs, also dielectric barrier discharges (DBDs) were used to produce PALs, even if less frequently. These devices are generally composed of a dielectric layer interposed between a high voltage electrode and a ground electrode, which generally consists of a metallic mesh.[39–42] Even in such cases, the volume of the treated solution does not exceed few milliliters (~ 3 ml).

An innovative plasma prototype, consisting of a ceramic box which encases a pin – to – pin arrangement of the high voltage and the ground electrodes, used to produce PALs is shown in Figure 1.2. The plasma device is composed of three different regions: gas diffusion region, main discharge region and radical transportation region. The gas injection was positioned on the top of the box; before reaching the discharge region, the working gas (pure argon or a mixture of argon and oxygen) passes through the diffusion region where it could mix. Subsequently it reaches the main plasma zone where the discharge occurs between the two cooled pin electrodes positioned opposite one to another.[43]

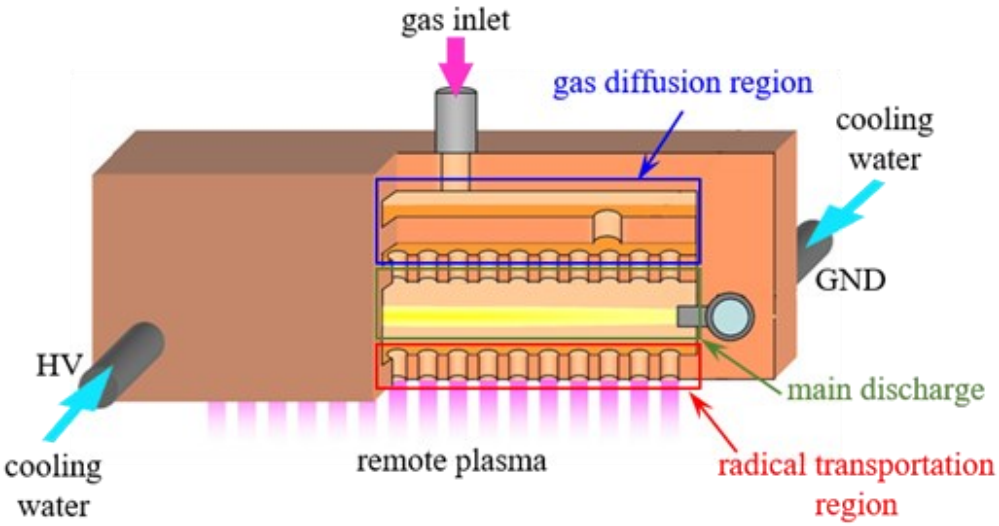

Figure 1.2 - CAP device characterized by ultrahigh electron density. With permission from [43].

Even if this device was successfully used for the production of PALs for the treatment of different types of cancer cells, healthy cells or chemo-resistant ones [11,12,14,20,24,43–51], further improvements are still necessary. Indeed, as reported by S. Takeda *et al*. [13] using the plasma device reported in Figure 1.2 and maintaining the same operating condition, an increase of the volume of the solution to be treated results in a reduction in the anti-tumor effect of the plasma treated solution.

The idea of using PAL to wash the peritoneal cavities of a woman suffering from ovarian cancer forces to imagine a plasma prototype capable of treating large volumes of liquid, since up to 6 l of chemotherapeutic solution may be required for an intraperitoneal administration.[52] In this regard, some of the plasma sources commonly used for the degradation of pollutants contained in liquid solution could represent a valid, albeit needing significant adaptations, alternative; one of the several possible configurations used in this application is the multiwire to plate configuration.[53–56] that also offer the advantage of using environmental air as working gas. Recently E. Ceriani *et al*. [57] reported a versatile multiwire prototype (Figure 1.3) that could work in two different discharge regimes (DBD and corona discharges) and could treat 200 ml of liquid solution. Despite the volume of the treated solution of this multiwire source was greater than the one used by CAP sources for the treatment of biologically compatible liquids, further efforts are still necessary to improve the design of such plasma sources to be able to treat a sufficient volume necessary for the intraperitoneal administration.

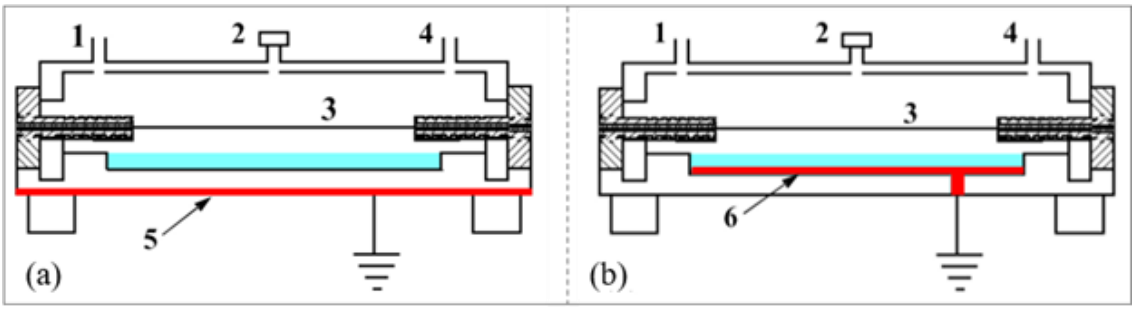

Figure 1.3 - Multiwire plasma source in (a) DBD and (b) corona configurations. These are composed by a 1) gas inlet, a 2) sampling port, 3) seven high voltage electrodes, a 4) gas outlet and the 5) ground electrode. With permission from [57].

1.1.2 Reaction pathways of biologically relevant RONS

Electrical discharges in contact with liquids are considered one of the most complex systems in plasma technology because it constitutes a highly non-equilibrium environment where the physical and chemical phenomena take place in multiple phases: gas phase, gas-liquid interface and liquid phase. Discharges in contact with liquids can produce a plethora of chemical reactions and consequently a large amount of reactive species in the underlying liquid substrate.[58,59] Currently, it is common knowledge that plasma-treated solutions exert biological effects in many different biomedical applications (including cancer treatment) which depend on the chemistry induced by plasma treatment in the treated liquid.[16, 46,60] Now the big challenge consists in the understanding of the reactions pathways in the liquid phase and consequently in controlling the reactive species concentration to obtain *ad hoc* composition for each specific application.

As reported in Figure 1.4, to study and characterize this complex system, usually the reaction environment is divided into three different regions: gas phase, gas – liquid interface and liquid phase. More in detail, when the electrical breakdown occurs, the discharge is formed in the gas phase leading to the formation of free radicals, ions, electrons and reactive species which chemistry is strongly influenced by the working gas (i.e., air, argon, helium, etc.…). The gas-liquid interface is characterized by a sub-nanometric layer of about 0.3 – 0.6 nm [58] and is involved in the transport phenomena governing the diffusion of charged particles and molecules in the underlying liquid substrate. Most of the phenomena taking place in the gas-liquid interface are still poorly understood due to the complex and multiscale (both temporal and spatial) nature of the involved mechanisms and reactions. As a consequence of solvation, diffusion and interaction with liquid substrate molecules, secondary reactions leading to the formation of RONS are established.[58–60]

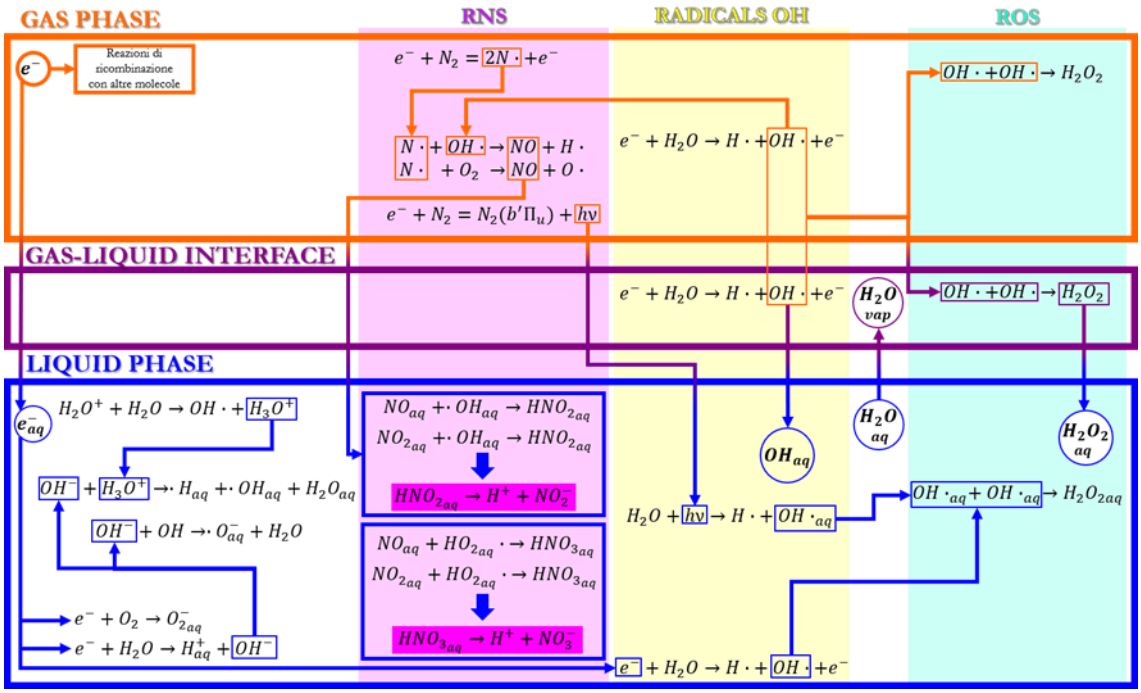

Figure 1.4 - Schematic diagram of the most important species and mechanisms involved in the formation of biologically relevant RONS.

To improve understanding of the results that will be presented below, it is useful to report the reactions involved in the formation of H_2O_2 and NO_2^- in the treated liquid.

1.1.2.1 Hydrogen peroxide formation

H_2O_2 concentration is influenced by the production of OH· in the gas phase, gas-liquid interface and liquid phase.[17,61–63] With specific reference to the gas phase, OH· is initially formed by electron impact dissociation of H_2O molecules during the interaction of the plasma and the humidity in the air or the evaporated water vapor above the underlying solution.

Different chemical reactions, whose reaction rates strongly depend on electron energy, lead to the formation of OH· radicals. For electron energies up to 1 eV, the vibrational excitation of water molecule (reaction (1)) is predominant; vibrationally excited water molecules (H_2O^*) could subsequently react (2) with an H_2O molecule to form the OH· radical.

$$H_2O + e^- \rightarrow H_2O^* + e^- \quad (1)$$

$$H_2O^* + H_2O \rightarrow H\cdot + OH\cdot + H_2O \quad (2)$$

On the contrary, for electron energy between 1.5 and 4 eV, the dissociative attachment predominates and results in the formation of a hydrogen ion (H^-) and a radical OH·.

$$H_2O + e^- \rightarrow H^- + OH\cdot \quad (3)$$

Once produced, due to its high reactivity, the OH· radical could react with a second OH· radical and form the H_2O_2 molecule:

$$OH\cdot + OH\cdot \rightarrow H_2O_2 \quad (4)$$

Since H_2O_2 is a very stable molecule, generally it does not react further with other molecules but diffuses in the liquid. Moreover, all the reactions reported above are even more important in the gas-liquid interface where the evaporation rate of water is higher compared with the gas phase.[64]

The presence of H_2O_2 in the liquid phase is not only due to the diffusion process but also to H_2O molecule photolysis:

$$e^- + N_2 \rightarrow N_2^* + h\nu \quad (5)$$

$$H_2O_{(aq)} + h\nu \rightarrow H_{(aq)} + OH\cdot_{(aq)} \quad (6)$$

$$OH\cdot_{(aq)} + OH\cdot_{(aq)} \rightarrow H_2O_{2(aq)} \quad (7)$$

In the immediate proximity of the water layer, as reported in equation (5), the impact between an electron and a nitrogen molecule (N_2) give rise to a vibrationally excited nitrogen molecule (N_2^*). From this excited state, N_2^* tends to spontaneously return to the ground state; the photons emitted during this relaxation process could reach the liquid and react with H_2O molecules as reported in reaction (6) leading to the formation of OH· directly in the liquid phase.[61,64] The OH· radicals contained in the liquid phase tend then to react together (7) with the production of H_2O_2 directly in the liquid phase.

1.1.2.2 Nitrites formation

NO_2^- concentration in the liquid phase strongly depends on the formation of nitrogen monoxide (NO) in the gas phase starting from monoatomic nitrogen (N).[65,66] In CAP, N could be produced starting from a vibrationally excited N_2 population:

$$O(^3P) + N_2^*(^1\Sigma_g^+, v) \rightarrow NO(^2\Pi) + N(^4S) \quad (8)$$

or through the dissociation of molecular nitrogen by direct impact of an electron with energy higher than 5 eV:

$$e^- + N_2(^1\Sigma_g^+) \rightarrow N_2\left(a^1\Pi_g, B^3\Pi_g, b^1\Pi_u\right) + e^- \rightarrow N + N + e^- \quad (9)$$

Subsequently, N could react with OH· radicals and O2 leading to the formation of NO, H and O.

$$N + OH \rightarrow NO + H \quad (10)$$

$$N + O_2 \rightarrow NO + O \quad (11)$$

After their production, NO molecules diffuse in the liquid phase and reacts with OH· radicals to form nitrous acid (HNO_2) which could dissociate and produce NO_2^- and hydrogen ions (H^+):

$$NO_{(aq)} + OH_{(aq)} \rightarrow HNO_{2(aq)} \quad (12)$$

$$HNO_{2(aq)} \rightarrow NO_{2(aq)}^- + H_{(aq)}^+ \quad (13)$$

In addition, NO_2^- could be generated in liquid from the dissolved gaseous NO and NO_2 through the following reactions reported by P. Lukes *et al*. [67]:

$$NO_{(aq)} + NO_{2(aq)} + H_2O \rightarrow 2NO_2{}^- + 2H^+ \quad (14)$$

$$NO_{2(aq)} + NO_{2(aq)} + H_2O \rightarrow NO_2^- + NO_3^- + 2H_{(aq)}^+ \quad (15)$$

1.1.3 The roles of RONS in antitumoral activity

The intracellular levels of reactive oxygen (ROS) and reactive nitrogen (RNS) species, together with those of antioxidant proteins, are of great relevance in human cells since they are correlated to several physiological and pathological conditions. In healthy cells, these agents are known for their importance in maintaining cellular homeostasis, namely the capacity to adjust the equilibrium between exogenous and endogenous stimuli. While in cancer cells, they are able to promote the many aspects of tumor development and progression.[68–70]

ROS can be divided into two main categories: free oxygen radicals (i.e. $O_2^{\bullet-}$, OH·, $NO^{\bullet}$, etc.…) and non-radical ROS (i.e. H_2O_2, O_3, $^1O_2$, etc.…). From Figure 1.5, it could be noticed that low levels of these reactive species promote cellular growth, migration and differentiation; while at high concentration (above a certain threshold level) they can cause irreversible damage to DNA proteins and lipids or even cell cycle arrest senescence and apoptosis.[18,71–74] Therefore, the equilibrium between ROS and antioxidants homeostasis is pivotal for regulating the cell biological functions.[75,76]

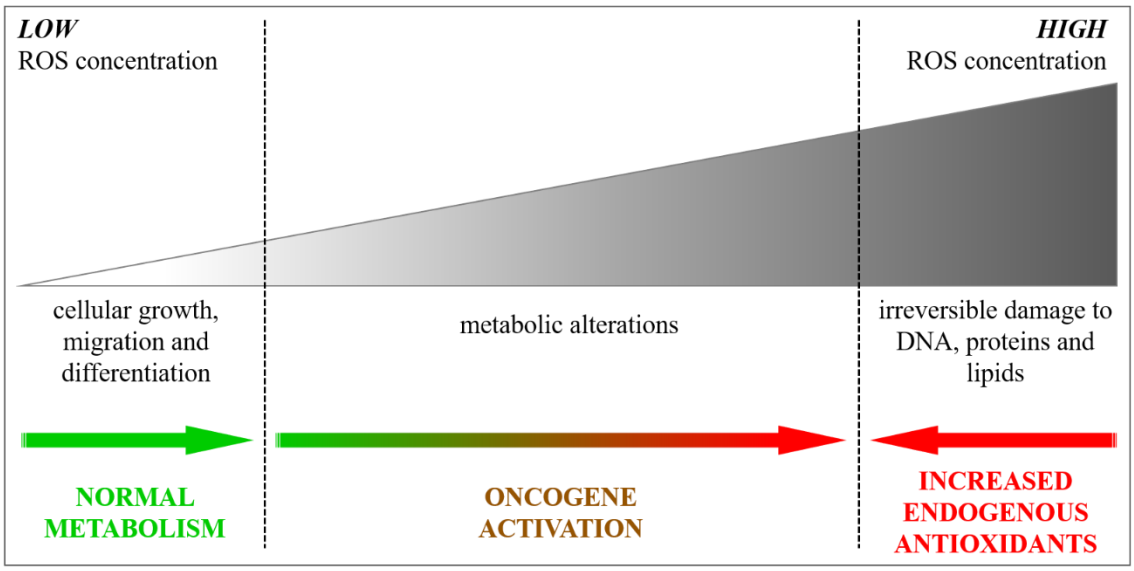

Figure 1.5 - ROS effects on cellular homeostasis: low levels of ROS promote cellular growth, migration and differentiation while high levels of ROS induce irreversible damage to DNA, proteins and lipids. In normal conditions, ROS levels are kept stable by several enzymes that neutralize toxic oxidants.[64]

Under normal physiological conditions, ROS levels are kept stable by non-enzymatic molecules (i.e., glutathione, flavonoids and vitamins A, C and E) or antioxidant enzymes (superoxide dismutase, catalase and glutathione peroxidase) which specifically scavenge different kinds of ROS. As reported in Figure 1.6, differently from their healthy counterparts, cancer cells are characterized by higher ROS levels due to, among many other reasons, the enhanced and abnormal metabolic activity, mitochondrial dysfunction and increased cellular receptor signaling. [74,77] This higher ROS content leads to an upregulation of the antioxidant levels and consequently to ROS levels close the toxic threshold.

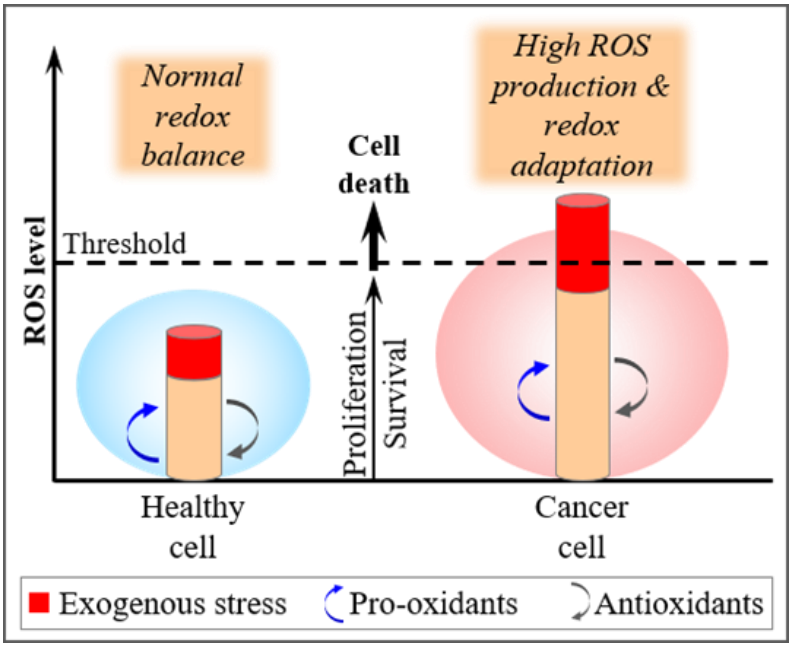

Figure 1.6 - Redox balance in cancer and healthy cells: beyond a certain threshold of toxicity, the antioxidants are no longer able to balance the toxic effect of ROS and the cell goes into apoptosis. Unlike cancer cells, whose ROS level is higher, in healthy cells the ROS levels are steadily maintained by antioxidants.[77]

RNS are also important molecules in cell signaling mechanisms. In particular, in hypoxic conditions NO_2^- (present in abundance blood and tissues) reacts with proteins and enzymes in order to produce nitric oxide (NO•).[78] This molecule is involved in many biological processes and, depending on its concentration it plays an important role in cell signaling, proliferation and survival or can subject the cells to nitrosative stress and consequently to death. More in detail, a low intracellular concentration (picomolar to nanomolar) of NO• exerts subtle effects in normal cells promoting cell survival and proliferation, while higher concentrations (micromolar) promote cell cycle arrest, apoptosis and senescence.[79] Cancer cells, as reported in Figure 1.7, are characterised by higher levels of nitric oxide synthase (NOS), which is involved in NO• production. This molecule is highly reactive and may interact with other species, leading to the formation of peroxynitrites, nitrogen dioxide or nitrogen trioxide, which in turn could lead to cell mutation and carcinogenesis. Moreover, it must be recorded that human solid tumors are characterized by the presence of numerous blood vessels with contractile cells and neural junctions able to regulate the blood flow. Consequently, a significant decrease (to around picomolar) or increase (to around millimolar) of NO• concentration can inhibit significantly the tumor growth or triggering apoptosis respectively.[19,80,81]

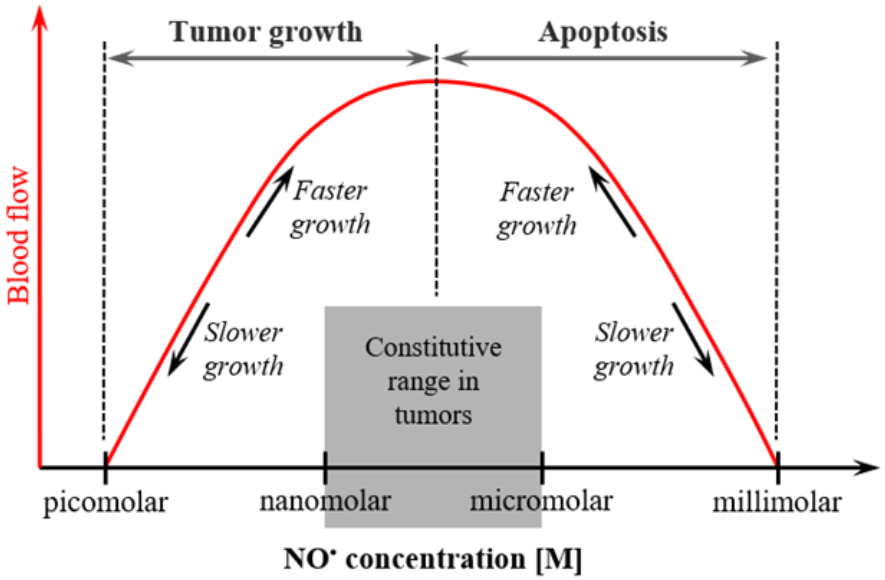

Figure 1.7 - Relation between blood flow and NO• concentration in tumor cells: normally tumor cells are characterized by higher values of NOS with the respect to healthy counterparts. A strong decrease (~ picomolar) or increase (~ millimolar) of NO• concentration could slower the tumor growth or conversely trigger apoptosis process.[79]

Under these assumptions, it appears that RONS can significantly influence cellular metabolism by inducing both proliferation and mutagenesis, depending on their concentration. Thus, they have a significant role in cancer therapy due to their influence on cell death mechanisms. In particular, in the right concentrations RONS can induce oxidative and nitrosative stresses leading to apoptosis, a programmed cell death not provoking the inflammation of the surrounding tissues.[68][82]

1.2 Materials and methods

1.2.1 Plasma device and electrical characterization

A multiwire plasma source (developed at the Alma Mater Studiorum – University of Bologna was used to produce PAL starting from a Ringer Lactate (RL, Fresenius Kabi Italia S.r.l.) solution (Figure 1.8a).[4] The high voltage electrodes consist of four stainless steel wires (with a diameter of 0.5 mm) individually fixed on aluminium supports (through threaded screws) and connected to the high voltage generator through a ballast resistor of 70 kΩ (Figure 1.8b). The ground electrode consists of an aluminium sheet fixed on the bottom of the 5 mm thickness polymethylmethacrylate (PMMA) vessel containing the liquid substrate; it is connected to the ground through a 30 kΩ resistor. To guarantee a controlled atmosphere during the plasma treatment, the entire structure is encased in a PMMA box on the cover of which was fixed a fan able to direct the plasma effluent towards the liquid surface. As an example, in Figures 1.8c/d is reported the behavior of plasma filaments using RL as liquid substrate.

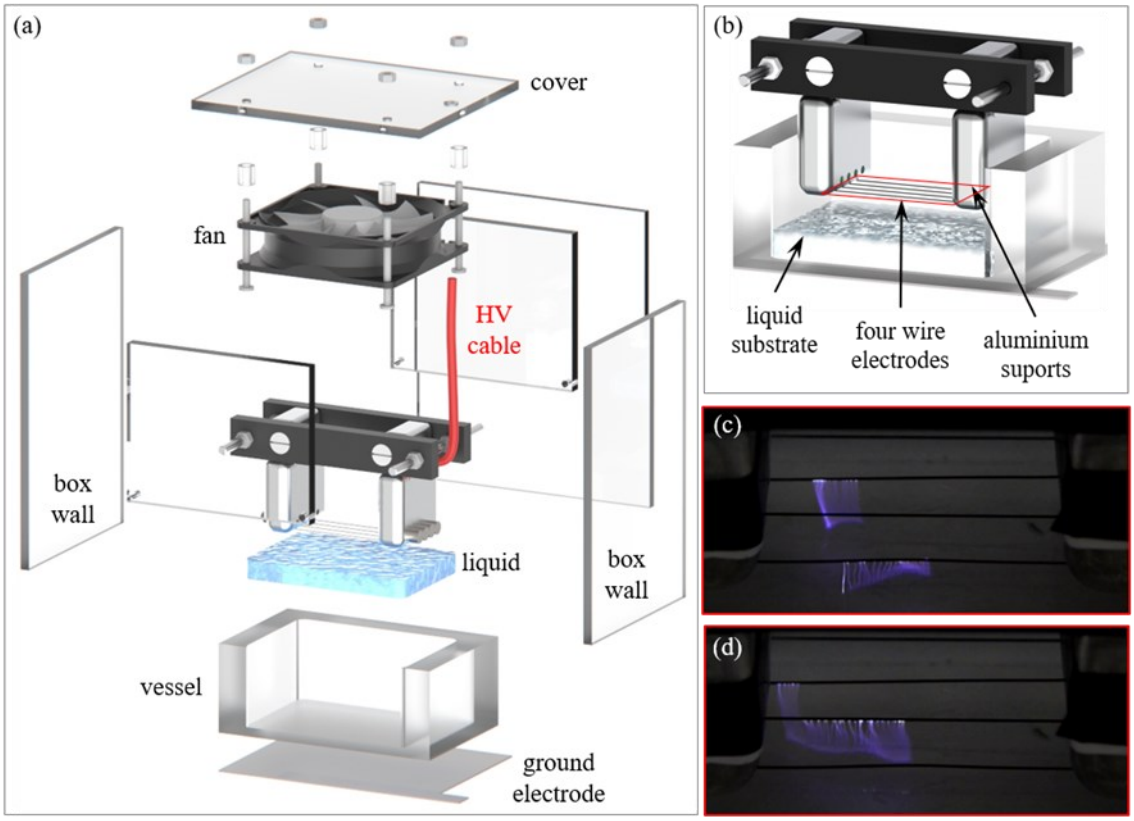

Figure 1. 8 - Render of the (a) exploded view of multiwire plasma source and its (b) electrodes configurations. Moreover, are reported the images of the plasma discharge during the treatment of (c, d) RL solution.

Figure 1.9 shows the setup used for the measure of the time evolution of the plasma discharge electrical parameters using 5 mm gap value between the high voltage electrodes and the liquid surface. The plasma device was driven by a micropulsed high voltage generator (AlmaPULSE, AlmaPlasma s.r.l.) delivering a peak voltage between 15 kV and 18 kV, pulse duration FWHM (Full Width at Half Maximum) of 8 μs and pulse repetition rate set at 1 kHz. As reported in Figure 1.9, two resistors of 70 kΩ and 30 kΩ were mounted on the high voltage and the ground cables,

respectively, to prevent arc discharges [83]. Moreover, two high voltage probes (Textronix P6015A) were used to measure the voltage before and after the high voltage resistor (70 kΩ), while the discharge current was measured by means of a current probe (Pearson 6585). All the probes were connected to an oscilloscope (Tektornix DPO4034, 350 MHz, 2.5 GSa s-1) and the average power (P) over a period (T) was calculated starting from current (I) and voltage (V) acquisitions:

$$P = \frac{1}{T}\int_T V(t)I(t)\,dt \tag{16}$$

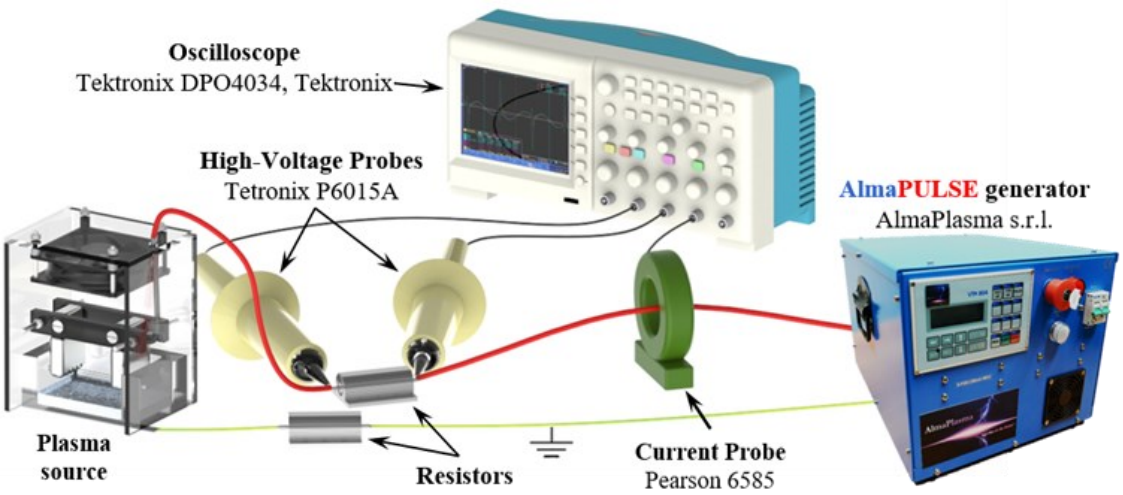

Figure 1.9 - Layout of the setup used for electrical characterization.

1.2.2 Plasma treatment and quantitative measure of RONS

PA-RL was produced by exposing 20 ml of RL to plasma for 10 minutes using a 5 mm gap between the high voltage wire electrodes and the liquid surface. The pulse repetition frequency (PRF) was fixed at 1 kHz, while the peak voltage (PV) was increased between 15 kV and 18 kV with the fan always on. After plasma treatment, quantitative measurements of H_2O_2, NO_2^- and O_3 were performed using Amplex® Red Hydrogen Peroxide Assay Kit (Thermo Fisher Scientific #A22188), Nitrite/Nitrate colorimetric assay (ROCHE #11746081001) [84][85] and a Photometer CHEMATEST (CH-8340 Hinwil/Switzeland), respectively. For H_2O_2 and NO_2^- measurements, to avoid secondary reactions which take place in acidic environments [86], the plasma treated liquid was diluted 40-fold in phosphate buffered (PB) solution (with a pH of 7.4) immediately after the treatment and the measurements were carried out under red light.[87]

Amplex Red Hydrogen Peroxide/Peroxidase Assay Kit is a highly accurate quantitative colorimetric method widely used for the detection of H_2O_2. As reported in Figure 1.10a, its simplified mechanism could be summarized as a peroxidase-catalyzed oxidation of Amplex Red reagent to resorufin in the presence of horseradish peroxidase (HRP); the resulting product is a colorimetric one and it is proportional to the H_2O_2 concentration.[88] The HRP (Figure 1.10c) is a monomeric enzyme which catalyzes the oxidation of a broad range of substrates with his prostheric heme group.[89,90] More specifically, the Figure 1.10b shows the reaction mechanism where in the first passage H_2O_2 initiates the peroxidase catalytic cycle leading the ferric ground-state HRP to compound 1 (porpyrin-π-cation radical). In the second passage a rapid one-electron

transfer reaction leads to the compound 2 following the formation of a phenoxyl-type radical from Amplex Red molecule. While in the third passage the one-electron transfer reaction leads the compound 2 back to the ground state following the formation of a second phenoxyl-type radical.[91] In the absence of $O_2^{\cdot -}$ and $ONOO^-$, the Amplex Red Hydrogen Peroxide/Peroxidase Assay Kit is considered a good indicator of H_2O_2 concentration.[90,92]

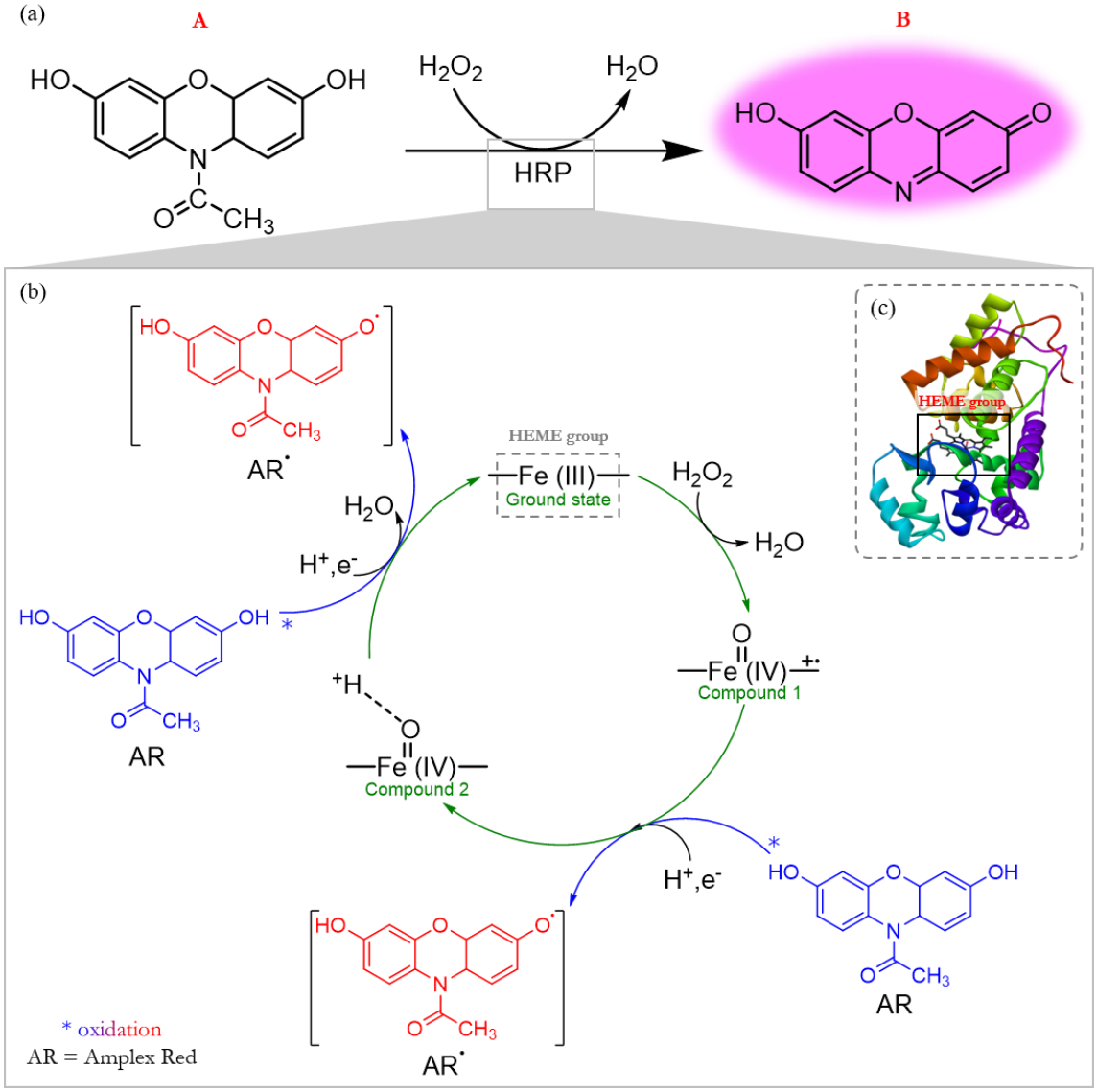

Figure 1. 10 – Simplified reaction mechanism showing the peroxidase-catalyzed oxidation of reagent A (1-(3,7-dihydroxy-4a,10a-dihydro-10H-phenoxazin-10-yl)ethan-1-one (Amplex Red)) with H_2O_2 (in the presence of HRP) to form the product B (7-hydroxy-3H-phenoxazin-3-one (resorufin)).[90,92]

The Nitrite/Nitrate colorimetric assay, based on the Griess assay's mechanism, was employed for the measure of NO_2^-; this mechanism is summarized in Figure 1.10a as the azo coupling between diazonium species, which are produced from sulfanilamide with NO_2^-, and N-(1-naphthyl)-ehthylenediamine (NED). The resulting reagent is a colorimetric product (diazo dye) proportional to the NO_2^- concentration with a maximum molar absorbance between 540 nm and 570 nm. The reaction mechanism is reported in detail in Figure 1.11; the reaction 1 is a two-passage, one of which carried out in acidic solution. The final product of these reaction is the diazonium cation which have a molar absorbance about 50 times lower that diazo dye product. The reaction 2 is an electrophilic aromatic substitution reaction with the diazonium cation

(produced from sulfanilamide) as the electrophilic agent and the aromatic amine (NED) as the nucleophilic base. In the diazo dye molecule –N = N– is the most important chromophore group which gives the red-violet color to the solution.[93]

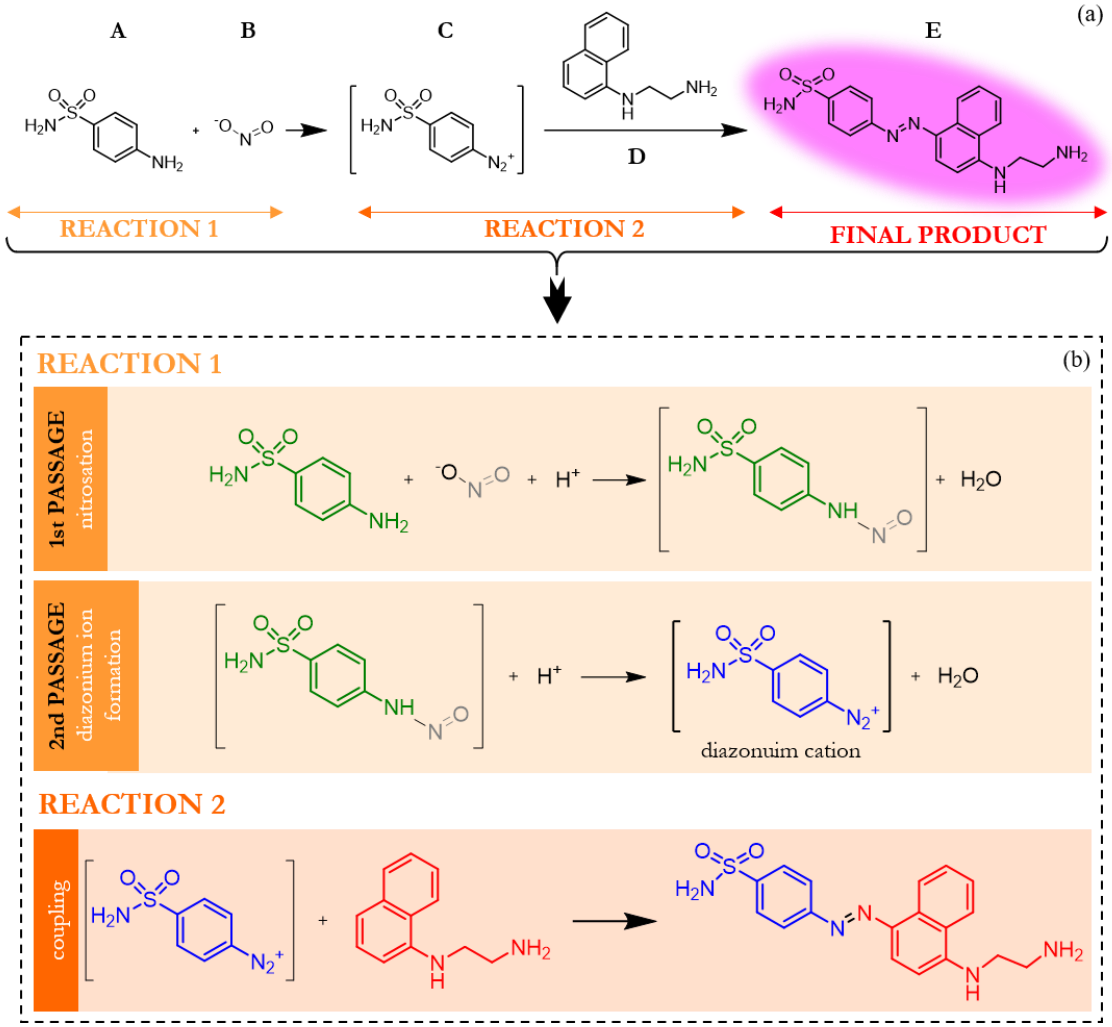

Figure 1. 11 – Griess mechanism showing the first reaction between 4-aminobenzenesulfonamide (A, sulfanilamide) and nitrites (B) having as product 4-sulfamoylbenzenediazonium (C) which in turn reacts with N1-(naphthalen-1-yl)ethane-1,2-diamine (D, sulphanilamide) to form (E)-4-((4-2-aminoethyl)amino)naphthalen-1-yl)benzenesulfonamide (E, diazo dye).[93]

In addition, before and after RL exposure to plasma, pH and conductivity were evaluated by means of inoLab® pH 7110 and Oakton Instrument: Con 6+ Meter, respectively.

1.2.3 Low-speed and high-speed filter imaging

Figure 1.12 shows the setup used for the evaluation of the plasma discharge behavior of the multiwire device. It was composed of a high-speed (HS) camera (Memrecam GX-3 NAC image technology) operated at 100 fps and 1/200 shutter time or a low-speed camera (Nikon D800) operated at 30 fps. Additionally, a camera lens (SIGMA 180 MM 1:3.5 APO macro DC HSM) equipped with a 402 nm filter (CHROMA, ET402/15x) was used to evaluate the emission of $N_2(C^3\Pi_u \rightarrow B^3\Pi_g)$ second positive system near 400 nm. During HS-filter imaging, the focus of the acquisitions was set in correspondence of the electrode closest to the filter.

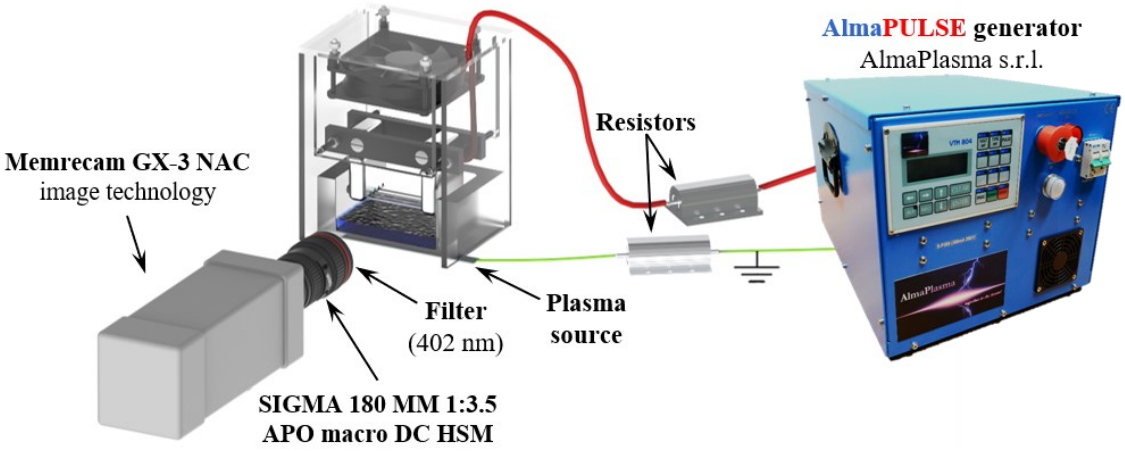

Figure 1.12 - Layout of the setup used for low-speed and high-speed characterization.

1.2.4 Optical absorption spectroscopy

The setup used for absorption spectroscopy is reported in Figure 1.13; a deuterium-halogen lamp (characterized by a broad spectrum from UV to NIR radiation) was used as a light source. The light beam emitted by the lamp was focused through an optical fiber and a fused silica lens (50 mm of focus length) through the discharge zone. In the same manner, the outgoing light beam was focused through a second focused silica lens and an optical fiber (Princeton Instruments, fiber optic bundle, 190 – 1100 nm) through the 500 mm spectrometer (Acton SP2500i, Princeton Instruments). For the NO_2 measurements (in the wavelength range 400 ± 1.2 nm), the grating resolution was fixed at 1200 mm^{-1} and the width of the inlet and the outlet slit of the spectrometer were fixed at 75 µm and 100 µm, respectively. While for O_3 measurements (in the wavelength range 253 ± 1.2 nm), the grating resolution was fixed at 150 mm^{-1} and the width of the inlet and the outlet slit of the spectrometer were fixed at 50 µm and 100 µm, respectively. A photomultiplier tube (PMT-Princeton Instruments PD439) connected to a fast oscilloscope (Tektoronix DPO 4034, 350 MHz, 2.5 GSa s^{-1}) was used as detector and its amplification factor was kept constant (1200) for all acquisitions.

Subsequently, NO_2 and O_3 concentrations were calculated using the Lambert – Beer law which correlates the absorbed light with the concentration of the specific molecule (n):

$$n = -\frac{1}{L\sigma} ln\left(\frac{I}{I_0}\right) \tag{17}$$

where I/I_0 is the ratio between the intensity of the lamp emitted (I_0) and the light intensity (I) after the optical path length (L) and σ is the cross-section of the absorber.

To avoid the emission of the plasma streamers, all the measurements were recorded every 60 s with both fan and power supply off. Moreover, the signal was recorded in continuous also in post discharge (for 120 s) to assess the composition of the treated gas.

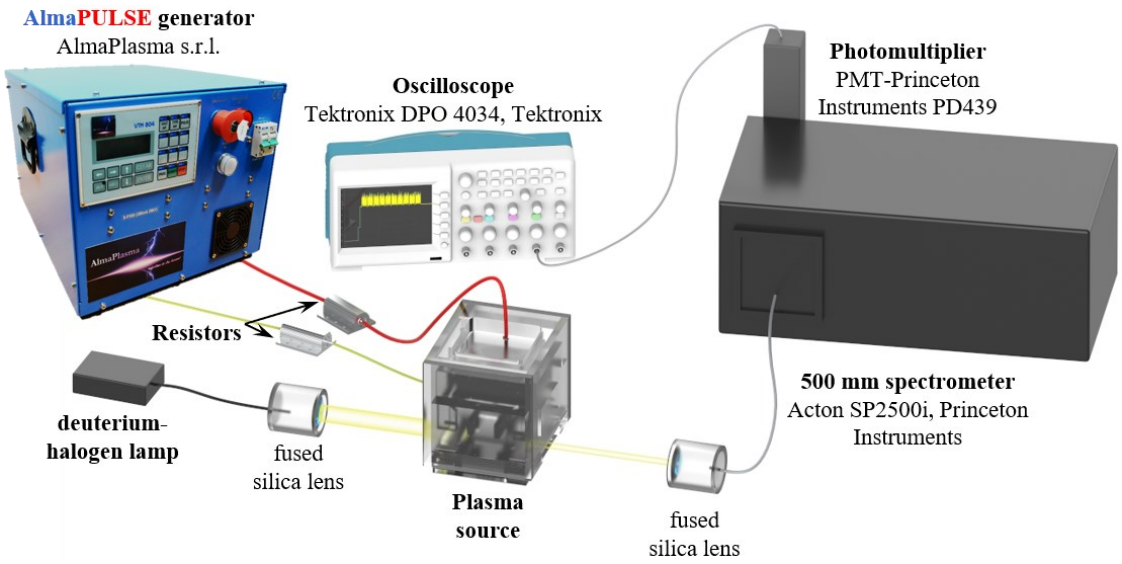

Figure 1.13 - Layout of the setup used for optical absorption spectroscopy.

1.2.5 Cell lines and culture conditions

SKOV3 and OV90 cell lines were purchased from ATCC®, while an immortalized line of fibroblasts (F) derived from a patient skin biopsy (obtained within the context of a protocol study approved by the Independent Ethics Committee of the S. Orsola-Malpighi Hospital (107/2011/U/Tess)) was used as non-cancer controls.

EOC cell lines and fibroblasts were grown in Roswell Park Memorial Institute 1640 medium (RPMI, EuroClone) and Dulbecco's modified Eagle's medium (DMEM High glucose, EuroClone), respectively. Both cell mediums were supplemented with 10 % heat-inactivated fetal bovine serum (FBS), 2 mM L-glutamine, 100 U/mL penicillin and 100 µg/mL streptomycin (EuroClone). The cells were maintained in an incubator with a humidified atmosphere of 5 % CO_2 at 37°C.

1.2.6 Cell treatment and viability assay

SKOV3 ($2x10^3$ cells/well), OV90 ($4x10^3$ cells/well), and F ($9x10^3$ cells/well) were seeded in 96-well plates in complete medium. After 24 hours, cells were treated with 100 µl of freshly produced PA-RL at different dilutions (1:4, 1:8 and 1:16) and RL. After 2 hours of treatment, cells were washed with phosphate buffered solution (PBS) and cultured in complete medium at 37°C and 5 % CO_2. Cell viability was assessed after the exposure of cells to the treatments and measured by using Sulforhodamine B (SRB) (Sigma-Aldrich, #S1402) assay at 2, 24, 48 and 72 hours after treatment. Treated cells were fixed with 50 % cold trichloroacetic acid (TCA) for 1 hour, washed 5 times with distilled water to eliminate TCA, and stained with 0.4 % SRB for 30 minutes. Protein-bound dye was dissolved in 10 mM pH 10.5 Tris base solution after 4 four washes with 1 % acetic acid to remove unbound dye. SRB was used to determine cell density, based on the measurement of cellular protein content. Absorbance values were determined at 570 nm using a 96-well Multilabel Plate Reader VICTOR3 (1420 Multilabel Counter-PerkinElmer, Turku, Finland).

1.3 Results and discussion

1.3.1 Electrical characterization

To evaluate the power dissipated by the resistance mounted on the high voltage cable and the average power of the plasma discharge, the temporal evolution of voltage and current waveforms (Figure 1.14 and Figure 1.15) was recorded during the treatment of RL solution (Figure 1.8c/d).[16] Two high voltage probes were used to measure the voltage drop across the 70 kΩ resistance mounted on the voltage cable (Figure 1.9) in order to calculate the power dissipated by the resistance; this procedure was performed to check if the measured power did not exceed the 100 W power rating of the resistance, namely the maximum power that can be dissipated from the resistor during operation without burning out. In Figure 1.14 an example of the voltage and current waveforms recorded before the 70 kΩ resistance is reported; the maximum and the minimum values reached by the voltage are 26 kV (Figure 1.14b) and -26.5 kV (Figure 1.14c), respectively. While the power calculated using equation (16) was about 30 W, noticeably lower than that reported by the manufacturer.

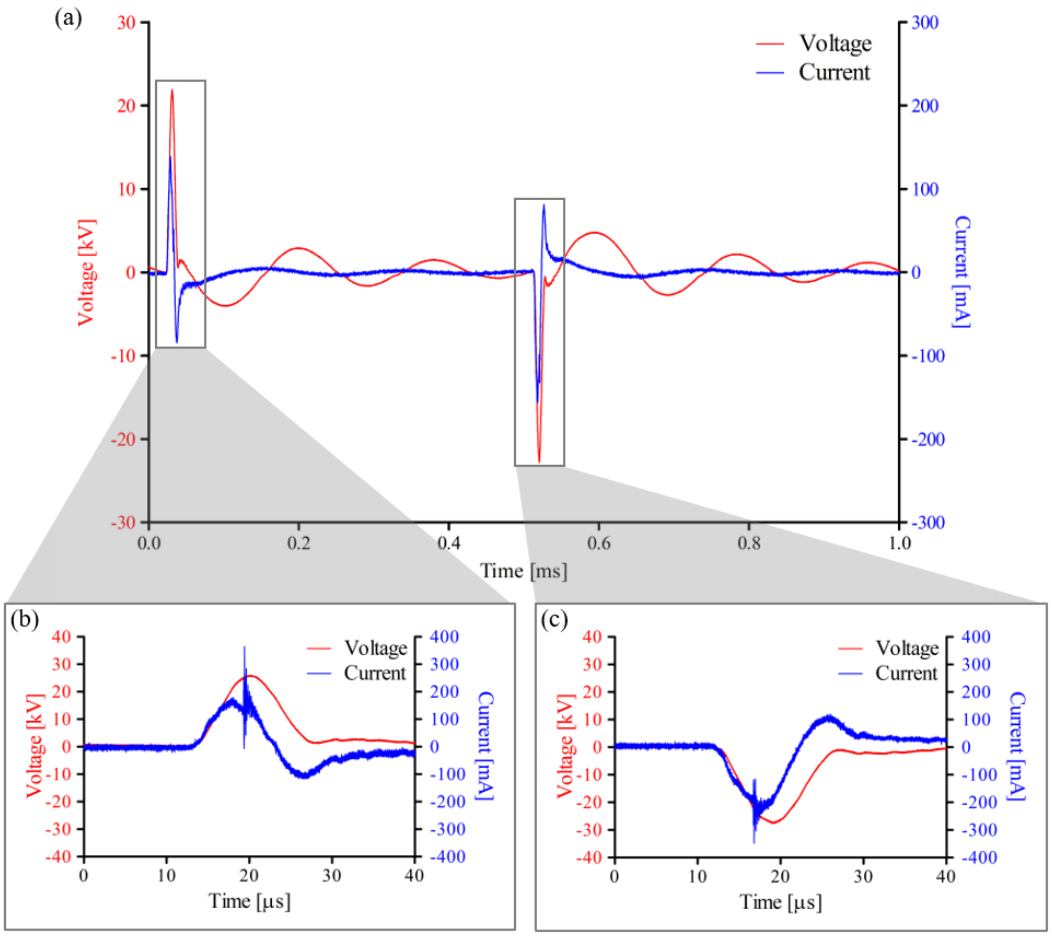

Figure 1.14 - Results of electrical characterization of the (a) entire period, single (b) positive and (c) negative peaks before the 70 kΩ resistance during multiwire plasma source operation with RL liquid substrate.

Subsequently, as reported in Figure 1.15, voltage data recorded by the high voltage probe placed after the 70 kΩ resistance and current were used for the calculation of the average power of the plasma discharge using equation (16) for different applied voltages. In Figure 1.15b/c was

reported an example of the presence of discharge activity; it can be distinguished by some current spikes superimposed on the displacement current waveform, in correspondence to a drop of voltage from 19 kV to 14.5 kV and from -9 kV to -11.2 kV. After the drop, the voltage waveform rises again and reaches a maximum of 18 kV or -13.2 kV.

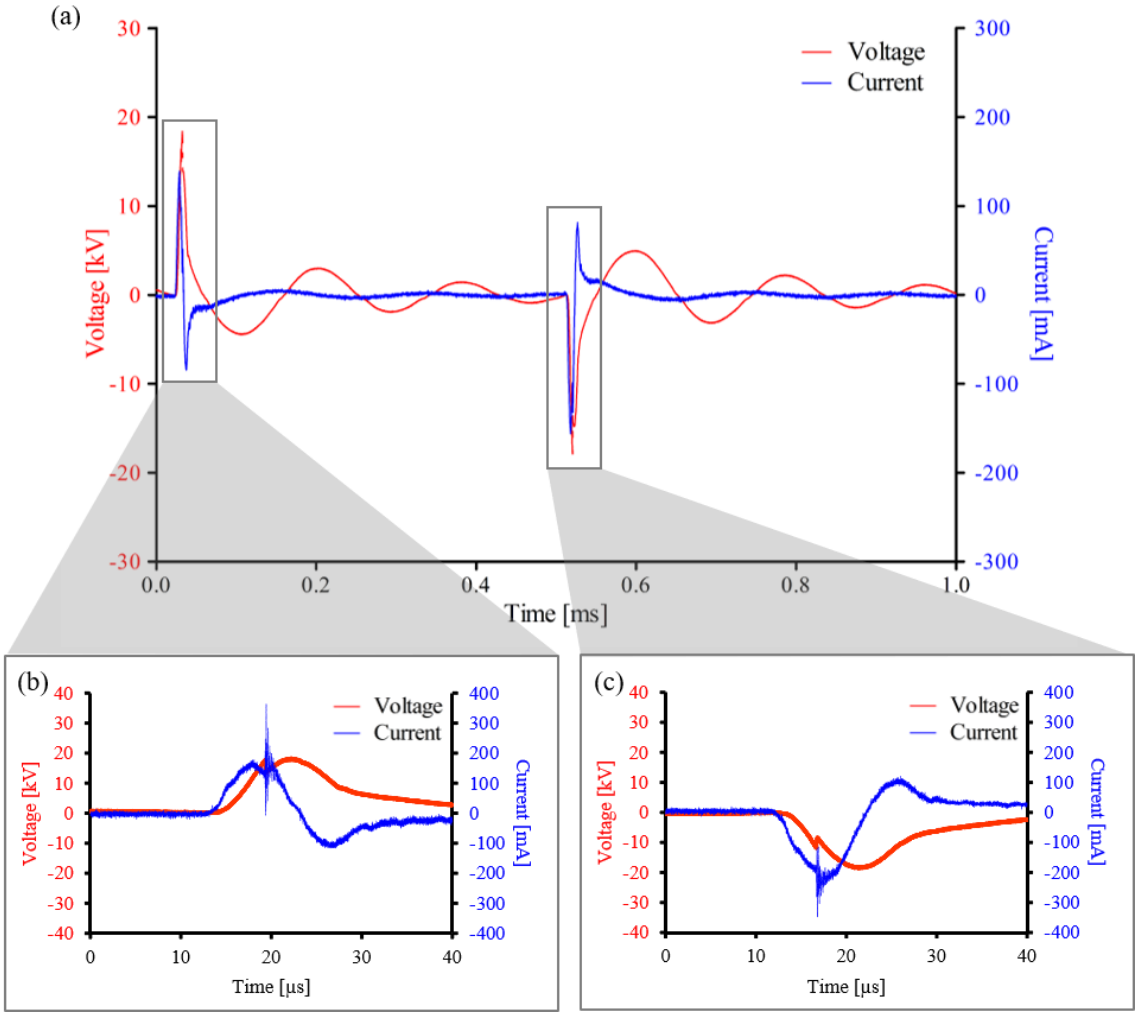

Figure 1. 15 - Results of electrical characterization of the (a) entire period, single (b) positive and (c) negative peaks after the 70 kΩ resistance during multiwire plasma source operation with RL liquid substrate.

As reported in Figure 1.16, the recorded data were used for the calculation of the average power as a function of the applied voltage, with a fixed frequency of 1 kHz; it results that an increase of the applied voltage from 15 kV to 18 kV determines an increase in the power values from a minimum of 5.2 W to a maximum of 12.4 W in agreement with the results reported by B. Dong *et al*. [94].

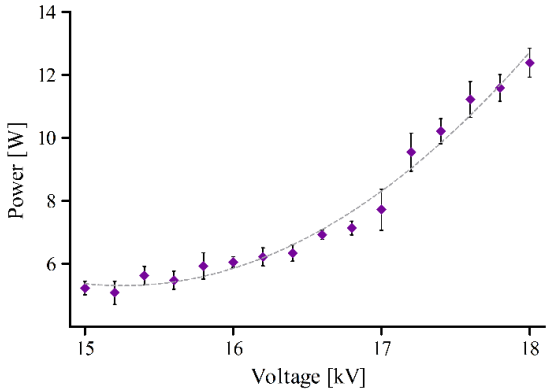

Figure 1.16 - Electrical characterization of plasma source during treatment of RL solution: power values as a function of the applied voltage. Data are presented as mean ± SD (n=3).

1.3.2 Chemical characterization of the treated liquid

The interaction of plasma discharges with liquid substrates leads to the formation of a high concentration of RONS.[62,86] In the cases under examination, RONS concentrations measured after the plasma treatment in the liquid substrate are shown in Figure 1.17; as previously reported by R. Laurita *et al*. [86], all the investigated concentrations strongly depend on the treatment time. More specifically, the H_2O_2 and NO_2^- concentrations increased with the treatment time (Figure 1.17a) and reached a maximum of 226 ± 12.5 µM and 658.6 ± 15.2 µM, respectively. The dependency of RONS concentration variation on the voltage values is shown in Figure 17b; in this case, H_2O_2 and NO_2^- concentrations measured in the liquid substrate resulted not to be influenced by the voltage and thus by the average power in the range of 5.2 ÷ 12.4 W.

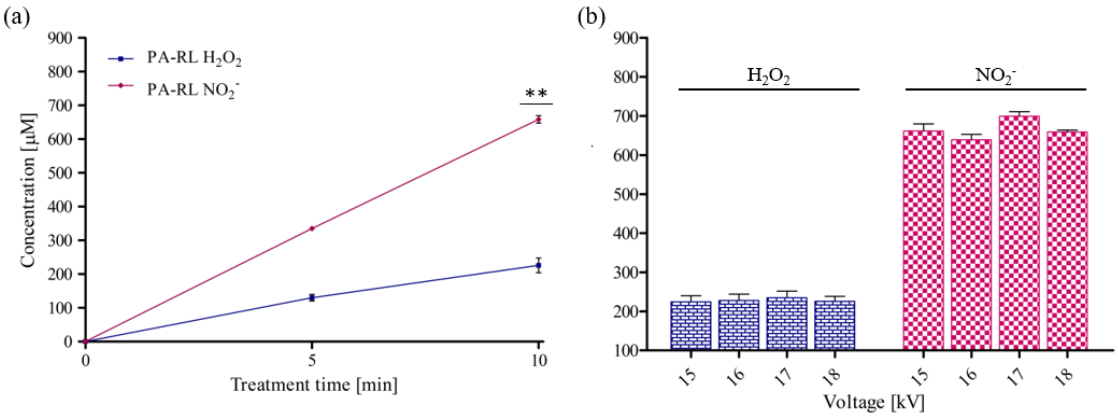

Figure 1.17 - Plasma treatment leads to the formation of H_2O_2 and NO_2^-. (a) RONS concentration as a function of average power after 10 min of plasma treatment. Data are presented as mean ± SEM (n=3). (b) H_2O_2 and NO_2^- concentrations as a function of treatment time. Data are presented as mean ± SEM (n=3) and statistical significance is specified with asterisks (**p ≤ 0.001 as determined by paired Student t-test, versus 5 min treatment).

In addition to the previous results, were also reported RONS concentration of diluted PA-RL solution (Figure 1.18); the choice of analyzing even PA-RL dilutions derives from the desire to analyze the efficacy of a plasma-treated liquid containing lower and lower RONS concentrations. The analyzed solution was obtained diluting 2-fold in RL. As expected, in both of cases H_2O_2 and NO_2^- concentrations decrease with increasing dilutions.

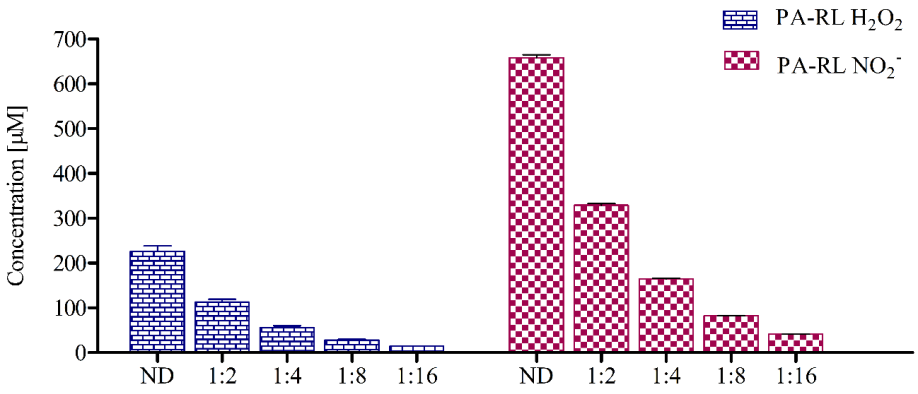

Figure 1.18 - H_2O_2 and NO_2^- concentration of not diluted (ND) PA-RL solutions after 10 min of plasma treatment and 1:2, 1:4, 1:8 and 1:16 dilutions. Data are presented as mean ± SEM (n=3).

Moreover, was reported the concentration of liquid phase O_3 as a function of the treatment time. As could be seen from Figure 1.19, O_3 concentration increases with the treatment time and reach a maximum value of 0.081 ± 0.0047 mg/l corresponding to a concentration of 1.69 ± 0.10 µM, considerably inferior with respect to H_2O_2 and NO_2^- concentrations.

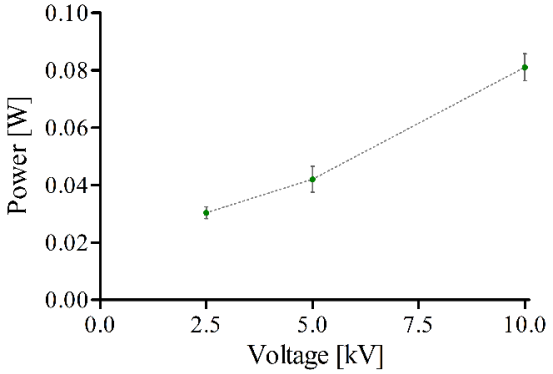

Figure 1.19 – O_3 concentrations in liquid phase as a function of the treatment time (150, 300 and 600 s). Data are presented as mean ± SEM (n=3)

In addition, pH and conductivity of PA-RL and their dilutions are reported in Figure 1.20. After 10 minutes of plasma treatment PA-RL pH decreased to 5.36 (PA-RL) whereby only dilutions starting from 1:4 were used for subsequent cell treatments. Plasma treatment also induced an increase of conductivity up to 15.13 mS/cm.

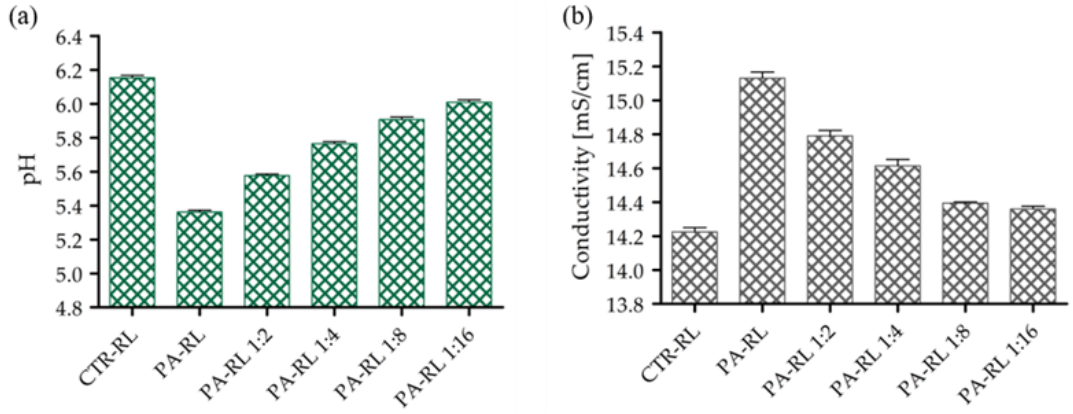

Figure 1.20 - Chemical characterization of PAM, PA-RL and its dilutions after 10 min of plasma treatment at 18 kV and 1 kHz. (a, b) pH and (c, d) conductivity as a function of serial dilutions. Data are presented as mean ± SEM (n=3).

1.3.3 Evaluation of plasma discharge behavior and emission by means of low-speed and high-speed filter imaging

Low-speed imaging was performed to assess the behavior of plasma filaments generated during the plasma treatment. The plasma discharge consisted of random streamers generated between the wire-electrodes and the liquid surface (Figure 1.21a). Figure 1.21b shows representative HS filter images of the multiwire discharge generated applying different voltages. In all investigated cases, it is possible to observe the single plasma filaments generated between the high voltage wire electrode and the liquid surface. Moreover, no relevant differences could be observed upon varying the input voltage between 15 kV and 18 kV.

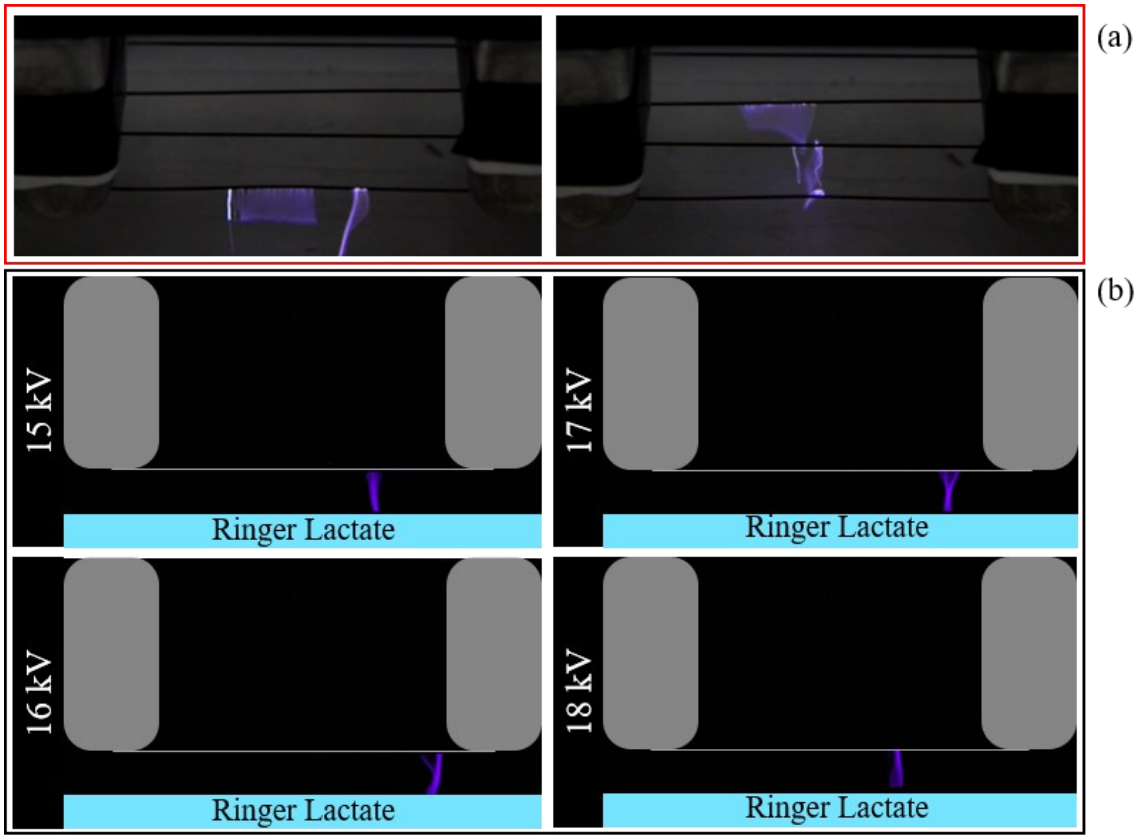

Figure 1.21 - Low-speed images and HS filter images of the multiwire plasma discharge during the treatment of RL. (a) Picture of plasma generated during the treatment of PA-RL with an applied voltage of 18 kV and 30 fps. (b) HS filter images of plasma filaments for different values of applied voltage (between 15 kV to 18 kV) and 100 fps.

As confirmed by HS filter images, the presence of vibrationally excited N_2 molecules support the idea that the reactions which lead to the production of RNS in the liquid phase involved chemical species generated in the plasma (gas phase) and diffusing into the liquid. Indeed, N_2^* molecules lead to N_2 dissociation and consequently formation of NO in the gas phase. As an example, the formation of NO_2^- involves the gas phase reaction of NO· molecules with OH· molecules (reaction 12), resulting in the production of HNO_2 that dissolves in the liquid phase and leads to the formation of NO_2^-. In non-equilibrium plasmas, gas phase NO is produced starting from a vibrationally excited N_2 population or via direct electron impact.[62] The presence of these molecules favors the cleavage breakage of N-N chemical bonds of nitrogen molecules to release N atoms that react with O_2 and ·O to produce NO molecules. As shown by M. Simek *et*

al. for in the case of a plasma discharge working in environmental air, vibrationally excited N_2 molecules emit light at a wavelength around 400 nm (second positive system, $C^3\Pi_u \rightarrow B^3\Pi_g$).[95] In this respect, Figure 1.18b confirms the presence of vibrationally excited N_2 molecules and thus the gas phase origin of the NO_2^- measured in the PAL.

1.3.4 Evaluation of RONS concentrations in gas phase

The interaction of CAP with a liquid substrate leads to the formation of numerous reactive species with biological importance. Since most of the chemical recitations involved in the formation of liquid phase RONS are still a big challenge, [58,59] during the course of my Ph.D. I investigated the concentration of O_3 (a long-life oxidant molecule) and NO_2 (one of precursors of NO_2^- in the liquid phase) molecules generated in the gas phase between the HV electrodes and the liquid substrate by means of OAS technique. Figure 1.22 shows a constant increase of O_3 concentration during the treatment time (600 s), reaching a maximum concentration of 8.04 ppm at the end of the treatment and then presenting a strong drop in the first few seconds of the post discharge phase. Differently from O_3, the NO_2 concentration maintains a constant value in the range of 0 ppm in both discharge and post discharge zone.

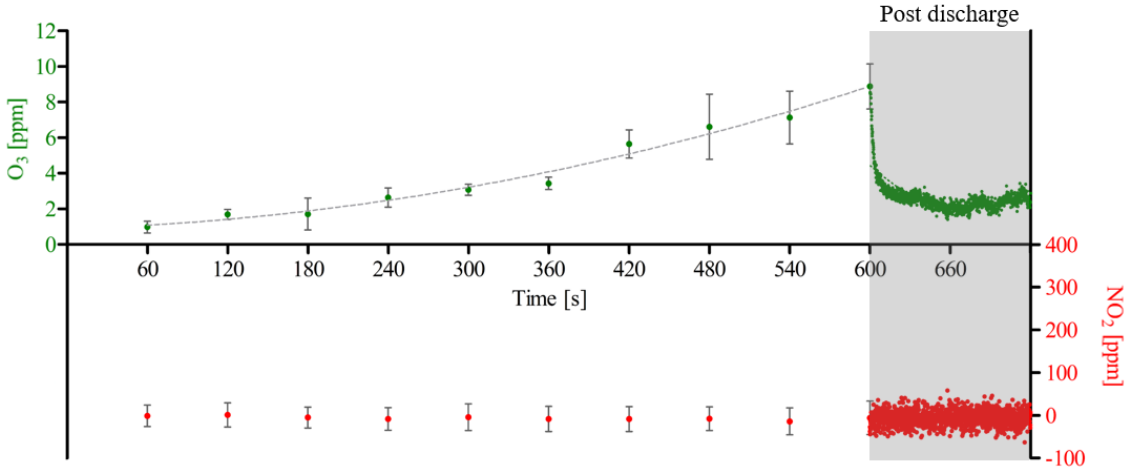

Figure 1.22 - O_3 and NO_2 concentrations during 600 s of plasma treatment and 120 s of post discharge.

As reported by E. Simoncelli *et al*. [66], when NO_2 concentration in gas phase is close to 0 ppm, O_3 molecules decomposition is limited and thus it could diffuse in the above liquid substrate. Part of the O_3 molecules formed in the gas phase diffuse in the liquid one as confirmed by the results reported in Figure 1.16; moreover, O_3 trend in the liquid phase is very similar to the gas phase one. The absence of NO_2 molecule in the gas phase confirms that the formation of NO_2^- in the liquid substrate did not involve the NO_2 pathway reactions.

1.3.5 Cell viability after PA-RL treatment

These results were reported to show the full picture of the effects of the multiwire source I developed. In this regard, experiments on cancer cells were performed in the Golgi BioPlasma Cell laboratory (DIN), while experiments on *ex vivo* fibroblasts were carried out in Genetica Medica Laboratory (DIMEC); my contribution in these experiments dealt with PA-RL production, while cell culturing and biological analyses were performed by Dr. Cristiana Bucci.

In order for the PA-RL to find applications in clinics, one of the most important requirements is that its cytotoxicity action needs to be specific for cancer cells; indeed, cancer cells are always surrounded by healthy ones. In this perspective, for the evaluation of the cytotoxic effect of PA-RL, two different EOC cell lines (namely SKOV3 and OV90) and primary fibroblasts were exposed for two hours to different PA-RL dilutions (1:4, 1:8 and 1:16); the results are shown in Figure 1.23.

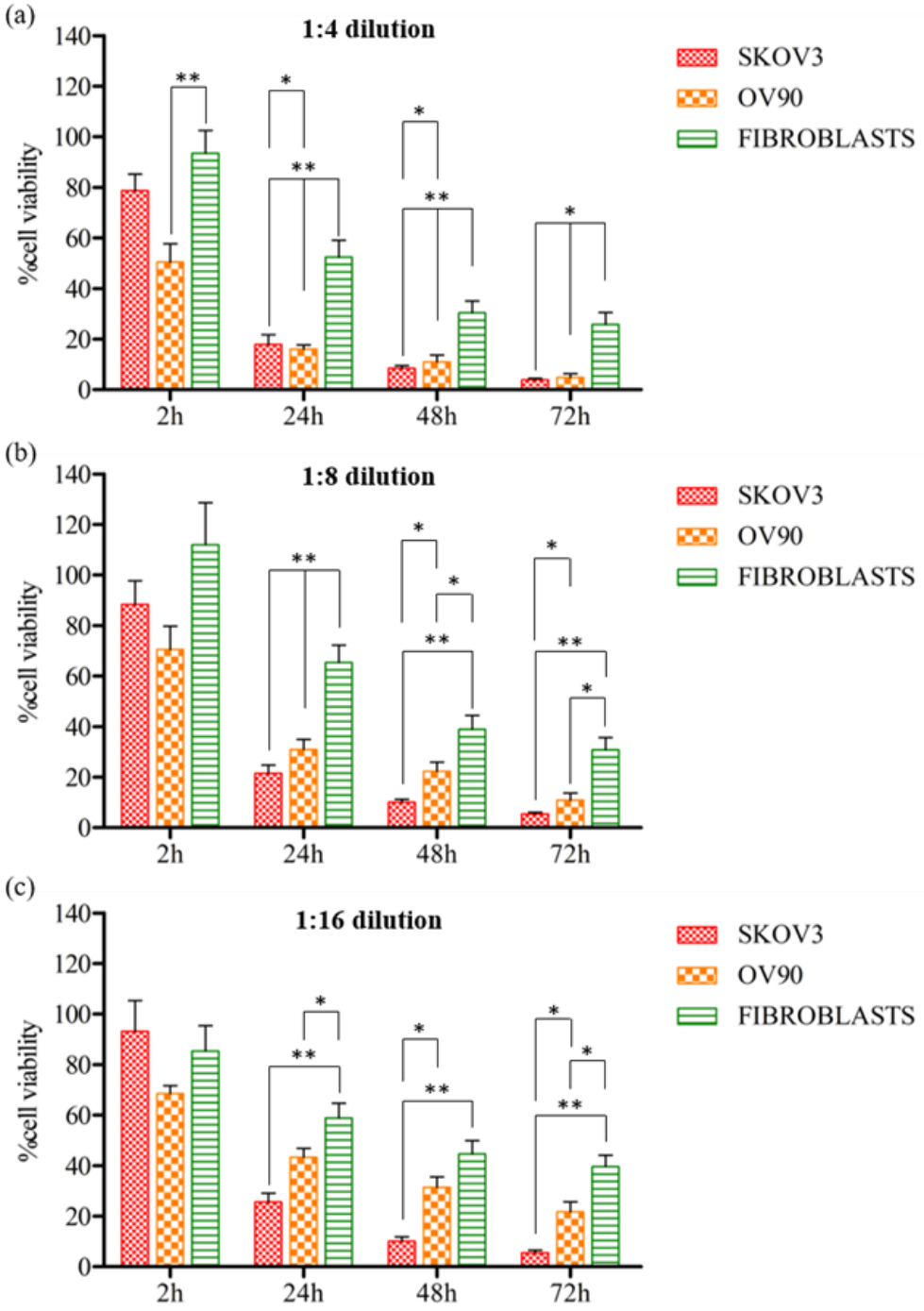

Figure 1.23 - PA-RL displays a selective cytotoxic effect on EOC cell lines with the respect to non-cancer cells. Viability of SKOV-3 (n=7), OV-90 (n=9) cell lines and primary fibroblasts (n=4) treated with PA-RL dilutions (1:4, 1:8 and 1:16). Cell viability was normalized to the corresponding control in RL at 2 hours and plotted as percentage relative to the corresponding control in RL, for all time points. In each panel, data are mean ± SEM and statistical significance is specified with asterisks (*$p \leq 0.05$, **$p \leq 0.001$ as determined by paired Student t-test).

After two hours of contact time, both SKOV3 and OV90 cell lines showed a decrease in viability only with 1:4 dilution, whereas only OV90 appeared to respond early to PA-RL even at higher dilution. Differently from EOC cells, primary fibroblasts seem not to be influenced by the treatment after two hours of contact time even with the smaller dilution (1:4, Figure 1.23a). In addition, both SKOV3 and OV90 cells were observed to be similarly affected in terms of viability when treated with the three PA-RL dilutions after 24, 48 and 72 hours of exposure, displaying a dose-dependent response. At the same time point, the dose-dependent response was more evident in the OV90 cell line. Indeed, considering as an example the 24 h time point it is possible to observe that 1:4, 1:8 and 1:16 dilution induce a cell viability of 0 ÷ 20 %, 20 ÷ 40 % and 40 ÷ 60 % for OV90 cell line and 0 ÷ 20 %, 20 ÷ 40 % and 20 ÷ 40 % for SKOV3 cell line. Similar effects could be seen also for the other time points. Overall, initially SKOV3 cells appeared to be less sensitive to the treatment, but at 24, 48 and 72 hours both cell populations showed to be severely affected by PA-RL. Also, primary fibroblasts display a dose dependent decrease of viability in response to all PA-RL dilutions. At the same time, however, the 1:16 dilution, seem to be the best compromise to obtain a high degree of mortality in cancer cells while sparing primary fibroblasts.

1.4 Conclusions and future perspectives

As reported above, the new therapeutic approaches for the treatment of EOC involve the combination of multiple therapies as cytoreductive surgery, intraperitoneal chemotherapy or, more recently, HIPEC therapy. However, ovarian cancer cells develop resistance against the currently employed drugs, through mechanisms that are still unclear, hence decreasing the long-term efficacy of therapies. Plasma-treated liquids, produced by means of cold atmospheric pressure plasma, thanks to their content of RONS, may respond to the requirement for new types of active treatments against ovarian cancer, which may be used in combination with other standard therapies. In this context, the novelty of this study consists in the use of a well-known clinically employed fluid (namely RL) treated with a multiwire device designed and engineered starting from a plasma device used for the degradations of pollutants in liquid phase. This latter device, differently from most CAP sources used for biomedical applications, is scaled for the treatment of larger volumes of liquids and generate high concentration of liquid phase RONS. Additionally, it was demonstrated that PA-RL produced by exposing RL to this plasma source has a degree of selectivity for cancer cells compared to fibroblasts, although further investigations need to confirm the exact mechanism underlying such preferential effect. Although far from clinical application, the achieved results are promising and therefore the topic deserves further investigation.

1.5 References

[1] J. Prat, "FIGO's staging classification for cancer of the ovary, fallopian tube, and peritoneum: abridged republication", *Journal of Gynecologic Oncology*, 26 (2) 87, (**2015**).

[2] J.O.A.M. Van Baal, *et al*., "Development of Peritoneal Carcinomatosis in Epithelial Ovarian Cancer : A Review", *Journal of Histochemistry & Cytochemistry*, 66 (2) 67, (**2018**).

[3] S. Lheureux, *et al*., "Epithelial ovarian cancer", *The Lancet*, 393 (10177) 1240, (**2019**).

[4] A. Jewell, *et al*., "Heated intraperitoneal chemotherapy in the management of advanced ovarian cancer", *Cancers*, 10 (9) 296, (**2018**).

[5] A. Rynne-Vidal, *et al*., "Mesothelial-to-mesenchymal transition as a possible therapeutic target in peritoneal metastasis of ovarian cancer", *The Journal of Pathology*, 242 (2) 140, (**2017**).

[6] B.C. Giovanella, *et al*., "Selective Lethal Effect of Supranormal Temperatures on Human Neoplastic Cells", *Cancer Research*, 36 (11 PART 1) 3944, (**1976**).

[7] A. Fagotti, "Peritoneal carcinosis of ovarian origin", *World Journal of Gastrointestinal Oncology*, 2 (2) 102, (**2010**).

[8] G. Zhang, *et al*., "The prognosis impact of hyperthermic intraperitoneal chemotherapy (HIPEC) plus cytoreductive surgery (CRS) in advanced ovarian cancer: The meta-analysis", *Journal of Ovarian Research*, 12 (1) 33, (**2019**).

[9] R.A. Cowan, *et al*., "Current status and future prospects of hyperthermic intraoperative intraperitoneal chemotherapy (HIPEC) clinical trials in ovarian cancer", *International Journal of Hyperthermia*, 33 (5) 548, (**2017**).

[10] E. Freund, *et al*., "Gas plasma-oxidized liquids for cancer treatment: pre-clinical relevance, immuno-oncology, and clinical obstacles", *IEEE Transactions on Radiation and Plasma Medical Sciences*, (**2020**).

[11] F. Utsumi, *et al*., "Effect of indirect nonequilibrium atmospheric pressure plasma on anti-proliferative activity against chronic chemo-resistant ovarian cancer cells in vitro and in vivo", *PLoS ONE*, 8 (12) e81576, (**2013**).

[12] H. Tanaka, *et al*., "Non-thermal atmospheric pressure plasma activates lactate in Ringer's solution for anti-tumor effects", *Scientific Reports*, 6 (1) 36282, (**2016**).

[13] S. Takeda, *et al*., "Intraperitoneal administration of plasma-activated medium: proposal of a novel treatment option for peritoneal metastasis from gastric cancer", *Annals of Surgical Oncology*, 24 (5) 1188, (**2017**).

[14] F. Utsumi, *et al*., "Selective cytotoxicity of indirect nonequilibrium atmospheric pressure plasma against ovarian clear-cell carcinoma", *SpringerPlus*, 3 (1) 398, (**2014**).

[15] E. Freund, *et al*., "In Vitro Anticancer Efficacy of Six Different Clinically Approved Types of Liquids Exposed to Physical Plasma", *IEEE Transactions on Radiation and Plasma Medical Sciences*, 3 (5) 588, (**2019**).

[16] A. Bisag, *et al*., "Plasma-activated ringer's lactate solution displays a selective cytotoxic effect on ovarian cancer cells", *Cancers*, 12 (2) 476, (**2020**).

[17] S. Nijdam, *et al*., Plasma Chemistry and Catalysis in Gases and Liquids, (**2012**).

[18] T. Finkel, *et al*., "Oxidants, Oxidative Stress and Biology of Ageing", *Insight Review Articles*, 408 (6809) 239, (**2000**).

[19] P. Sonveaux, *et al*., "Nitric oxide delivery to cancer: Why and how?", *European Journal of Cancer*, 45 (8) 1352, (**2009**).

[20] H. Tanaka, *et al*., "Selective killing of ovarian cancer cells through induction of apoptosis by a nonequilibrium atmospheric pressure plasma", *Applied Physics Letters*, 100 (11) 113702, (**2012**).

[21] K. Nakamura, *et al*., "Novel Intraperitoneal Treatment With Non-Thermal Plasma-Activated Medium Inhibits Metastatic Potential of Ovarian Cancer Cells", *Scientific Reports*, 7 (1) 6085, (**2017**).

[22] E. Biscop, *et al*., "Influence of Cell Type and Culture Medium on Determining Cancer Selectivity of Cold Atmospheric Plasma Treatment", *Cancers*, 11 (9) 1287, (**2019**).

[23] T. Matsuzaki, *et al*., "Enhanced ability of plasma-activated lactated Ringer's solution to induce A549 cell injury", *Archives of Biochemistry and Biophysics*, 656 19, (**2018**).

[24] H. Tanaka, *et al*., "Oxidative stress-dependent and -independent death of glioblastoma cells induced by non-thermal plasma-exposed solutions", *Scientific Reports*, 9 (1) 13657, (**2019**).

[25] Y. Sato, *et al*., "Effect of plasma-activated lactated ringer's solution on pancreatic cancer cells in vitro and *in vivo*", *Annals of Surgical Oncology*, 25 (1) 299, (**2018**).

[26] A. Khlyustova, *et al*., "Important parameters in plasma jets for the production of RONS in liquids for plasma medicine: A brief review", *Frontiers of Chemical Science and Engineering*, 13 (2) 238, (**2019**).

[27] X. Lu, *et al*., "On atmospheric-pressure non-equilibrium plasma jets and plasma bullets", *Plasma Sources Science and Technology*, 21 (3) 034005, (**2012**).

[28] E. Robert, *et al*., "Experimental study of a compact nanosecond plasma gun", *Plasma Processes and Polymers*, 6 (12) 795, (**2009**).

[29] A. Stancampiano, *et al*., "The effect of cold atmospheric plasma (CAP) treatment at the adhesive-root dentin interface", *The Journal of Adhesive Dentistry*, 21 (3) 229, (**2019**).

[30] E. Simoncelli, et al., "Preliminary investigation of the antibacterial efficacy of a handheld Plasma Gun source for endodontic procedures", *Clinical Plasma Medicine*, 3 (2) 77, (**2015**).

[31] R. Zaplotnik, *et al*., "Influence of a sample surface on single electrode atmospheric plasma jet parameters", *Spectrochimica Acta - Part B Atomic Spectroscopy*, 103 124, (**2015**).

[32] F. Girard-Sahun, *et al*., "Reactive oxygen species generated by cold atmospheric plasmas in aqueous solution: Successful electrochemical monitoring *in situ* under a high voltage system", *Analytical Chemistry*, 91 (13) 8002, (**2019**).

[33] C. Canal, *et al*., "Plasma-induced selectivity in bone cancer cells death", *Free Radical Biology and Medicine*, 110 72, (**2017**).

[34] E. Turrini, *et al*., "Plasma-activated medium as an innovative anticancer strategy: Insight into its cellular and molecular impact on *in vitro* leukemia cells", *Plasma Processes and Polymers*, 17 (10) e2000007, (**2020**).

[35] M. Mateu-Sanz, *et al*., "Cold plasma-treated ringer's saline: A weapon to target osteosarcoma", *Cancers*, 12 (1) 227, (**2020**).

[36] J. Chauvin, *et al*., "Elucidation of *in vitro* cellular steps induced by antitumor treatment with plasma-activated medium", *Scientific Reports*, 9 (1) 1, (**2019**).

[37] F. Judée, *et al*., "Short and long time effects of low temperature Plasma Activated Media on 3D multicellular tumor spheroids", *Scientific Reports*, 6 21421, (**2016**).

[38] T.H. Chung, *et al*., "Cell electropermeabilisation enhancement by non-thermal-plasma-treated PBS", *Cancers*, 12 (1) 219, (**2020**).

[39] M. Gherardi, *et al*., "Atmospheric non-equilibrium plasma promotes cell death and cell-cycle arrest in a lymphoma cell line", *Plasma Processes and Polymers*, 12 (12) 1354, (**2015**).

[40] Y. Li, *et al*., "Effects of atmospheric-pressure non-thermal bio-compatible plasma and plasma activated nitric oxide water on cervical cancer cells", *Scientific Reports*, 7 45781, (**2017**).

[41] A. Azzariti, *et al*., "Plasma-activated medium triggers cell death and the presentation of immune activating danger signals in melanoma and pancreatic cancer cells", *Scientific Reports*, 9 (1) 1, (**2019**).

[42] M. Adhikari, *et al*., "Melanoma growth analysis in blood serum and tissue using xenograft model with response to cold atmospheric plasma activated medium", *Applied Sciences (Switzerland)*, 9 (20) 4227, (**2019**).

[43] M. Iwasaki, *et al*., "Nonequilibrium atmospheric pressure plasma with ultrahigh electron density and high performance for glass surface cleaning", *Applied Physics Letters*, 92 (8) (**2008**).

[44] N. Kurake, *et al*., "Effects of •OH and •NO radicals in the aqueous phase on H_2O_2 and NO_2^- generated in plasma-activated medium", *Journal of Physics D: Applied Phys*ics, 50 (15) 155202, (**2017**).

[45] K. Ishikawa, *et al*., "Non-thermal plasma–activated lactate solution kills U251SP glioblastoma cells in an innate reductive manner with altered metabolism", *Archives of Biochemistry and Biophysics*, 688 (April) 108414, (**2020**).

[46] K. Nakamura, *et al*., "Adjusted multiple gases in the plasma flow induce differential antitumor potentials of plasma-activated solutions", *Plasma Processes and Polymers*, 17 (10) 1900259, (**2020**).

[47] N. Yoshikawa, *et al*., "Plasma-activated medium promotes autophagic cell death along with alteration of the mTOR pathway", *Scientific Reports*, 10 (1) 1, (**2020**).

[48] H. Tanaka, *et al*., "Plasma-activated medium selectively kills glioblastoma brain tumor cells by down-regulating a survival signaling molecule, AKT kinase", *Plasma Medicine*, 1 (3–4) 265–277, (**2011**).

[49] H. Tanaka, *et al*., "Cell survival and proliferation signaling pathways are downregulated by plasma-activated medium in glioblastoma brain tumor cells", *Plasma Medicine*, 2 (4) 207–220, (**2012**).

[50] T. Adachi, *et al*., "Plasma-activated medium induces A549 cell injury via a spiral apoptotic cascade involving the mitochondrial-nuclear network", *Free Radical Biology and Medicine*, 79 28, (**2015**).

[51] N. Kurake, *et al*., "Cell survival of glioblastoma grown in medium containing hydrogen peroxide and/or nitrite, or in plasma-activated medium", *Archives of Biochemistry and Biophysics*, 605 102, (**2016**).

[52] K. Van Der Speeten, *et al*., "Overview of the optimal perioperative intraperitoneal chemotherapy regimens used in current clinical practice", *Pleura and Peritoneum*, 2 (2) 63, (**2017**).

[53] A. Pokryvailo, *et al*., "A compact high-power pulsed corona source for treatment of pollutants in heterogeneous media", *Digest of Technical Papers-IEEE International Pulsed Power Conference*, 34 (5) 1188, (**2007**).

[54] L.R. Grabowski, *et al*., "Corona above water reactor for systematic study of aqueous phenol degradation", *Plasma Chemistry and Plasma Processing*, 26 (1) 3, (**2006**).

[55] E. Marotta, *et al*., "Advanced oxidation process for degradation of aqueous phenol in a dielectric barrier discharge reactor", *Plasma Processes and Polymers*, 8 (9) 867, (**2011**).

[56] M. Magureanu, *et al*., "Pulsed corona discharge for degradation of methylene blue in water", *Plasma Chemistry and Plasma Processing*, 33 (1) 51, (**2013**).

[57] E. Ceriani, *et al*., "A versatile prototype plasma reactor for water treatment supporting different discharge regimes", *Journal of Physics D: Applied Physics*, 51 (27) 274001, (**2018**).

[58] P. Bruggeman, *et al*., "Non-thermal plasmas in and in contact with liquids", *Journal of Physics D: Applied Physics*, 42 (5) 053001, (**2009**).

[59] P.J. Bruggeman, *et al*., "Plasma-liquid interactions: A review and roadmap", *Plasma Sources Science and Technology*, 25 (5) 053002, (**2016**).

[60] N.K. Kaushik, *et al*., "Biological and medical applications of plasma-activated media, water and solutions", *Biological Chemistry*, 400 (1) 39, (**2018**).

[61] B.R. Locke, *et al*., "Review of the methods to form hydrogen peroxide in electrical discharge plasma with liquid water", *Plasma Sources Science and Technology*, 20 (3) 034006, (**2011**).

[62] Z. Machala, *et al*., "Chemical and antibacterial effects of plasma activated water: Correlation with gaseous and aqueous reactive oxygen and nitrogen species, plasma sources and air flow conditions", *Journal of Physics D: Applied Physics*, 52 (3) 034002, (**2019**).

[63] S. Kanazawa, *et al*., "Observation of OH radicals produced by pulsed discharges on the surface of a liquid", *Plasma Sources Science and Technology*, 20 (3) 034010, (**2011**).

[64] S.A. Norberg, *et al*., "Atmospheric pressure plasma jets interacting with liquid covered tissue: Touching and not-touching the liquid", *Journal of Physics D: Applied Physics*, 47 (47) 475203, (**2014**).

[65] A. Fridman, Plasma Chemistry, (**2008**).

[66] E. Simoncelli, *et al*., "UV-VIS optical spectroscopy investigation on the kinetics of long-lived RONS produced by a surface DBD plasma source", *Plasma Sources Science and Technology*, 28 (9) 095015, (**2019**).

[67] P. Lukes, *et al*., "Aqueous-phase chemistry and bactericidal effects from an air discharge plasma in contact with water: Evidence for the formation of peroxynitrite through a pseudo-

second-order post-discharge reaction of H_2O_2 and HNO_2", *Plasma Sources Science and Technology*, 23 (1) (**2014**).

[68] D.B. Graves, "The emerging role of reactive oxygen and nitrogen species in redox biology and some implications for plasma applications to medicine and biology", *Journal of Physics D: Applied Physics*, 45 (26) 263001, (**2012**).

[69] T. Von Woedtke, *et al*., "Plasma medicine: A field of applied redox biology", *In Vivo*, 33 (4) 1011, (**2019**).

[70] G. Bauer, *et al*., "Dynamics of singlet oxygen-triggered, RONS-based apoptosis induction after treatment of tumor cells with cold atmospheric plasma or plasma-activated medium", *Scientific Reports*, 9 (1) 1, (**2019**).

[71] P.L. De Sá Junior, *et al*., "The roles of ROS in cancer heterogeneity and therapy", *Oxidative Medicine and Cellular Longevity*, 2017 (**2017**).

[72] C.C. Winterbourn, "Reconciling the chemistry and biology of reactive oxygen species", *Nature Chemical Biology*, 4 (5) 278, (**2008**).

[73] E. Veal, *et al*., "Hydrogen peroxide as a signaling molecule", *Antioxidants and Redox Signaling*, 15 (1) 147, (**2011**).

[74] G.Y. Liou, *et al*., "Reactive oxygen species in cancer", *Free Radical Research*, 44 (5) 479, (**2010**).

[75] A. Kirtonia, *et al*., "The multifaceted role of reactive oxygen species in tumorigenesis", *Cellular and Molecular Life Sciences*, 77 (22) 4459, (**2020**).

[76] G. Bauer, "Targeting extracellular ROS signaling of tumor cells", *Anticancer Research*, 34 (4) 1467, (**2014**).

[77] D. Trachootham, *et al*., "Targeting cancer cells by ROS-mediated mechanisms: A radical therapeutic approach?", *Nature Reviews Drug Discovery*, 8 (7) 579, (**2009**).

[78] M.T. Gladwin, *et al*., "The Emerging Biology of the Nitrite Anion", *Nature Chemical Biology*, 1 (6) 308, (**2005**).

[79] C. Napoli, *et al*., "Effects of nitric oxide on cell proliferation: Novel insights", *Journal of the American College of Cardiology*, 62 (2) 89, (**2013**).

[80] D.G. Hirst, *et al*., "Nitrosative stress in cancer therapy", *Frontiers in Bioscience*, 12 (9) 3406, (**2007**).

[81] D. Hirst, *et al*., "Nitrosative stress as a mediator of apoptosis: implications for cancer therapy", *Current Pharmaceutical Design*, 16 (1) 45, (**2009**).

[82] P. Bruggeman, *et al*., "Non-thermal plasmas in and in contact with liquids", *Journal of Physics D: Applied Physics*, 42 (5) 053001, (**2009**).

[83] H. Li, *et al*., "Realization of DC atmospheric pressure glow discharge without external airflow", *Vacuum*, 113 28–35, (**2015**).

[84] L. Crestale, *et al*., "Cold Atmospheric Pressure Plasma Treatment Modulates Human Monocytes/Macrophages Responsiveness", *Plasma*, 1 (2) 261, (**2018**).

[85] C.Y. Chen, *et al*., "Synergistic effects of plasma-activated medium and chemotherapeutic drugs in cancer treatment", *Journal of Physics D: Applied Physics*, 51 (13) 13LT01, (**2018**).

[86] R. Laurita, *et al*., "Chemical analysis of reactive species and antimicrobial activity of water treated by nanosecond pulsed DBD air plasma", *Clinical Plasma Medicine*, 3 (2) 53, (**2015**).

[87] B. Zhao, *et al*., "Photooxidation of Amplex red to resorufin: Implications of exposing the Amplex red assay to light", *Free Radical Biology and Medicine*, 53 (5) 1080, (**2012**).

[88] M. Zhou, *et al*., "A stable nonfluorescent derivative of resorufin for the fluorometric determination of trace hydrogen peroxide: Applications in detecting the activity of phagocyte NADPH oxidase and other oxidases", *Analytical Biochemistry*, 253 (2) 162, (**1997**).

[89] N.C. Veitch, "Horseradish peroxidase: A modern view of a classic enzyme", *Phytochemistry*, 65 (3) 249, (**2004**).

[90] D. Debski, *et al*., "Mechanism of oxidative conversion of Amplex® Red to resorufin: Pulse radiolysis and enzymatic studies", *Free Radical Biology and Medicine*, 95 323, (**2016**).

[91] H.H. Gorris, *et al*., "Mechanistic aspects of horseradish peroxidase elucidated through single-molecule studies", *Journal of the American Chemical Society*, 131 (17) 6277, (**2009**).

[92] B. Kalyanaraman, *et al*., "Measuring reactive oxygen and nitrogen species with fluorescent probes: Challenges and limitations", *Free Radical Biology and Medicine*, 52 (1) 1, (**2012**).

[93] D. Tsikas, "Analysis of nitrite and nitrate in biological fluids by assays based on the Griess reaction: Appraisal of the Griess reaction in the l-arginine/nitric oxide area of research", *Journal of Chromatography B: Analytical Technologies in the Biomedical and Life Sciences*, 851 (1–2) 51, (**2007**).

[94] B. Dong, *et al*., "Experimental study of a DBD surface discharge for the active control of subsonic airflow", *Journal of Physics D: Applied Physics*, 41 (15) 155201, (**2008**).

[95] M. Simek, *et al*., "Time and space resolved analysis of N2($C^3\Pi_u$) vibrational distributions in pulsed positive corona discharge", *Journal of Physics D: Applied Physics*, 35 (16) 1981, (**2002**).

1.6 Appendix

Chapter 1.2.1 shows the last version of a multiwire source designed and engineered for the treatment of clinically approved solutions. However, before achieving this result, I realized several plasma devices for the treatment of liquids. Set out below, I will briefly report the most important steps made at the beginning of the project.

1.6.1 CAP prototypes for the treatment of a liquid substrate

Corona discharge takes place at atmospheric pressure in a strong and non uniform electric field generally associated with needles or thin wires. As can be seen in Figure 1.24, five different prototypes of multipin plasma sources were designed, realized and subsequently tested to produce a plasma interacting with a liquid substrate. All these prototypes are characterized by a cylindrical geometry, but they differ in the number, diameter, length of needles and pin-to-pin distance.

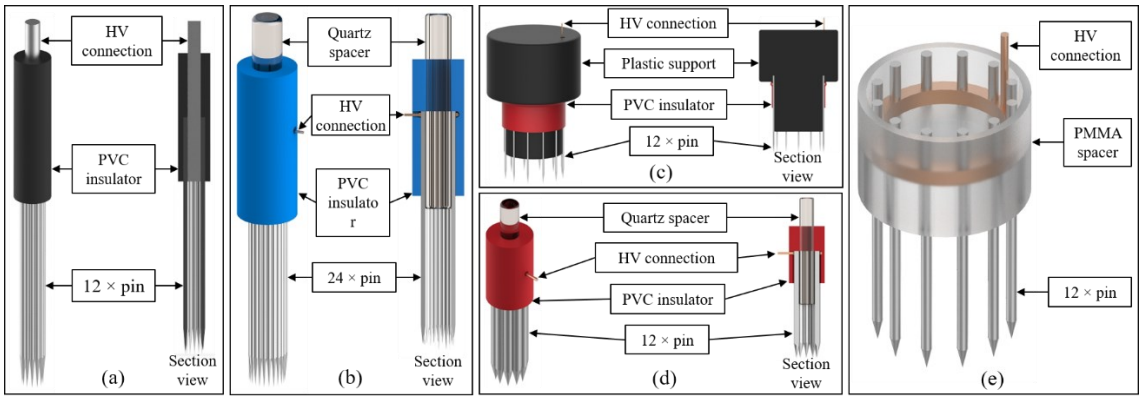

Figure 1.24 - Multipin plasma sources: a) prototype with a steel central spacer of 2 mm and 12 steel needles (0.7 mm in diameter) b) prototype with a quartz central spacer and 24 steel needles (0,7 mm in diameter) c) prototype with 12 needles (0.7 mm in diameter) placed on a 3D printed support d) prototype with a quartz central spacer and 12 needles (2 mm in diameter) e) prototype with 12 needles (2 mm in diameter) fixed on a PMMA support.

The multipin devices shown in Figure 1.24, due to the geometry of high voltage electrodes, have a limited plasma region (only near the sharp points of the needle electrodes) and consequently a limited interaction region between plasma and liquid substrate. In order to maximize the region of interaction, a different type of plasma source was designed (Figure 1.25). Instead of needle electrodes, the device is characterized by four copper wires fixed on two plastic supports. Even if this configuration was significantly better in terms of RONS production in the liquid phase, wire assembly proved difficult since the tension of the wires could not be adjusted separately, leading to their frequent break-ups. Another equally important problem involved the plastic supports, as they were damaged by the high temperatures reached by the electrodes during prototype operation.

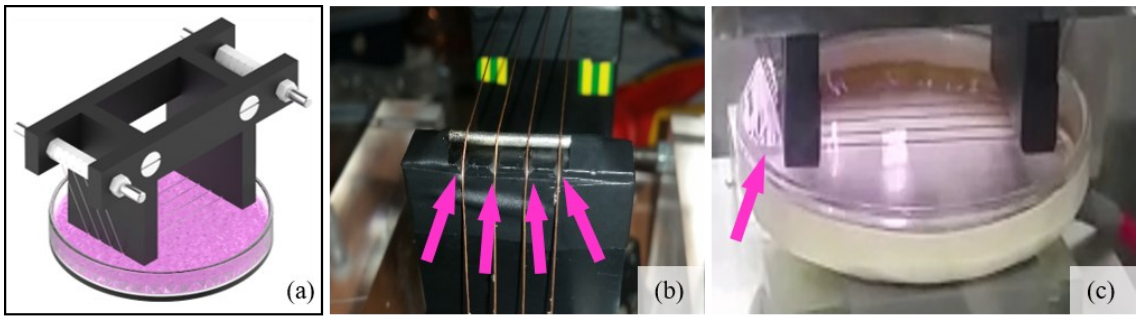

Figure 1.25 - Multiwire plasma sources a) prototype with a four copper wires electrode (0.4 mm in diameter) fixed on PVC supports. Even if the generation zone was higher compared to the generation zone of multipin devices, the (b) plastic supports were frequently damaged during plasma operation leading to (c) abnormal discharges near the liquid container extremity.

For this reason, a second prototype characterized by a more robust design was realized (Figure 1.26): stainless steel wires were individually fixed on aluminum supports through threaded screws. A polymethylmethacrylate (PMMA) box was designed to encase the plasma source, guaranteeing operation under a controlled atmosphere; the box was equipped with a fan able to direct the plasma effluent towards the liquid surface, also avoiding wires thermal expansion due to the high temperature reached by the electrodes (about 70°C). In order to maximize the interaction between plasma and liquid substrate the liquid vessel was properly designed to allow the housing of the multiwire source and to keep the required distance between HV electrodes and liquid surface.

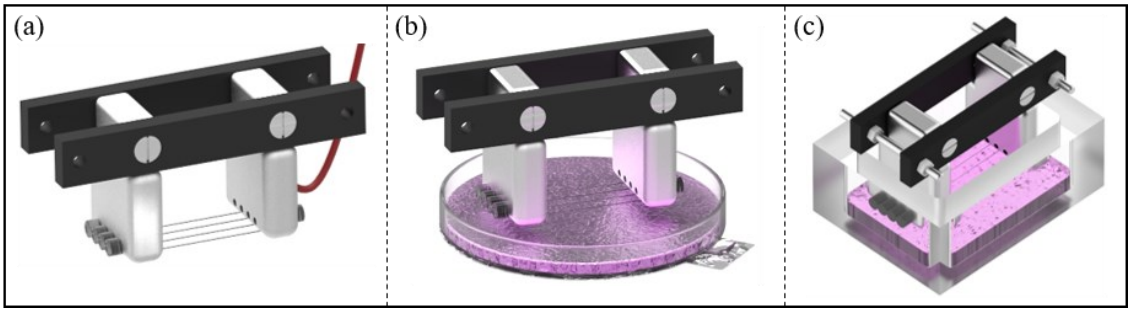

Figure 1.26 - Multiwire plasma sources a) prototype with a four steel wires electrode (0.5 mm in diameter) fixed on aluminum supports and positioned firstly over a (b) Petri dish with a diameter of 60 mm containing the liquid substrate and secondly (c) over a specifically liquid container.

1.6.2 Plasma device and electrical characterization

The advanced prototype of the multiwire plasma source described in detail in the paragraph 1.2.1 and reported in Figure 1.8, was used to produce PAM by exposing Roswell Park Memorial Institute 1640 medium (RPMI, EuroClone, Milan, Italy) to the plasma discharge. As reported in Figure 1.27a, the behavior of the discharge was quite similar to the one reported in Figure 1.8c/d; indeed, plasma filaments are formed randomly on the four high voltage electrodes. At the same time, also the voltage – current waveforms were characterized by similar trends. Moreover, this similarity was to find also in the average power: 12.1 ± 0.1 W in the case of RPMI-1640 substrate and 12.4 ± 0.1 W in the case of RL substrate (with an applied voltage of 18 kV and a frequency of 1 kHz).

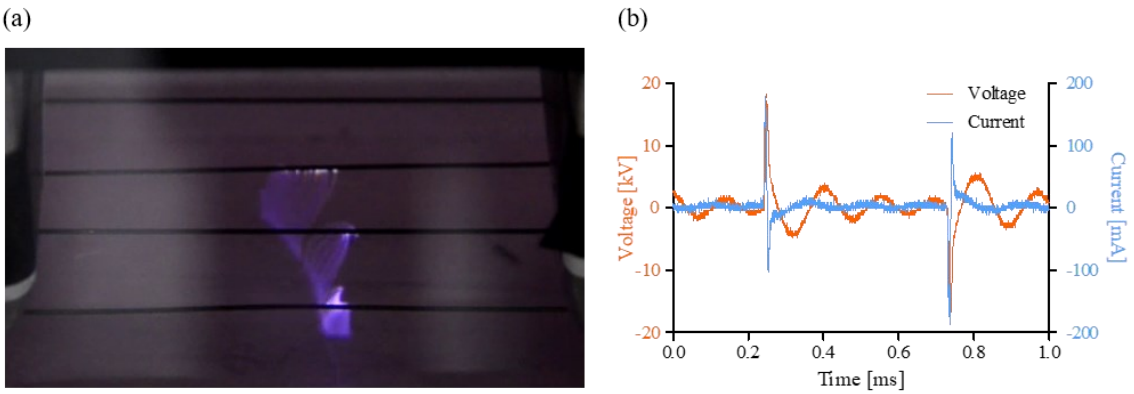

Figure 1.27 - (a) plasma discharge behavior using RPMI-1640as liquid substrate and (b) results of the electrical characterization using a voltage of 18 kV and a frequency of 1 kHz for 600 s of plasma treatment.

1.6.3 Chemical characterization of the treated liquid

As reported in Figure 1.28a, similarly to the results presented in Figure 1.17a of the paragraph 1.3.2, also in this case the H_2O_2 and NO_2^- concentrations increased linearly with the treatment time and reach a maximum of 265 ± 4.5 µM and 673 ± 11 µM, respectively. These values are consistent with the measured average power which is higher for RL instead of RPMI-1640and consequently also RONS concentration in PA-RL results a slightly greater.

At the same time also in this case were performed serial dilutions which were subsequently used for biological experiments.

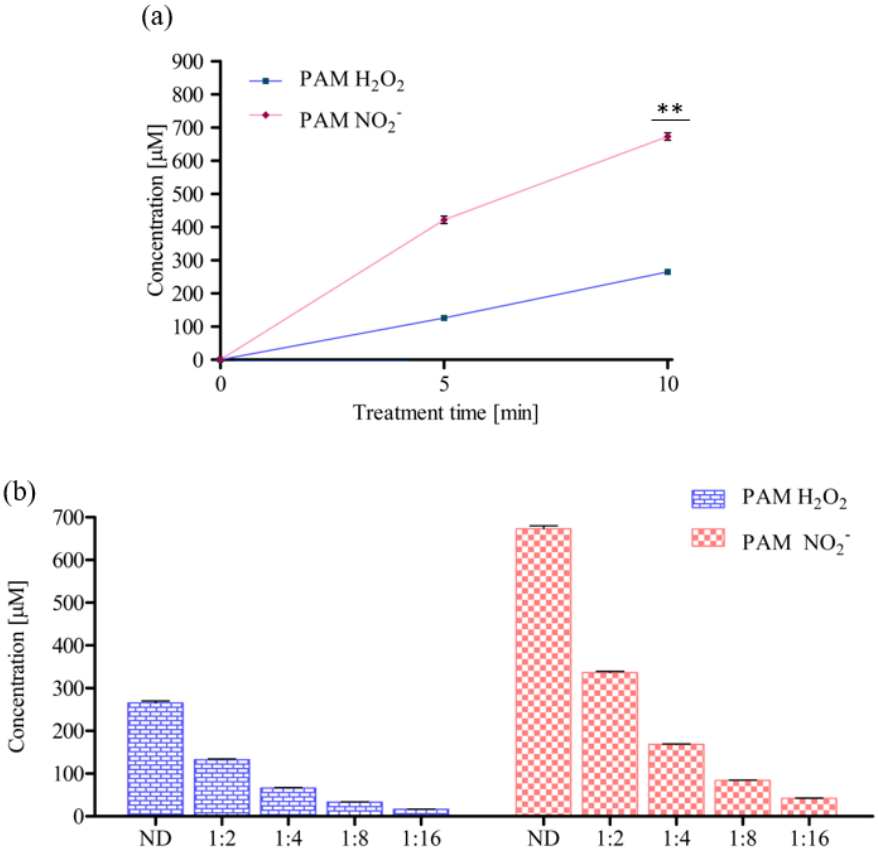

Figure 1.28 - Plasma treatment leads to the formation of H_2O_2 and NO_2^-. (a) RONS concentration as a function of treatment time and (b) dilutions in RPMI-1640.

In addition, pH and conductivity of PAM and their dilutions are reported in Figure 1.29. After 10 minutes of plasma treatment PA-RL pH increased to 8.1 ± 0.01 differently from PA-RL which drop immediately after the plasma treatment with the respect to its control. At the same manner, the conductivity increases up to 15.5 mS/cm.

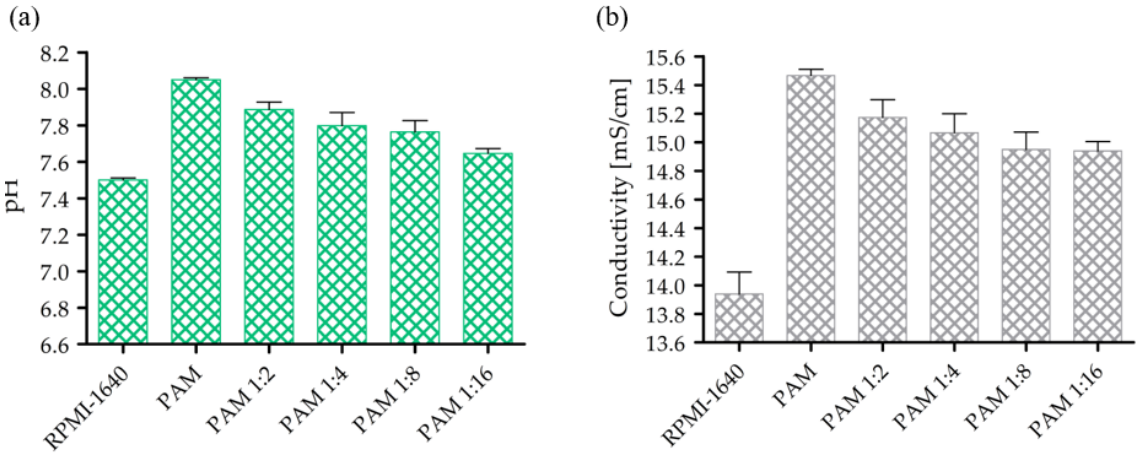

Figure 1.29 - Chemical characterization of PAM and its dilutions after 10 min of plasma treatment at 18 kV and 1 kHz. (a, b) pH and (c, d) conductivity as a function of serial dilutions. Data are presented as mean ± SEM (n=3).

1.6.4 Biological results

In order to assess the biological effect of different activated liquids, PAM and PA-RL were used for the treatment of two different EOC cell lines, namely SKOV3 and OV90. Cell lines conditions and treatment was reported more in detail in the paragraphs 1.2.5 and 1.2.6.

As could be seen in Figure 1.30, in both cell lines, after the 2 hours of plasma contact, PAM induced a cytotoxic effect of 40 ÷ 50 % while PA-RL over 80%. For both PAM and PA-RL treatments, the dilution 1:4 induces a cytostatic effect with a viability less than 40% in both cellular lines analyzed. While dilution 1:8 leads to an increase of viability after 24 hours from the treatment. This effect is higher using 1:16 PAM dilution. Differently from PAM, PA-RL also PA-RL dilutions up to 1:8 induce a cytotoxic effect. For this reason, more detail studies were carried out using PA-RL. Moreover, the possibility to use it also in clinical application make this liquid substrate more suitable for all the investigations reported below.

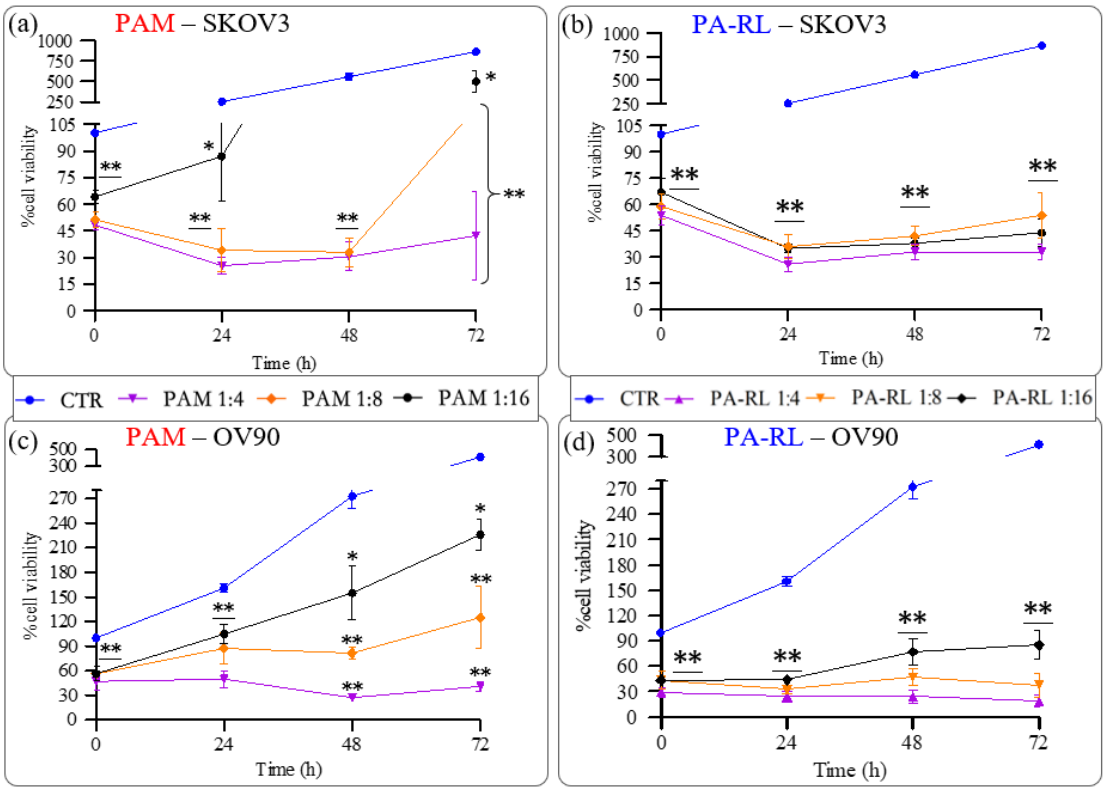

Figure 1.30 - PAM and PA-RL effect on EOC cell lines. Viability of SKOV-3 treated with (a) PAM and its dilutions (1:4, 1:8 and 1:16, n=4) and (b) PA-RL and its dilutions (1:4, 1:8 and 1:16, n=6). Viability of OV-90 treated with (c) PAM and its dilutions (1:4, 1:8 and 1:16, n=3) and (b) PA-RL and its dilutions (1:4, 1:8 and 1:16, n=5). Cell viability was normalized to the corresponding control in RPMI-1640 at 2 hours and plotted as percentage relative to the corresponding control in RPMI-1640, for all time points. In each panel, data are mean ± SEM and statistical significance is specified with asterisks (*$p \leq 0.05$, **$p \leq 0.001$ as determined by paired Student t-test).

2

Design and realization of a Cold Atmospheric Plasma (CAP) device for dental applications

2.1 Introduction

In recent years, atmospheric pressure plasma jets (APPJs) have been increasingly used in many different applications (i.e. wound healing, cancer treatment or dental applications), due to their combination of plasma stability and excellent reaction chemistry.[1–7] As reported by X. Lu *et al*. [8], there are many types of APPJs working with various noble gasses (i.e. argon, helium, neon, etc…) and characterized by many different configurations. Generally, the most employed configuration for biomedical applications consists of a long (several centimeters) dielectric cylindrical tube of a few millimeters in diameter (used for the injection of plasma gas) equipped with an inner high voltage (HV) electrode and an outer ground electrode. When a high voltage of a few kV is applied, a plasma discharge takes place between the two electrodes. After the ignition, the plasma propagates inside the dielectric tube as ionization wavefronts (FIWs), leading to a separation between the generation region and the application zone located at the end of the tube; FIWs are thus guided for several centimeters towards the extremity of the dielectric tube and then ejected in the surrounding environment, where a plasma plume is formed.[9] Plasma plume expanding in air has been widely investigated since allows the production of short life and long life reactive oxygen and nitrogen species (RONS) which play a key role in biomedical applications. [10–14] As reported by X. Lu *et al*. [15] the plasma plume in the surrounding air depends on the operating conditions and could reach lengths greater than 10 cm. These characteristics make this plasma source suitable for the direct treatment of objects characterized by arbitrary forms. Moreover, from the electrical configuration of this plasma source [4,16,17], it is possible to notice that only a small part of the discharge current reaches the substrate to be treated; this aspect makes the APPJs very interesting from a biomedical point of view.

The use of CAPs for dental applications is a quite new argument introduced initially by Goree *et al*.[18]; in this work, a plasma needle prototype was used for the first time to inactivate *Streptococcus mutans* (a gram-positive and facultatively anaerobic microorganism considered as the major responsible for the development of dental caries [19]). The plasma device consists of a high voltage needle electrode placed inside a glass nozzle where helium gas was flowed; due to its small dimensions, this APPJ easily enables the treatment of small targets (approximately of a few millimeters). Moreover, the prototype resulted in a limited increase of the intra-pulpal temperature (about 2.3°C), below the 5.5°C considered as a threshold value beyond which pulpal necrosis can occur.[20] Starting from this pioneering study, many other research groups designed

increasingly advanced devices for various fields of dental applications, namely tooth blanching/whitening, bacterial inactivation, and root canal restoration.

Nowadays, dental whitening has become one of the most frequently requested aesthetic treatment; as such it has now assumed considerable importance both in the domestic and in the professional field. In most cases it requires the use of H_2O_2 based gels together with a high-intensity light source to oxidize the discolorations or chromophores (organic pigments generally present in drinks, food or tobacco) inside the teeth.[21] To get optimum results, the bleaching technique generally requires the use of gels containing a high concentration of H_2O_2 (about 35 ÷50 %); however, such concentration could potentially lead to tooth sensitivity, alteration of enamel surfaces, or in the worst case to thermal damage of the pulp.[22] In this perspective, APPJ sources, thanks to their ability of producing high concentrations of oxidizing species without a significant temperature increase could be used for bleaching applications without or in synergy with conventional procedures.[23–25] In support of these hypothesis, various research groups around the world tested and successfully demonstrated the ability of APPJs alone or in synergy with H_2O_2 solution to provide dental whitening.[22,26–28] More recently, Y. C. Cheng *et al*. [29] demonstrated that the use of a APPJ source was less harmful than H_2O_2 based gel solution to the enamel.

Alongside the use for aesthetic purposes, APPJ devices were also successfully employed for endodontic treatments, required when a caries degenerates in the infection of the dental pulp. Actually, the current gold standard of endodontic therapy consists of various steps which comprise the tooth opening, pulp and nerve removal, root canal shaping and disinfection, and finally tooth restoration. Generally, chlorhexidine (CHX) or sodium hypochlorite (NaClO) based solutions are used in the disinfection phase; as a limiting factor, their effectiveness depends on concentration, but concentrations beyond a certain threshold (CHX > 0.2 % and NaClO > 6 %) may be toxic.[30,31] Moreover, due to the complex shape and tiny dimensions of the root canals, proper disinfection is not always assured. In this context, the use of highly ionized gas produced by APPJ devices have yielded encouraging results. M. Habib *et al*. [32] obtained a reduction of 99.999% against *Enterococcus faecalis* biofilm after only 2 min of plasma treatment; in the same manner, J. Pan *et al*. [33] used an APPJ device for the decontamination of *E. faecalis* biofilm and obtained a complete inactivation after 10 min of treatment. On the contrary, X. Lu *et al*. [34] claimed that more than 10 minutes of treatment are needed to obtain a complete inactivation. Differently from these studies, X. C. Zhou *et al*. [35] obtained a logarithmic reduction of *E. faecalis* biofilm of about 7 after 4 minutes of treatment with an APPJ device through which was flown 3 % hydrogen peroxide solution. In this context, E. Simoncelli *et al*. [7] used for the first time a Plasma Gun (PG) configuration (introduced for the first time by E. Robert *et al*. [36]) for dental applications, specifically for the decontamination of *E. faecalis* through a direct treatment (the tooth model was directly exposed to the plasma plume) and an indict treatment (using a plasma-treated liquid); as the authors reported, the efficacy of PG treatment was proven in both direct and indirect conditions.

In dentistry, CAP applications are not limited to tooth bleaching or root canal disinfection, since more recently CAP has been investigated to prepare the root canal for restoration, namely the final phase of the Endodontic Triad which consists of shaping, cleaning, and filling.[37] In this case, CAPs were used to improve the adhesive performance of restorations inside root canals.

As reported by different authors [5,6,38] the use of APPJ devices leads to an enhancement of bonding strength between filling materials and CAP-treated dentine.

Despite the number of works that report the numerous advantages in using APPJ for dental applications, plasma devices have yet to be translated to the clinical environment. As could be observed from Figure 2.1, the main reason is related to the fact that the plasma devices used for such kind of applications are both ergonomically unsuitable for a real application and not safe from an electrical point of view. Indeed, as shown in Figure 2.1b, the electrical connections are not encased inside an external housing and therefore represents a risk for the operator.

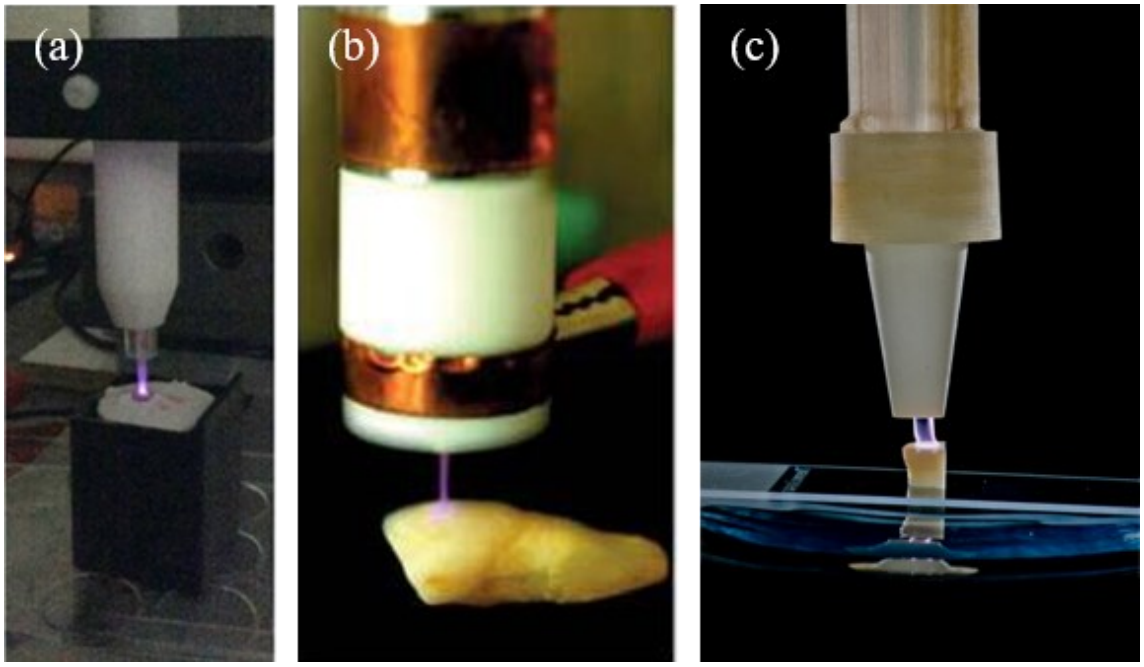

Figure 2.1 – Examples of APPJs for dental applications. All the images are reported with permission from [29][22][38].

In recent years, there was a growing awareness of the need to improve the electrical characteristics and the ergonomics of APPJ devices for dental applications. In this regard, Y. Yue *et al*. [39] report an interesting study related to different configurations of APPJ devices for dental applications including also the PG described by E. Simoncelli *et al*. [7]. While this prototype was a first step towards the reduction of the electrical risks through distancing the generation zone from the application one, the possibility that the main current could flow from the pin electrode to the patient to be treated was non negligible. This plasma source was later ameliorated from the ergonomics perspective by A. Stancampiano *et al*. [5], who introduce for the first time a PG configuration aimed to bring plasma technology closer to a clinical environment (Figure 2.2). Although this work represents a big step forward in the field of plasma dentistry, further efforts are still necessary for the development of a plasma device designed according to the standard regulations for medical devices.

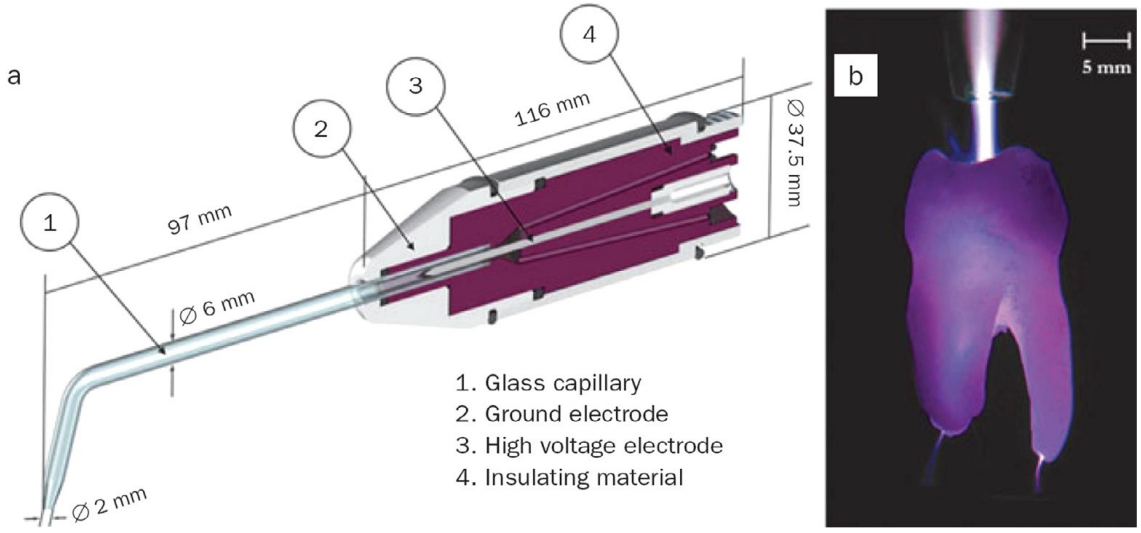

Figure 2.2 – APPJ device for the improvement of the bond strength of a dental adhesive in root canal restoration. With permission from [5].

2.1.1 Development and regulation of medical devices

As reported by the World Health Organization (WHO), a medical device can be defined as follows: "*any instrument, apparatus, implement, machine, appliance, implant, reagent for in vitro use, software, material or other similar or related article, intended by the manufacturer to be used, alone or in combination, for human beings, for one or more medical purpose(s)… and does not achieve its primary intended action by pharmacological, immunological, or metabolic means, but which may be assisted in its intended function by such means*".[40] As recently reported by J. K. Aronson *et al*. [41], the first step for the regulation of a medical device consists of identifying its category of belonging. By way of example, Figure 2.3 reports a classification of the types of medical devices and the respective regulations to refer to. However, this work does not consider CAP devices, which have been developed intensively only over the past few years. The difficulties in identifying national or international standards covering the field of plasma medicine were overcome only recently with the development of the German DIN SPEC 91315, a document describing the general requirements for medical plasma sources to comply with the continuous development of novel plasma sources for therapeutic applications. The suggested physical tests reported on the DIN SPEC 91315 include the UV irradiation measurement (which should not exceed 30 J/m^2 or 3 mJ/cm^2 as a daily dose), the leakage current (which should not exceed 100 mA), gas emission (used to identify the emission of UV radiation which depending on its energy could be efficiently used for specific dermatological applications [42,43] or could cause toxic effects [44]) and the temperature measurement (which should not exceed 40°C). In this perspective, none of the above-mentioned plasma sources were developed considering the standard regulations for medical devices. To overcome with this lack, my research activity deals with the design of a PG device complying with the DIN SPEC 91315 and the standard regulations reported in Figure 2.3.

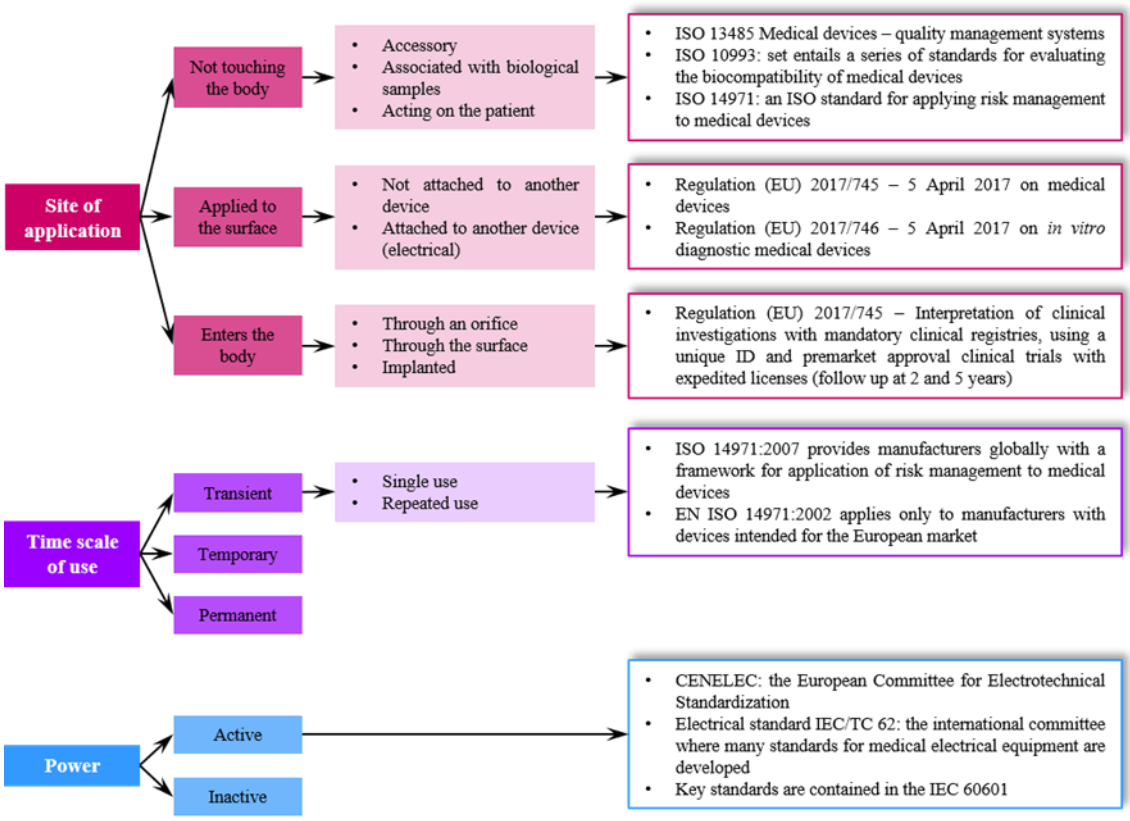

Figure 2.3 – Classification of medical devices based on the type of application.[41]

For a plasma prototype to be considered a medical device, several regulations have to be taken into account. In particular, it must be designed and realized in such a way that its use does not compromise the clinical condition or the safety of patients or operators. In this regard, as the first step of a plasma prototype design, the standard ISO 14971 (Medical devices - Application of risk management to medical devices) [45] and IEC 60601 (Medical electrical equipment – Part 1: General requirements for basic safety and essential performance) [46] have to be taken into account. Therefore, early in the design phase all factors of risk must be identified and carefully analyzed before the realization of the final prototype. According to the standard ISO 14971, a proper risk management consists of the following steps: identification of the risks associated with the medical device, analysis of the risk, risk assessment, and finally risk reduction. Within a risk analysis, all qualitative and quantitative characteristics that could affect the safety of the device must be taken into account.

During my Ph.D., I focused on many different aspects of the design phase of a plasma source for medical applications complying with the standard regulations, such as: analysis of the risk of a structural nature, measurements of temperature, UV irradiation and leakage currents. In this perspective, during the initial design phase, the main elements that have been taken into consideration are:

1. Electrical connections: these must be designed to ensure a stable contact between the high voltage and the ground cable with the respective electrodes. The damage of a connection during the device operation could compromise the operation of the plasma device or could cause a severe electric shock to both the patient and the operator.

2. Gas connection: this must ensure an optimal gas sealing, resistant to mechanical and thermal stresses. Indeed, a gas leak could cause plasma formation in areas not designed for this occurrence leading to prototype damages.
3. Outer casing: the purpose of such element must be the isolation of the generation zone from the external environment (containing liquids or powders which could penetrate inside the device) and protect the patient and the operator from any electric shock.

After prototypes realization, the risks directly involving the operator or the patient were taken into account. In this regard, the standard "DIN EN 60601-1 – Medical electrical equipment" on which the DIN-specification 91315 (General requirements for medical plasma sources) is based, established thresholds for several types of leakage currents when electrical medical devices potentially interface with a patient, or a soft tissue in general. The measurement of this "leakage currents" generally can help to verify whether or not a medical device is electrically safe. Although electrical fields on the biological targets can play an important and benefic role in the complex biological interaction between plasma and living tissue [47], during the development process of a plasma source for medical applications it is highly recommended to first check the intensity and characteristics of the currents that these electric field can induce in the target tissue. Subsequently, the temperature of the dielectric capillary, being the most thermally stressed element of the source and the UV irradiance and, were evaluated.

2.2 Materials and methods

The design of PG prototypes used for dental applications was carried out using two different softwares: Creo | PTC and Solid Edge. Both of these programs for computer-aided design (CAD) were used to create the digital models of the plasma devices and subsequently to carry out a specific analysis of each critical point before its realization. Thanks to its instant feedback for design changes, Creo | PTC was always used in the first step of prototyping. On the other hand, Solid Edge was used only in the last phase of the design to realize the 2D drafts and the models subsequently implemented on KeyShot, a 3D rendering program which allows to obtain photorealistic real-time models. In the following chapters will be reported the design evolution of three plasma devices. After the realization of CAD models, two of the three prototypes were realized in the machine workshop of Alma Mater Studiorum – University of Bologna and then characterized during the various phases of development of the project.

2.2.1 Temperature measurements

During the initial phase of experimentation, the temperature of the borosilicate capillary, the most thermally stressed element of the plasma device, was measured. The measurements were performed by means of the Optris® CSlaser LT (Luchsinger s.r.l., Curno (BG)), a two-wire infrared thermometer characterized by a response time up from 150 ms. Its double-laser sighting was focused on the borosilicate tube near the cap as reported in Figure 2.4.

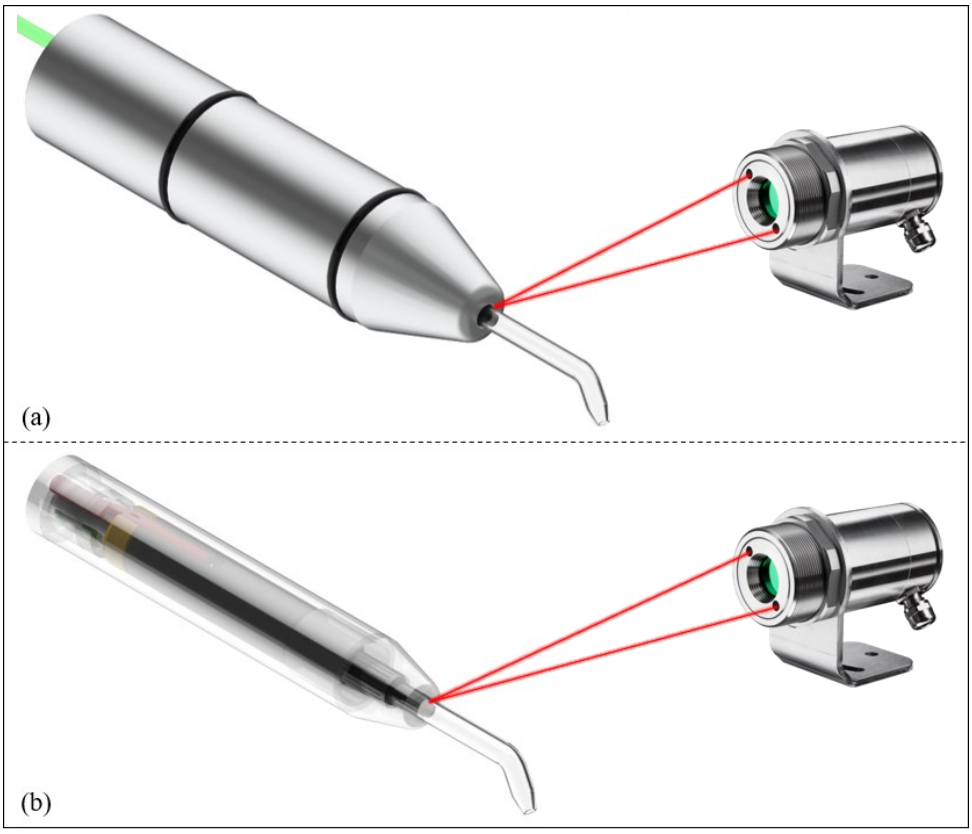

Figure 2.4 - Temperature measurements of the borosilicate capillary, the most thermally stressed element of (a) first prototype and (b) second prototype.

2.2.2 UV irradiance measurements and optical emission spectroscopy

The UV irradiance produced by the plasma plume was evaluated using the UV power meter Hamamatsu C9536/H9535-222 (measurement range of 0.001–200 mW/cm^2, high spectral response in the range 150 ÷ 350 nm). The sensor was placed 2 mm far away from the end of capillary of the plasma sources. Moreover, using the setup reported in Figure 2.5, optical emission spectroscopy (OES) measurements were carried out to obtain mainly information about the excited species of the plasma plume. In this perspective, the plasma emission was collected through a fused silica lens (positioned at about 2 mm from the end of capillary) by means of an optical fiber (Princeton Instruments, fiber optic bundle, 190 – 1100 nm) and a 500 mm spectrometer (Acton SP2500i, Princeton Instruments). In order to achieve highly resolved spectra, the inlet and the outlet slit width were set to 5 µm and 25 µm, respectively. In addition, a photomultiplier tube (PMT-Princeton Instruments PD439) connected to a fast oscilloscope (Tektoronix DPO 4034, 350 MHz, 2.5 GSas-1) was used as detector and its amplification factor was kept constant (1230) for all acquisitions.

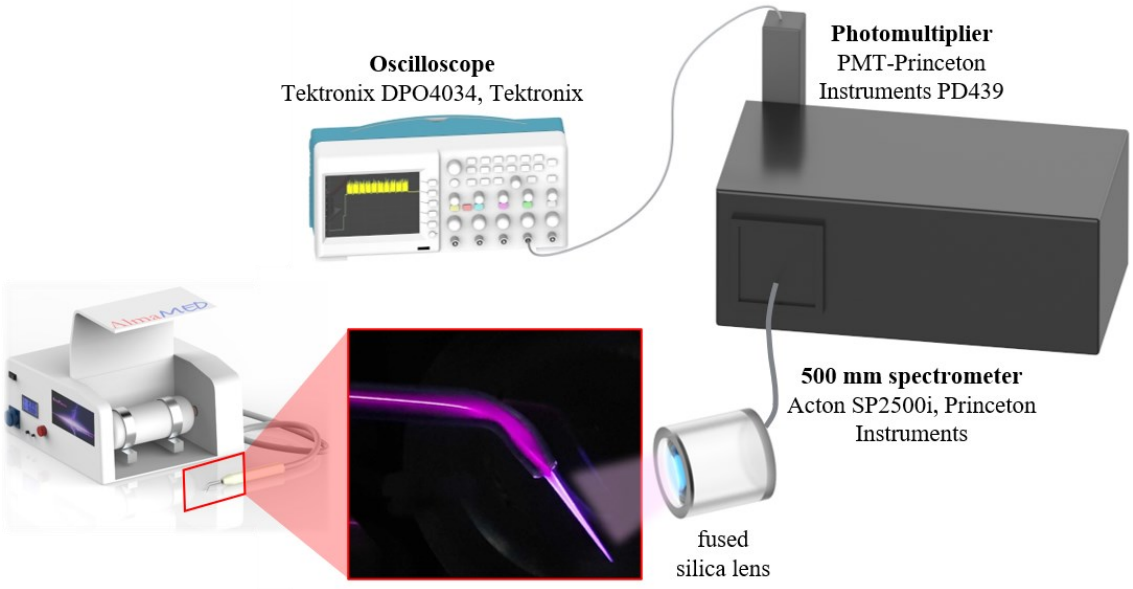

Figure 2.5 - Layout of the setup used for OES characterization.

2.2.3 Leakage current measurements

As suggested by the standard DIN EN 60601-1, the investigation of leakage current was carried out by measuring the maximum values of current (I_{rms}) flowing through a human finger (used as soft tissue) and through a metal wire, as reported in Figure 2.6. The human finger was positioned at 2, 5 and 12 mm of distance from the source outlet, respectively. The measurement of all leakage currents was performed by the means of a digital oscilloscope (Tektronix DPO4034, 350 MHz, 2.5 GSa s^{-1}) and two current probes (Pearson 6585). In all investigated cases the first current probe (A1) was used to measure the current flowing through the finger touching the plasma plume. Instead, the second current probe (A2) was used to measure the current flowing

through the metal wire having the first extremity positioned in the hand of the patient and the second one positioned in four different configurations. For the measurement of the current passing through a floating patient the second extremity of the metal wire was kept free from any connection. For the measurement of the auxiliary leakage current, also the second extremity of the metal wire was positioned in the hand of the patient. Differently from the above setups, in the ground patient configuration, the wire was connected to the ground while in ground to source patient it was connected to the ground electrode of the plasma source.

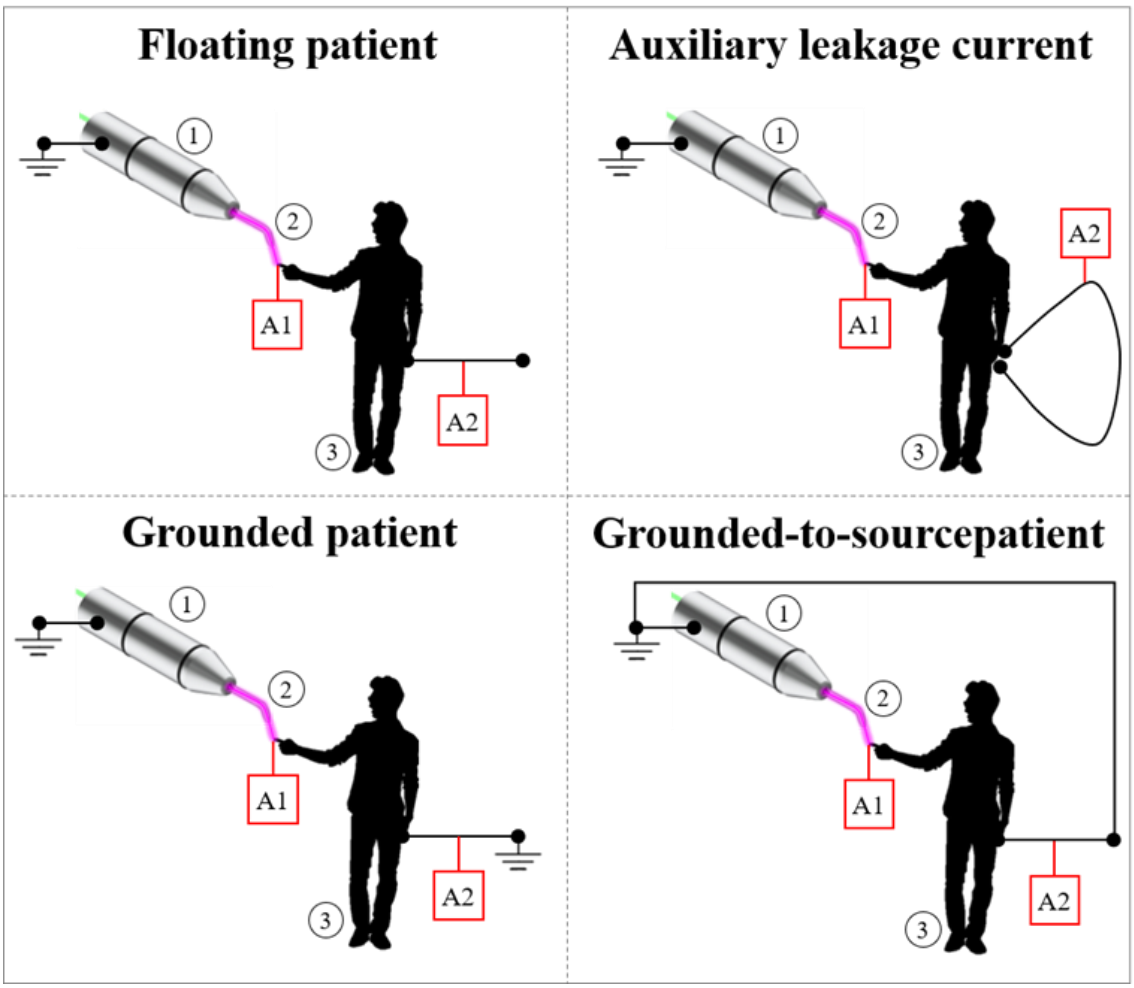

Figure 2.6 – Schematics of leakage current measurements. 1) plasma source, 2) plasma plume, 3) patient, A1) current probe 1, A2) current probe 2.[6]

2.3 Results and discussion

2.3.1 First prototype

The design of a plasma source which could be translate to the clinical environment is a very complex process which take long time and cross various steps of design and prototyping. The approach adopted during the course of my PhD consisted in the development and improvement of a laboratory device whose efficacy was already assessed. In this case, the laboratory device reported in Figure 2.7 (fully described by E. Simoncelli *et al*. [7] and proposed for the first time for dental applications) was considered as starting point for the design of a plasma source more suitable for medical applications.

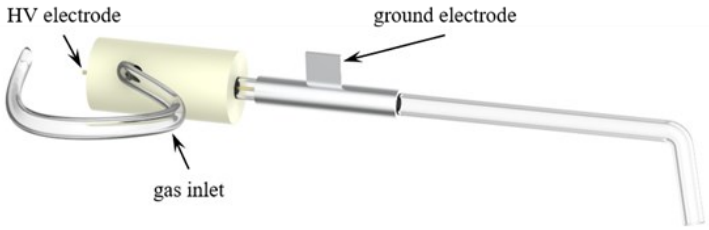

Figure 2.7 – APPJ laboratory prototype use to assess the efficacy of CAP treatments for endodontic procedures.[7]

The first step necessary for the realization of a medical device consists in providing an external housing for encasing the electrical connections and for increasing the ergonomics of the device. In this framework, an aluminium housing was designed to encase both HV and ground electrodes maintaining the same configuration of the plasma source reported in Figure 2.7. Altogether, as reported in Figure 2.8, the first prototype consists of two separated elements: the handpiece (Figure 2.8b) and the connector (Figure 2.8c). The choice of dividing the prototype into two separate pieces is due to facilitate mounting and dismounting of the device during the cleaning procedure.

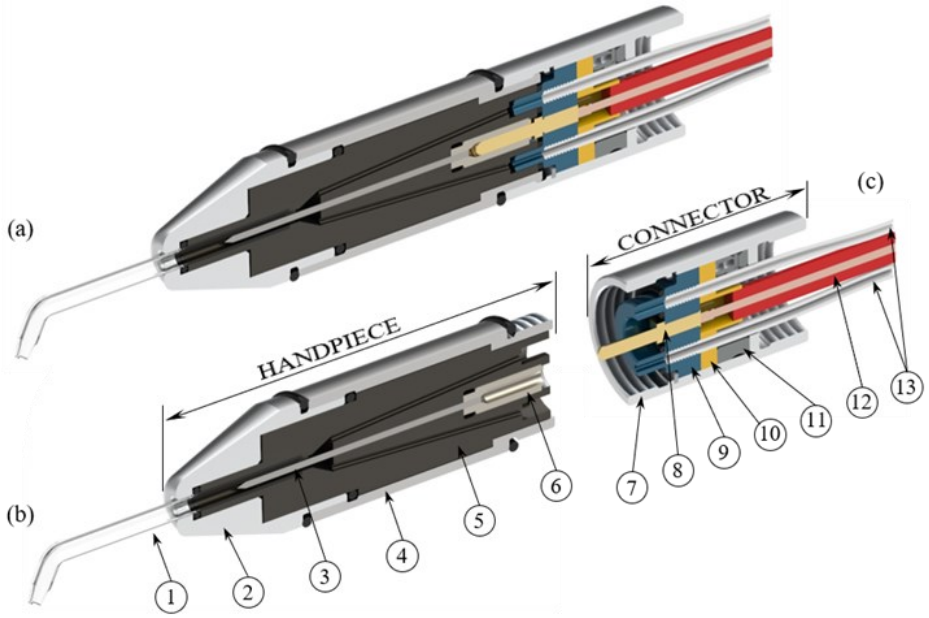

Figure 2.8 – (a) Handheld device for dental application made of (b) handpiece and a (c) connector. More specifically, the handpiece consists of 1) glass capillary, 2) aluminum cap, 3) high voltage tip, 4) aluminum housing which acts as ground electrode, 5) polymeric support and 6) high voltage connector. While the connector consists of 7) outer

aluminum housing, 8) banana socket, 9) gas & HV connector, 10) gas & HV fixing, 11) ring electrode for the ground connection, 12) high voltage cable, and 13) gas inlet tubes.

The handpiece (Figure 2.8a) consists of an external aluminum housing (acting as a ground electrode) which encases a 3D printed polymeric support on whose central axis was encased the HV electrode. As reported in Figure 2.9, in the initial design phase three different geometries of the polymeric support were taken into consideration; these elements are characterized by three different geometries of the channels for the introduction of gas (helium) in the generation zone. The first solution (Figure 2.9a) was characterized by the presence of two linear and symmetrical holes both overlooking a conical chamber, while in the second and the third solution (Figure 2.9b/c) helical gas channels were realized to guarantee a better gas mixing in case of using a gas mixture. However, to simplify the geometry of each component of the device and to avoid the obstruction of the gas channel due to the manufacturing process, only the polymeric support reported in Figure 2.9a was realized.

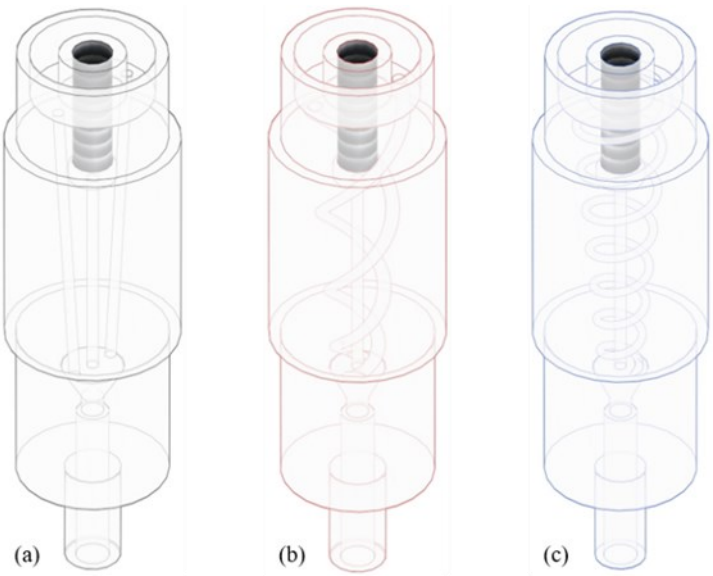

Figure 2.9 - Polymeric support characterized by: (a) two linear and symmetrical gas inlets, (b) two helical gas inlets, and (c) one helical gas inlet.

Referring to Figure 2.10, from the left of the handpiece, the assembly phase envisages the mounting of a glass tube, necessary for directing the plasma effluent from the generation zone to the application one; this element also acts as a dielectric material between the HV and the ground electrodes. As reported above, the connector contains all the electrical and gas connections. The banana socket connector, used to make the electrical contact between the HV connector and the power supply through an HV cable, is placed on the central axis of the connector. The gas tubes are fixed through barbed connections whose particular geometry allows the two tubes to be fixed by mechanical interference. Moreover, the connector is equipped with a ring electrode used for the ground connection.

The design of an advanced plasma prototype not only involved the 3D modeling of all its components. In order to realize a reliable device from a mechanical and electrical point of view, it was necessary to design and dimension every single component having in mind the final product and the type of coupling between each single element. Figure 2.10 shows an example of the handpiece section view; as could be seen from Detail A, to ensure the mounting of the polymeric

support inside the external casing composed by the aluminium cap (2) and the aluminium housing (5) it is necessary to realize a coupling with large tolerances (+ 0.25 mm and + 0.2 mm). On the contrary, in the generation zone (Detail B) the tolerance between the cap and the polymeric support (0.009 mm) is lower than the previous one in order to ensure the contact between the ground electrode and the dielectric material.

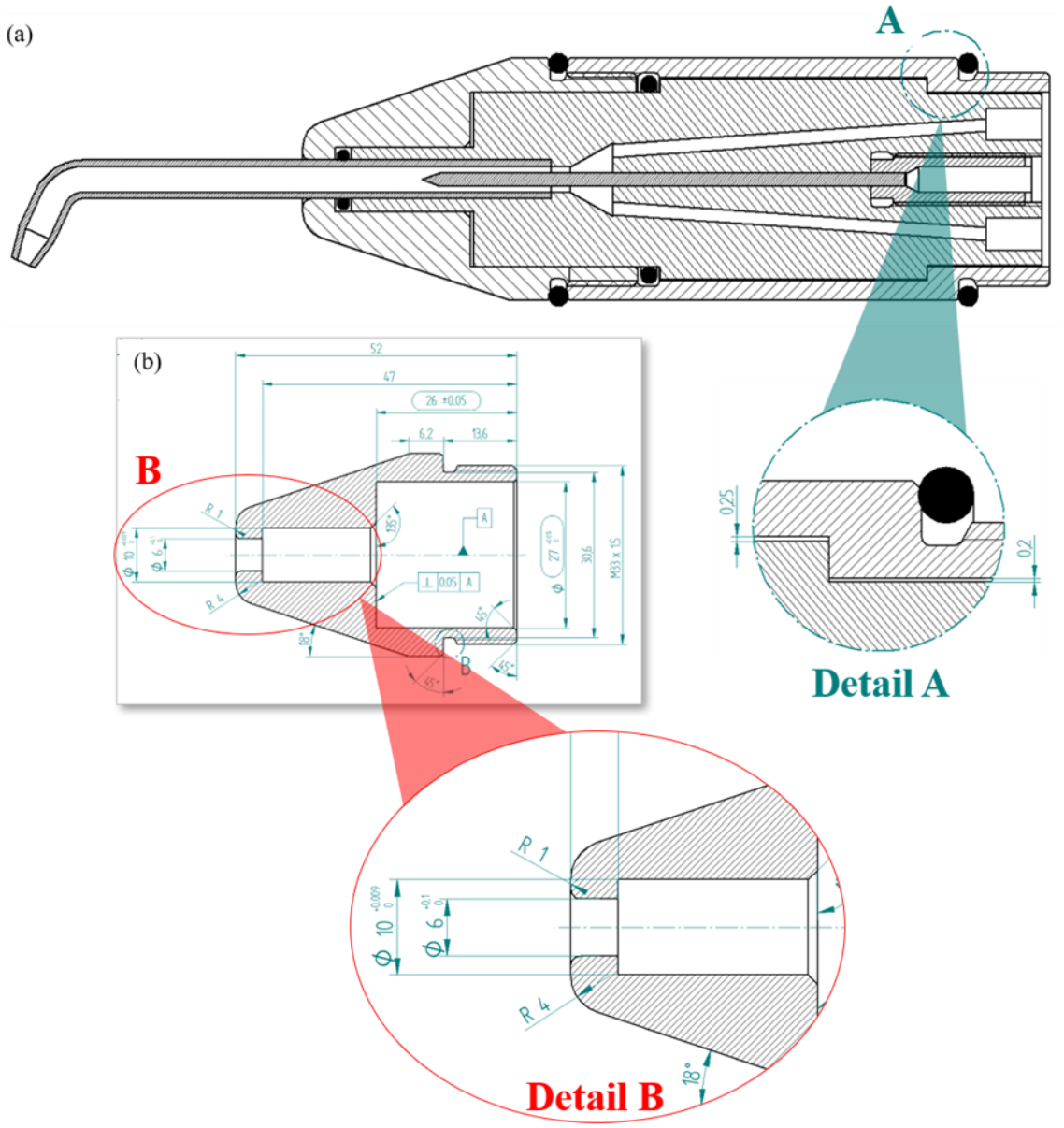

Figure 2.10 - (a) Section view of the handpiece and the (b) cover.

Despite the careful dimensioning, initially the prototype was not free from malfunctions (Figure 2.11a/b); the presence of two separate components which form the plasma source (handpiece and connector) leads to gas leakages and consequently to electrical arches as reported in Figure 2.11b. To avoid this problem, additional O-Rings were placed in the junction area. Following this improvement, the APPJ device reported in Figure 2.8 was successfully used to enhance the bond strength between filling materials and dentine in coronal-medial and apical restoration of the root canal.[5,6]

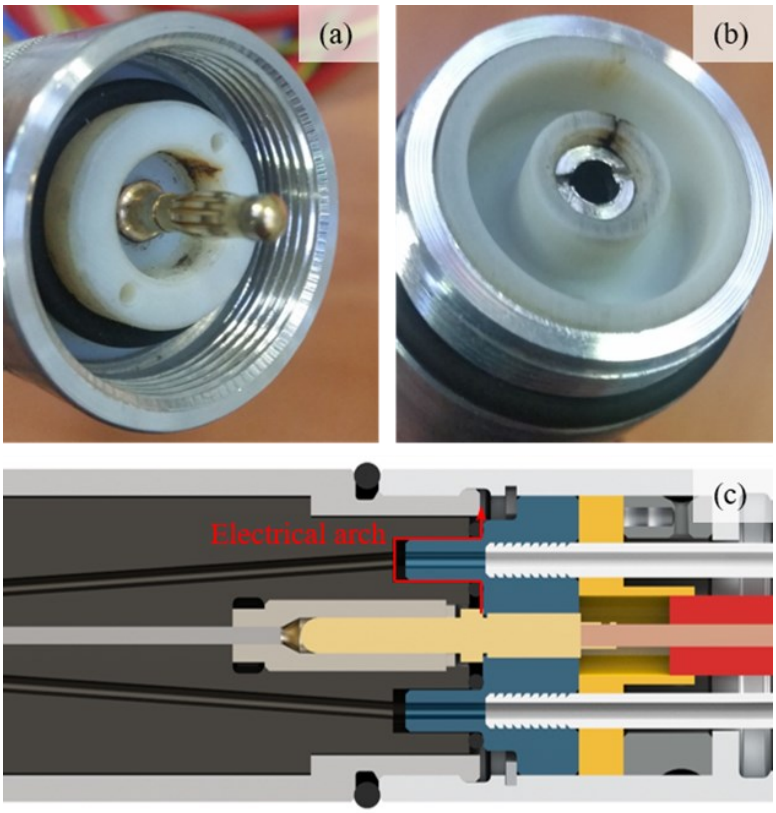

Figure 2.11 – Problems related to the first prototype (gas leakages).

Even if the device is characterized by good handling, the external diameter of the device (37.5 mm) is bigger than the diameter of the devices commonly used in the dental field. Moreover, due to the geometry of the polymeric support and gas & HV connector, it is necessary to use the 3D printing technology which offer a great flexibility with the respect of traditional machine tools (drill, milling machine and lathe). Indeed, as reported in Figure 2.10a, the conic chamber, the gas channels (characterized by an angled axis) and the barbed connections are impossible to realize with the tools of drill, milling machine or lathe. However, despite the numerous advantages of 3D printing, production costs would currently be too high to ensure market penetration.

2.3.2 Second prototype

Starting from the first prototype, the idea was to optimize the existing geometry to realize a second device with a smaller diameter avoiding the aforementioned leakages problematics. In this case, the outer casing (acting as ground electrode) was intended to maintain the same characteristics as the previous prototype and to contain all the elements that make up the plasma device. However, to minimize the geometry dimensions, as reported in Figure 2.12, one of the two gas tubes was to be removed and the banana socket used for the HV connection was to be repositioned in order to compact the overall size (resulting in a diameter of 22.5 mm instead of 37.5 mm). In this second prototype, the same dimensions of the generation zone, and consequently the same characteristics of the plasma, were maintained.

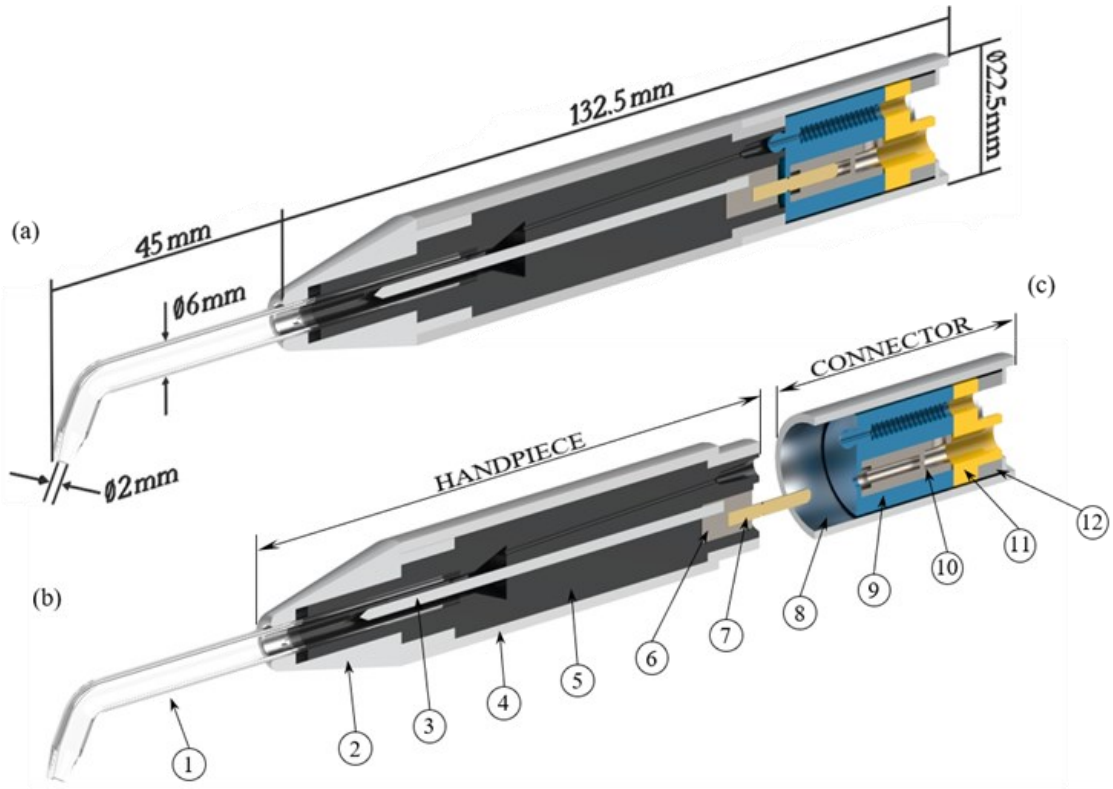

Figure 2.12 – (a) Second prototype with a dimeter of 22.5 mm made of (b) handpiece and a (c) connector. More specifically, the handpiece consists of: 1) glass capillary, 2) aluminum cap, 3) high voltage tip, 4) aluminum housing which acts as ground electrode, 5) polymeric support, 6) high voltage support and a 7) commercial banana socket. While the connector consists of: 8) outer aluminum housing, 9) gas & HV connector, 10) high voltage connector, 11) gas & HV fixing, and a 12) ring electrode for the ground connection.

During the initial phases of the source development, it became clear from the analysis of CAD models that the prototype presented a critical issue: as reported in Detail A of Figure 2.13, the distance between HV and ground electrodes in the proximity of the gas injection was approximately 2.2 mm. Such proximity between the two electrodes could lead to unwanted electrical arches and subsequently to damage of the plasma prototype if the operating conditions were too high.

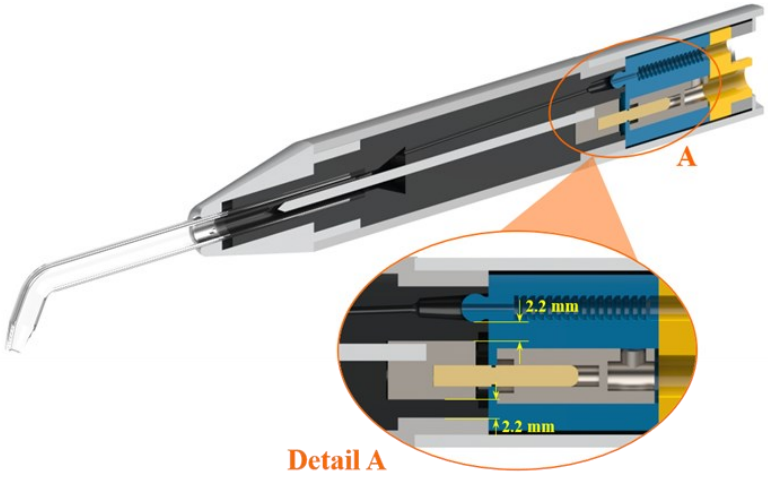

Figure 2.13 - Detail of the junction area between the handpiece and the connector which reports the distances between the high voltage, the ground connections and gas inlet.

The second prototype, although it could have been interesting to use in the laboratory for scientific purposes, has therefore never gone into production because it would never have presented the robustness of operation required for the clinic. Despite this first defeat, the second prototype has given inspiration for the design of the third one.

2.3.3 Third prototype

Further efforts were undertaken to improve the ergonomics of the devices shown in Figure 2.8 and 2.12. More specifically, to comply with the dimensions of devices commonly used in the dental practice, the geometry of each component of the second prototype of the APPJ plasma source (Figure 2.12) was optimized and adapted to an external housing design having a diameter of 21.5 mm (Figure 2.14).

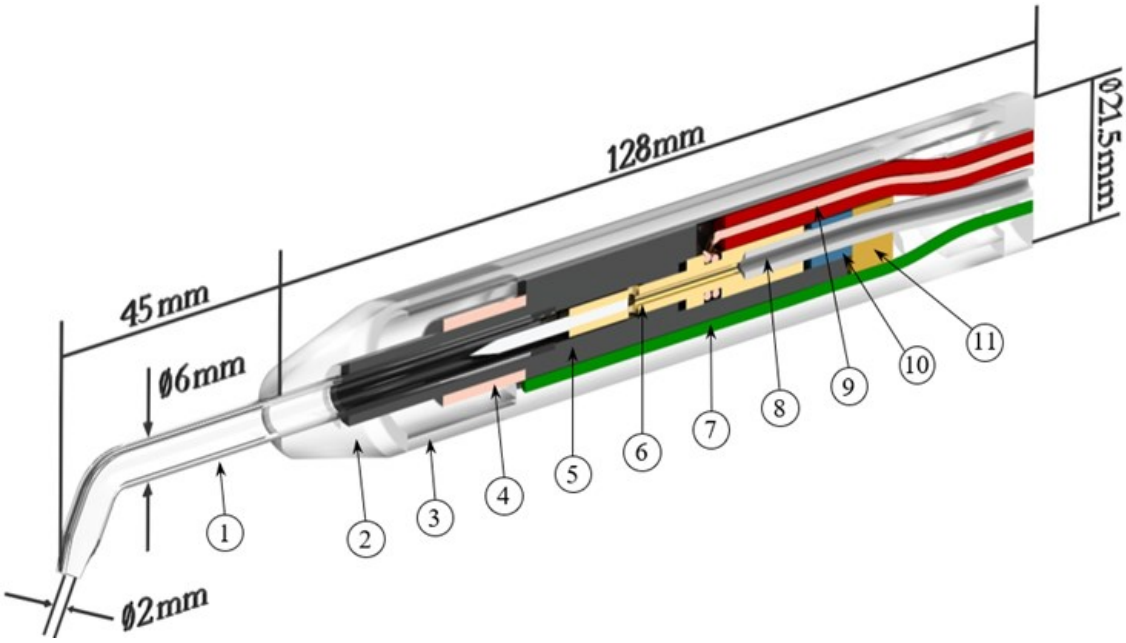

Figure 2.14 – (a) Third prototype with a dimeter of 21.5 mm; it consists of: 1) glass capillary, 2) PMMA cap, 3) PMMA housing, 4) aluminum ground electrode, 5) polymeric support, 6) high voltage electrode, 7) ground cable, 8) gas inlet tube, 9) HV cable, 10) PMMA ring for fixing the gas tube, and 11) PMMA spacer.

The need to minimize the weight of the device resulted in changes of the external housing material: instead of aluminum, it was realized in polymethylmethacrylate (PMMA), a transparent material of low density that also allows the operator to monitor the discharge zone during operation of the plasma source. Moreover, in order to avoid the risks associated with the proximity between the high voltage and the ground electrode, the geometry of the high voltage connector was completely modified. To compact the radial dimensions of the device maintaining the same geometry of the generation zone, the high voltage connector has taken two distinct functions: high voltage electrode and gas connector (Figure 2.15).

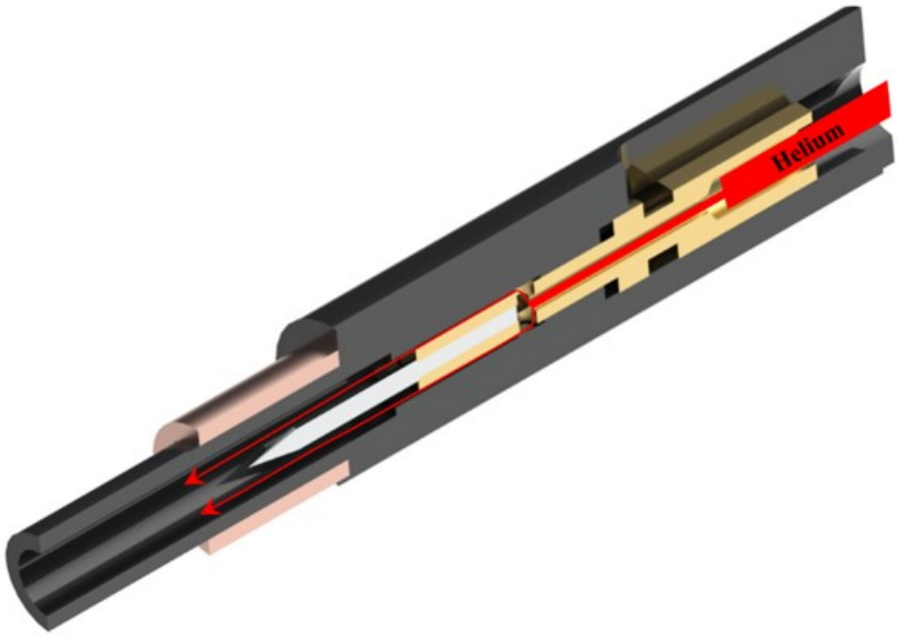

Figure 2.15 – High voltage connector with dual-function of high voltage electrode and gas connector.

Figure 2.16 shows the section view of both first and third prototypes; even if the number of components was unchanged, electrical and gas connections were improved to take up as little space as possible. More in detail, the axial inlet of helium gas through the upper part of high voltage electrode has allowed a considerable reduction of the plasma source diameter (from 37.5 mm to 21.5 mm). The design changes involved only the geometry of the support elements necessary to encase the electrodes and the dielectric capillary and to fix gas and electrical connections. Therefore, the relative position between high voltage and ground electrode remained unchanged.

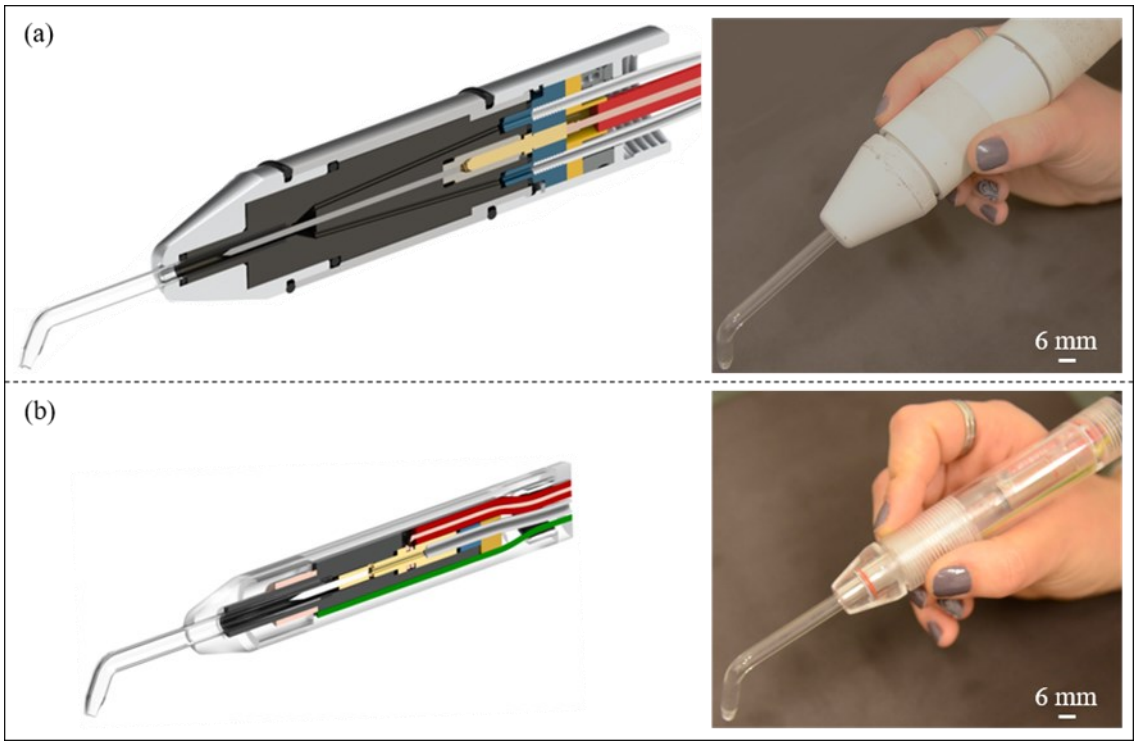

Figure 2.16 – (a) first prototype and (b) third prototype of the APPJ plasma source.[6]

2.3.4 AlmaMED: a tabletop device for dental applications

As the last step of the design and the realization of a plasma device for clinical applications, the prototype reported in Figure 2.14 was connected to a tabletop device containing a small disposable high-purity (99.99999 %) helium tank (0.66 l) and a compact dedicated pulse generator working with a single operating condition (Figure 2.17a/b). Each helium tank was capable of providing about 20 min of plasma treatment and when it ends, could be easily replaced. This choice results from the need to realize a device that could be easily used by a dental practitioner, instead of a person not an expert in the plasma sector.

Being designed to work with different types of replaceable disposable, this system is characterized by high versatility; Figure 2.17c shows the plasma device working with a borosilicate glass capillary terminating with a 25 mm long section characterized by an inclination of 75° and a tapered orifice (inner diameter of 2 mm). In addition, the later borosilicate capillary could be easily replaced with a linear one on which was possible to fix different replaceable polymeric tips (Figure 17d-g). This possibility facilitates the sterilization of the terminal part of the device and at the same time allows the use of tips characterized by different shapes that can be adapted to the complex morphology of human teeth.

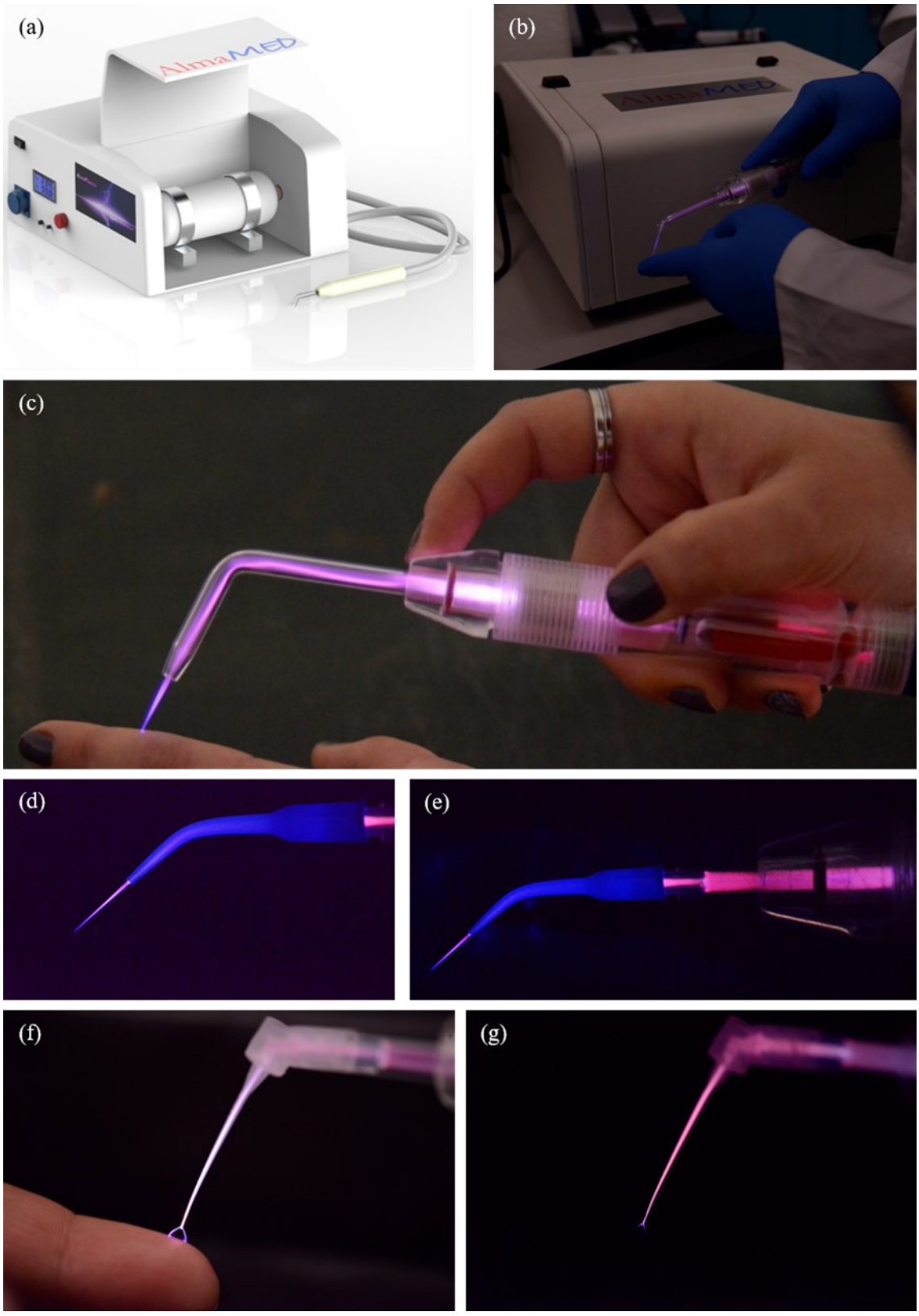

Figure 2.17 – (a) Render and (b) image of AlmaMED; a tabletop system composed by a dedicate pulse generator, a helium supply and an APPJ device. The latter one could work with (c) borosilicate gas capillary and (d, e, f, g) different types of replaceable polymeric tips.

2.3.5 Evaluation of temperature profile evolution

Figure 2.18a shows the temperatures reached by the borosilicate capillaries during the plasma treatment; the red dotted curve represents the threshold value bearable by the human body. In both cases the temperature of the borosilicate capillary increases with the treatment time. With regard to the first prototype, the temperature increases rapidly in the first 2.5 min of plasma treatment and subsequently remains constant near 47°C. Differently from the first prototype, the temperature of the third one increased slowly and reach a maximum of 42°C after 17 min of continuous plasma treatment. As reported in Figure 2.18b, this higher temperature registered for the first prototype could be linked with the formation of undesired plasma between the extremity of the aluminum cap and the borosilicate capillary related to the first prototype. Thus, considering that the effectiveness of the plasma treatment was assessed after a few minutes of plasma treatment [5–7], only the third prototype ensures effective decontamination without risk of exceeding the threshold.

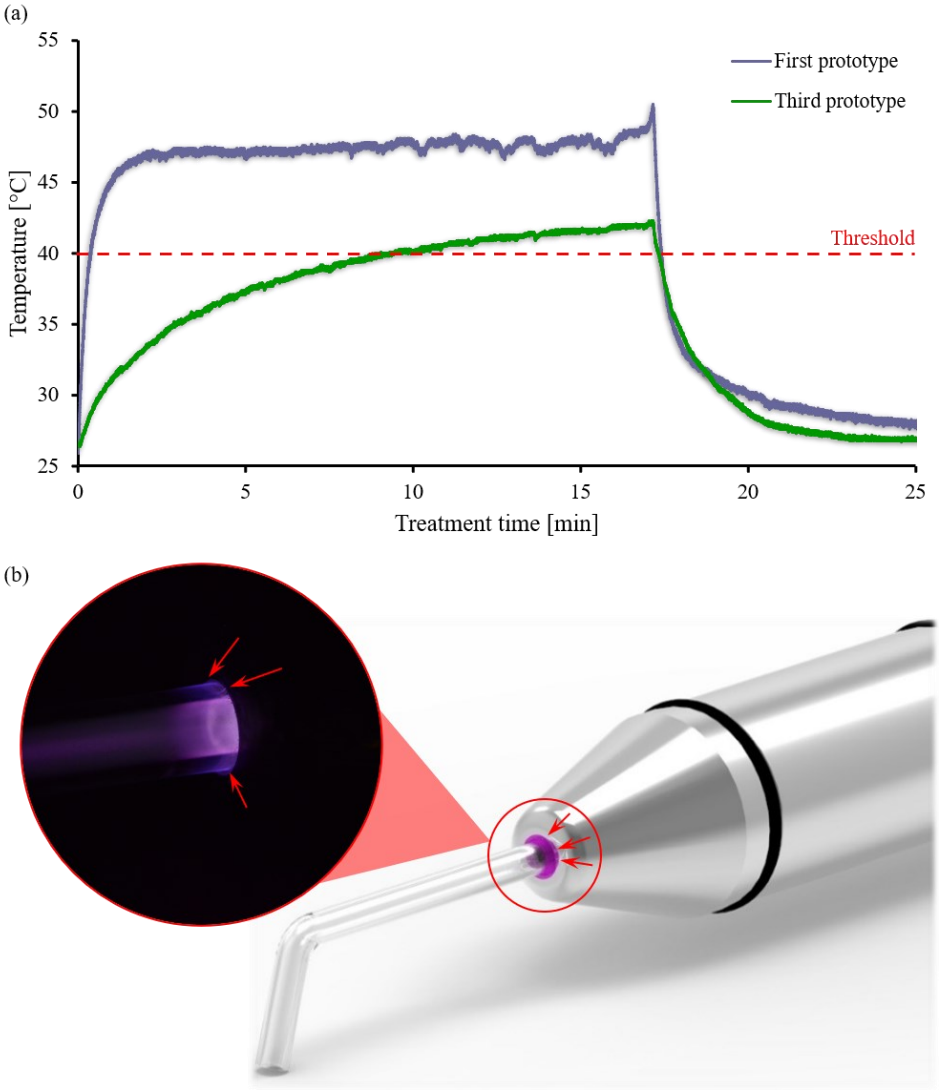

Figure 2.18 – Temperature profiles measured on the borosilicate tube near the extremity of the (a) aluminum cap pf the first prototype and the (b) PMMA cap of the third prototype. Undesired plasma discharges (c) between the extremity of the aluminum cap and the borosilicate capillary in the first prototype are indicated by red arrows.

2.3.6 Evaluation of the UV irradiance and the OES spectrum

As far as the UV irradiance is concerned, the UV radiation produced by the two APPJ devices (Figure 2.8 and 2.14) was always under the instrument sensitivity (<1μW/cm^2) and, in turn, under the imposed limit. For this reason, to analyze in more detail the plasma characteristics, the OES method was used to determine the optical emission spectra in the UV-VIS-NIR regions as a function of wavelength.[48] Figure 2.19 shows the normalized (on the first negative system of N_2^+ at 391 nm) spectra of the APPJ devices where have been identified the regions: UV-A (400 ÷ 315 nm), UV-B (315 ÷ 280 nm) and UV-C (280 ÷ 100 nm). For both plasma devices there were reordered the same emission lines corresponding to the same reactive species; the only difference between the two spectra consists in the intensity of emission which in some cases results to be higher for the first prototype (Figure 2.8).

In the UV-A and UV-B regions a strong emission of N_2 and OH was detected; in particular, the emission is higher for the first prototype with respect to the third one. A faint emission of NO in the UV-B region (283 nm) was observed, but no distinct emission lines were measured in UV-C region. In VIS-NIR only a few lines of He (587.6 nm, 667.8 nm and 706.5 nm), O (616 nm, 715 nm, 777.3 nm and 782 nm), O_2^+ (673.8 nm), N (750.8 nm) and N_2 (760.6 nm) were detected. The emission spectra, while being only indicative for excited state population during plasma generation on microsecond time scales, show that both prototypes allow for RNS production. At the same time, the first prototype is characterized by higher emission in UV-B and UV-A regions which could be detrimental in outbreaks of dermatological diseases.[49]

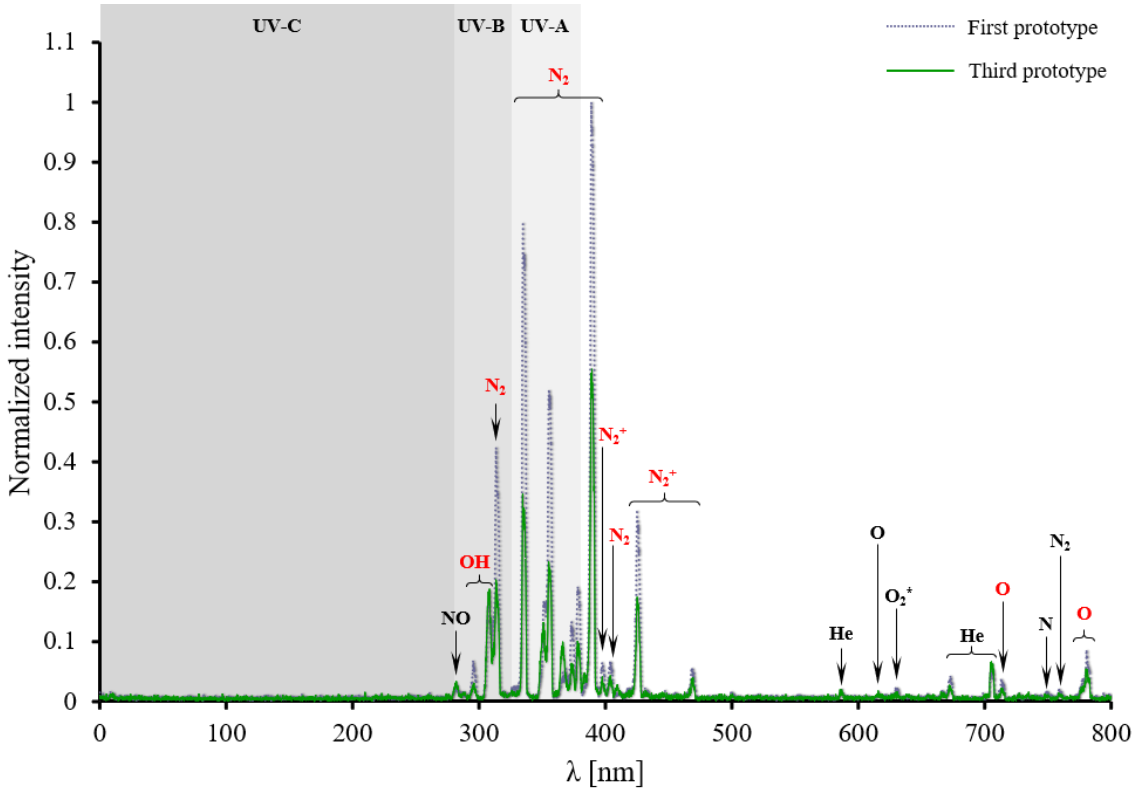

Figure 2.19 – Spectral emission in the UV-VIS-NIR regions

2.3.7 Leakage current measurements

In Table 2.1, the recorded values of maximum current are reported for the investigated cases and distances, as described in paragraph 2.2.7. As clearly shown by the results, the highest values of leakage current were measured using the first prototype and these were observed in the case of the floating patient; in this case, the measured current overcomes the threshold value of 100 μA. The safest condition was individuated when the patient is grounded-to-source: all the recorded values of IRMS are under the threshold limit. On the contrary, current values measured using the first prototype were over the threshold value and in particular, are much higher than those measured with the third prototype. As could be seen in Table 2.1, the measurements related to the ground-to-source patient are not reported because in the third prototype the ground electrode was positioned inside a PMMA housing far away from the patient or the operator.

The distance between the source outlet and the soft tissue (the human finger in the present study) relevantly affects the leakage current in the case of the not-grounded patient.

	Gap	**First prototype**		**Third prototype**	
		I_{RMS_1}	I_{RMS_2}	I_{RMS_1}	I_{RMS_2}
	[mm]	[μA]	[μA]	[μA]	[μA]
Floating patient	2	140	30	<1	<1
	5	120	< 10	<1	<1
	12	100	30	<1	<1
Auxiliary leakage current	2	90	110	<1	<10
	5	20	40	<1	<1
	12	<10	230	<1	<10
Grounded patient	2	87	70	<10	<10
	5	38	10	<10	<10
	12	130	40	<10	<10
Grounded-to-source patient	2	80	50	-	-
	5	100	100	-	-
	12	80	50	-	-

Table 2.1 – Recorded values of IRMS for three different distances between human finger and the source outlet: 2, 5 and 12 mm.

2.4 Conclusions and future perspectives

The design and the engineering of a plasma device exploitable in the clinical environment is a long and complex activity that requires numerous steps and detailed analysis of the geometry, the mounting procedure, and especially the technology and the procedures necessary to realize every single component. In the great majority of the cases, this procedure was not easy or exempt from failures. In this perspective I reported the most important steps in the design of a plasma device easy to handle and expected to be mounted on a tabletop device that could be used for dental clinical applications. Moreover, during the design I focused on different aspects of standard regulations for medical devices, including the German DIN SPEC 91315, and significant time was dedicated to the identification of the risks that could compromise the good functioning of the plasma device and the safety of both patient and operator.

The first prototype, characterized by a compact geometry and quite easy handling despite its dimensions far away from the devices commonly used in the dental field, represented an enormous step forward compared to the previously employed laboratory prototype.[5,6] Despite the accurate design and realization, many problems related to gas leakages were encountered and resulted in compromising the internal polymeric elements of the device. A second prototype, promising to solve these issues, was deemed unadapt for clinical practice due to the risk of formation of stray discharges within the plasma source. However, identifying problems and finding suitable solutions is part of the engineering process and so these initial failures were considered as the starting point for the design of another plasma device, characterised by a lower diameter, improved gas connection and with no risk of internal stray discharges. After its realization phase, I focused on three relevant parameters indicated by the standard regulations as important for considering a prototype as a medical device: temperature, UV irradiance and leakage currents measurement. With reference to the third prototype, all the measurement results do not exceed the thresholds reported in DIN SPEC 91315; this provides a very first estimation of the applicability of the third PG prototype as medical plasma source. Even if future clinical *in vivo* studies are still required, the potential for future success of a CAP-assisted dental procedure appears day by day more certain.

2.5 References

[1] G. V. Naidis, "Production of active species in cold helium-air plasma jets", *Plasma Sources Science and Technology*, 23 (6) 065014, (**2014**).

[2] S.A. Norberg, *et al*., "Formation of reactive oxygen and nitrogen species by repetitive negatively pulsed helium atmospheric pressure plasma jets propagating into humid air", *Plasma Sources Science and Technology*, 24 (3) (**2015**).

[3] G. Busco, *et al*., "The emerging potential of cold atmospheric plasma in skin biology", *Free Radical Biology and Medicine*, 161 290, (**2020**).

[4] F. Judée, *et al*., "Atmospheric pressure plasma jets applied to cancerology: correlating electrical configurations with in vivo toxicity and therapeutic efficiency", *Journal of Physics D: Applied Physics*, 52 (24) 245201, (**2019**).

[5] A. Stancampiano, *et al*., "The Effect of Cold Atmospheric Plasma (CAP) Treatment at the Adhesive-Root Dentin Interface", *The Journal of Adhesive Dentistry*, 21 (3) 229, (**2019**).

[6] A. Bisag, *et al*., "Cold atmospheric pressure plasma treatment to assist the restoration of the apical region of a root canal in endodontic procedures", *Clinical Plasma Medicine*, 19–20 (May) 100100, (**2020**).

[7] E. Simoncelli, *et al*., "Preliminary investigation of the antibacterial efficacy of a handheld Plasma Gun source for endodontic procedures", *Clinical Plasma Medicine*, 3 (2) 77, (**2015**).

[8] X. Lu, *et al*., "On atmospheric-pressure non-equilibrium plasma jets and plasma bullets", *Plasma Sources Science and Technology*, 21 (3) 034005, (**2012**).

[9] E. Robert, *et al*., "Characterization of pulsed atmospheric-pressure plasma streams (PAPS) generated by a plasma gun", *Plasma Sources Science and Technology*, 21 (3) 034017, (**2012**).

[10] S.A. Norberg, *et al*., "Atmospheric pressure plasma jets interacting with liquid covered tissue: Touching and not-touching the liquid", *Journal of Physics D: Applied Physics*, 47 (47) 475203, (**2014**).

[11] A. Khlyustova, *et al*., "Important parameters in plasma jets for the production of RONS in liquids for plasma medicine: A brief review", *Frontiers of Chemical Science and Engineering*, 13 (2) 238, (**2019**).

[12] E. Turrini, *et al*., "Plasma-activated medium as an innovative anticancer strategy: Insight into its cellular and molecular impact on in vitro leukemia cells", *Plasma Processes and Polymers*, 17 (10) e2000007, (**2020**).

[13] J.S. Oh, *et al*., "Effect of plasma jet diameter on the efficiency of reactive oxygen and nitrogen species generation in water", *Japanese Journal of Applied Physics*, 55 (6S2) 06HD01, (**2016**).

[14] K. Ogawa, *et al*., "Modulating the concentrations of reactive oxygen and nitrogen species and oxygen in water with helium and argon gas and plasma jets", *Japanese Journal of Applied Physics*, 58 (SA) B01, (**2019**).

[15] X. Lu, *et al*., "An 11 cm long atmospheric pressure cold plasma plume for applications of plasma medicine", *Applied Physics Letters*, 92 (8) 10, (**2008**).

[16] F. Judée, *et al*., "Plasma gun for medical applications: Engineering an equivalent electrical Title target of human body and deciphering relevant electrical parameters", *Journal of Physics D: Applied Physics*, 52 (16) 16LT02, (*2019*).

[17] Z. Fang, *et al*., "Discharge processes and an electrical model of atmospheric pressure plasma jets in argon", *European Physical Journal D*, 70 (1) (**2016**).

[18] J. Goree, *et al*., "Killing of *S. mutans* bacteria using a plasma needle at atmospheric pressure", *IEEE Transactions on Plasma Science*, 34 (4 II) 1317–1324, (**2006**).

[19] S. Hamada, *et al*., "Biology, immunology, and cariogenicity of Streptococcus mutans", *Microbiological Reviews*, 44 (2) 331, (**1980**).

[20] R.E.J. Sladek, *et al*., "Plasma treatment of dental cavities: a feasibility study", *IEEE Transactions on Plasma Science*, 32 (4) 1540, (**2004**).

[21] C. Kurzmann, *et al*., "In vitro evaluation of experimental light activated gels for tooth bleaching", *Photochemical and Photobiological Sciences*, 18 (5) 1009, (**2019**).

[22] S.H. Nam, *et al*., "High-efficiency tooth bleaching using nonthermal atmospheric pressure plasma with low concentration of hydrogen peroxide", *Journal of Applied Oral Science*, 21 (3) 265, (**2013**).

[23] J. Winter, *et al*., "Tracking plasma generated H_2O_2 from gas into liquid phase and revealing its dominant impact on human skin cells", *Journal of Physics D: Applied Physics*, 47 (28) (**2014**).

[24] S.A. Norberg, *et al*., "Formation of reactive oxygen and nitrogen species by repetitive negatively pulsed helium atmospheric pressure plasma jets propagating into humid air", *Plasma Sources Science and Technology*, 24 (3) 035026, (**2015**).

[25] J. Pan, *et al*., "A novel method of tooth whitening using cold plasma microjet driven by direct current in atmospheric-pressure air", *IEEE Transactions on Plasma Science*, 38 (11) 3143, (**2010**).

[26] H.W. Lee, *et al*., "Tooth Bleaching with Nonthermal Atmospheric Pressure Plasma", *Journal of Endodontics*, 35 (4) 587, (**2009**).

[27] H.W. Lee, *et al*., "Atmospheric pressure plasma jet composed of three electrodes: Application to tooth bleaching", *Plasma Processes and Polymers*, 7 (3–4) 274, (**2010**).

[28] V. Šantak, *et al*., "Optical Emission Spectroscopy of an Atmospheric Pressure Plasma Jet during Tooth Bleaching Gel Treatment", *Applied Spectroscopy*, 69 (11) 1327, (**2015**).

[29] Y.C. Cheng, *et al*., "Tooth bleaching by using a helium-based low-temperature atmospheric pressure plasma jet with saline solution", *Plasma Processes and Polymers*, 14 (11) 1600235, (**2017**).

[30] M. Zehnder, "Root Canal Irrigants", *Journal of Endodontics*, 32 (5) 389, (**2006**).

[31] V.C. Nakamura, *et al*., "*Ex vivo* evaluation of the effects of several root canal preparation techniques and irrigation regimens on a mixed microbial infection", *International Endodontic Journal*, 46 (3) 217, (**2013**).

[32] M. Habib, *et al*., "Antimicrobial effects of non-thermal atmospheric plasma as a novel root canal disinfectant", *Clinical Plasma Medicine*, 2 (1) 17, (**2014**).

[33] J. Pan, *et al*., "Cold plasma therapy of a tooth root canal infected with enterococcus faecalis biofilms in vitro", *Journal of Endodontics*, 39 (1) 105, (**2013**).

[34] X. Lu, *et al*., "An RC plasma device for sterilization of root canal of teeth", *IEEE Transactions on Plasma Science*, 37 (5) 668, (**2009**).

[35] X.C. Zhou, *et al*., "Bactericidal effect of plasma jet with helium flowing through 3% hydrogen peroxide against *Enterococcus faecalis*", *Experimental and Therapeutic Medicine*, 12 (5) 3073, (**2016**).

[36] E. Robert, *et al*., "Experimental study of a compact nanosecond plasma gun", *Plasma Processes and Polymers*, 6 (12) 795, (**2009**).

[37] C.J. Ruddle, "Endodontic triad for success: The role of minimally invasive technology", *Dentistry Today*, 34 (5) 76, (**2015**).

[38] Y. Zhang, *et al*., "Non-thermal atmospheric plasmas in dental restoration: Improved resin adhesive penetration", *Journal of Dentistry*, 42 (8) 1033, (**2014**).

[39] Y. Yue, *et al*., "Comparison on the Absolute Concentrations of Hydroxyl and Atomic Oxygen Generated by Five Different Nonequilibrium Atmospheric-Pressure Plasma Jets", *IEEE Transactions on Radiation and Plasma Medical Sciences*, 1 (6) 541, (**2017**).

[40] "Medical Device", World Health Organization, Accessed 2 (October) (**2019**). http://www.who.int/medical_devices/full_deffinition/en/.

[41] J.K. Aronson, *et al*., "Medical Devices: Definition, Classification, and Regulatory Implications", Drug Safety, 43 (2) 83, (**2020**).

[42] A. Kreuter, *et al*., "A randomized controlled study of low-dose UVA1, medium-dose UVA1, and narrowband UVB phototherapy in the treatment of localized scleroderma", *Journal of the American Academy of Dermatology*, 54 (3) 440, (**2006**).

[43] G. Von Kobyletzki, *et al*., "Medium-dose UVA1 cold-light phototherapy the treatment of severe atopic dermatitis", *Journal of the American Academy of Dermatology*, 41 (6) 931, (**1999**).

[44] Y. Matsumura, *et al*., "Toxic effects of ultraviolet radiation on the skin", *Toxicology and Applied Pharmacology*, 195 (3) 298, (**2004**).

[45] "Medical devices - Application of risk management to medical devices", International Standard ISO 14971, (**2007**).

[46] "Medical electrical equipment- General requirements for basic safety and essential performance", International Standard Iec60601-1, (**2005**).

[47] T.H. Chung, *et al*., "Cell electropermeabilisation enhancement by non-thermal-plasma-treated PBS", *Cancers*, 12 (1) 219, (**2020**).

[48] B.B. Sahu, *et al*., "Development and characterization of a multi-electrode cold atmospheric pressure DBD plasma jet aiming plasma application", *Journal of Analytical Atomic Spectrometry*, 32 (4) 782, (**2017**).

[49] J. D'Orazio, *et al*., "UV radiation and the skin", *International Journal of Molecular Sciences*, 14 (6) 12222, (**2013**).

3

Design and realization of a Cold Atmospheric Plasma (CAP) device for the inactivation of airborne pathogens

3.1 Introduction

Bioaerosols are generally defined as aerosolized particles with a biological origin (plants or animals) having a drop diameter in a range of 0.001 ÷ 100 μm and eventually containing living microorganisms like e. g. bacteria, viruses, or fungi. Currently, bioaerosols have become an important topic in daily life because are strongly suspected to play a significant role in spreading events under certain conditions.[1] Indeed, in both occupational and residential environments, bioaerosol was associated with a wide range of diseases, for instance, influenza, allergies, and respiratory syndromes.[2,3] Even if the importance of infectious bioaerosol in disease transmission was still poorly understood [4], generally many respiratory viruses are believed to transmit over multiple routes: direct spray route (through respiratory droplets having a diameter higher than 5 μm), long-range airborne route (through aerosols containing droplets with a diameter from submicron to approximately 5 μm), and the fomite route.[5,6] Nowadays, these themes have become dramatically topical due to the occurrence of the COVID-19 crisis. To date, the confirmed cases worldwide since the beginning of the pandemic are 75.479.471 while the dead are 1.686.267 and the situation is not over yet.

Several studies reported that the transmission via bioaerosols is of great importance in the COVID-19 pandemic caused by the Severe Acute Respiratory Syndrome Coronavirus 2 (SARS-CoV-2) identified in Wuhan (China) in December 2019.[7,8] Indeed, viruses could be released in small droplets (within a respirable size range) during breathing, talking, sneezing, coughing or laughing; the viral load emitted by an infected person generally depends on the location within the respiratory tract from which the droplets originated.[9,10] In the simplest of the cases, as reported by S. H. Smith *et al*. [11], the speech produces a single-peak drop size distribution (1 ÷ 10 μm) while cough produces a double-peak distribution (1 ÷ 10 μm and 100 ÷ 1000 μm). The larger drops (d > 100 μm) tend to settle on the ground (in about 3 s) due to the force of gravity while smaller droplets remain suspended for longer periods of time. Moreover, the smaller droplets could also evaporate into aerosols or droplet nuclei having a long-range transmission risk.[8]

Based on the studies of X. Xie *et al*. [12], M. Jayaweera *et al*. [13] have reported the trajectory of both large particles and aerosols during sneezing, coughing and exhaling events in indoor environments. The trajectory of large particles (60 – 100 μm) depends strongly on the air velocity and the relative humidity. Generally, during sneezing event the largest particles travel at a speed of 50 m/s and can travel a horizontal distance of 6 m. During the coughing event, the particle's

speed was about 10 m/s leading to horizontal dispersion of about 3 m; while for exhaling events, the particles have a trajectory of about 1 m. On the contrary, smaller particles emitted as aerosols could contain the viral agents and could remain potentially infectious over time and distances higher than 6 m.[1, 10,14–16] In this perspective, S.H. Smith, *et al*. find out that SARS-CoV-2 remains viable for more than 3 hours in aerosol while N. van Doremalen, *et al*. observe that the virus remains viable for up to 72 hours also on different surfaces (i.e., plastic, stainless steel, copper, and cardboard).[17,18]

Due to the significant implications of droplets and aerosol on the health of citizens around the world, face masks became popular as one of the most effective devices in preventing both aerosol and droplets from transmitting the viral load.[19,20] Surgical masks in combination with social distancing and frequent hand-washing become increasingly important in avoiding the spread of COVID-19 disease. Indeed, the face masks have the double task of controlling the contact of droplets and avoiding the droplets outgoing from an infected patient. In these regards, M. Jayaweera *et al.* [13] take into consideration different types of facial masks and study the leakage of large droplets and aerosol coming from an infected person who worn it (Figure 3.1). As reported in Figure 3.1b, even wearing a surgical mask, about 20 ÷ 30 % of droplets were dispersed. This percentage decrease to 5 % with N95 or elastomeric respirators (Figure 3.2c/d).

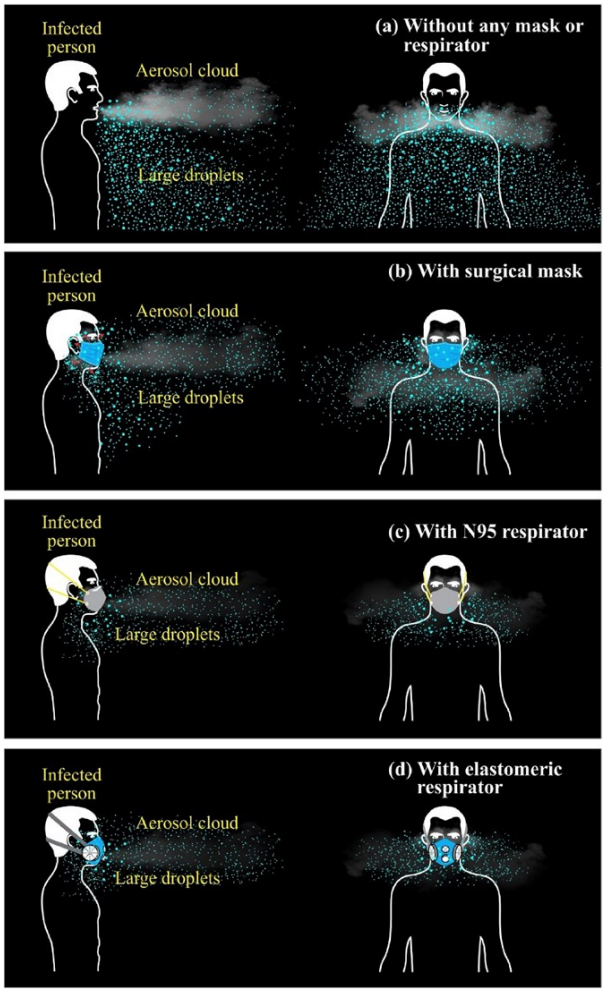

Figure 3.1 – Aerosol and large droplets emitted by an infected person who (a) do not wear any mask or respirator, (b) wear a surgical mask, (c) wear a N95 respirator and (d) wear an elastomeric respirator. From the images it is evident that none of the face masks can completely avoid the emission of viral load contained in droplets or aerosols. With permission from [13].

As reported above, of all the measures adopted for the containment of the SARS-CoV-2 virus, the safe distance (about 1 m) have assumed considerable importance; in this perspective, several numerical simulations have been conducted for both outdoor and indoor environments.[8,21–25] In the last case, droplet lifetimes and transport distances were significantly affected by environmental conditions, especially in poorly ventilated spaces.[10,26] In this regard, many examples were reported starting from two Wuhan hospitals used exclusively for the treatment of patients with COVID-19 during the lockdown.[27] After the sampling different locations, namely, patient areas (which include intensive care unit, coronary care units and ward rooms), medical staff areas (places exclusively accessed by the medical staff who had direct contact with patients) and public areas (pharmacy, doctor's office, outpatient hall, supermarket, etc.…) Y. Liu *et al*. [27] find out that the highest virus concentration was in a temporary single toilet room of about 1 m^2 in area and without ventilation. Moreover, Y. Li *et al*. [28] analyzed an interesting case study regarding teen members of three different families who were found to have been infected with SARS-CoV-2 after lunch in a Chinese restaurant. The people were sitting at neighboring tables while none of the other 68 customers became infected. The result of this fluid dynamic analysis was reported in Figure 3.2 which shows a recirculation envelope created in the most critical zone of the restaurant. In that area was supposed a high concentration of exhaled droplet nuclei from the index patient confined in an individual circulation zone formed due to the spatial configuration of the air-conditioning units and the absence of open windows.

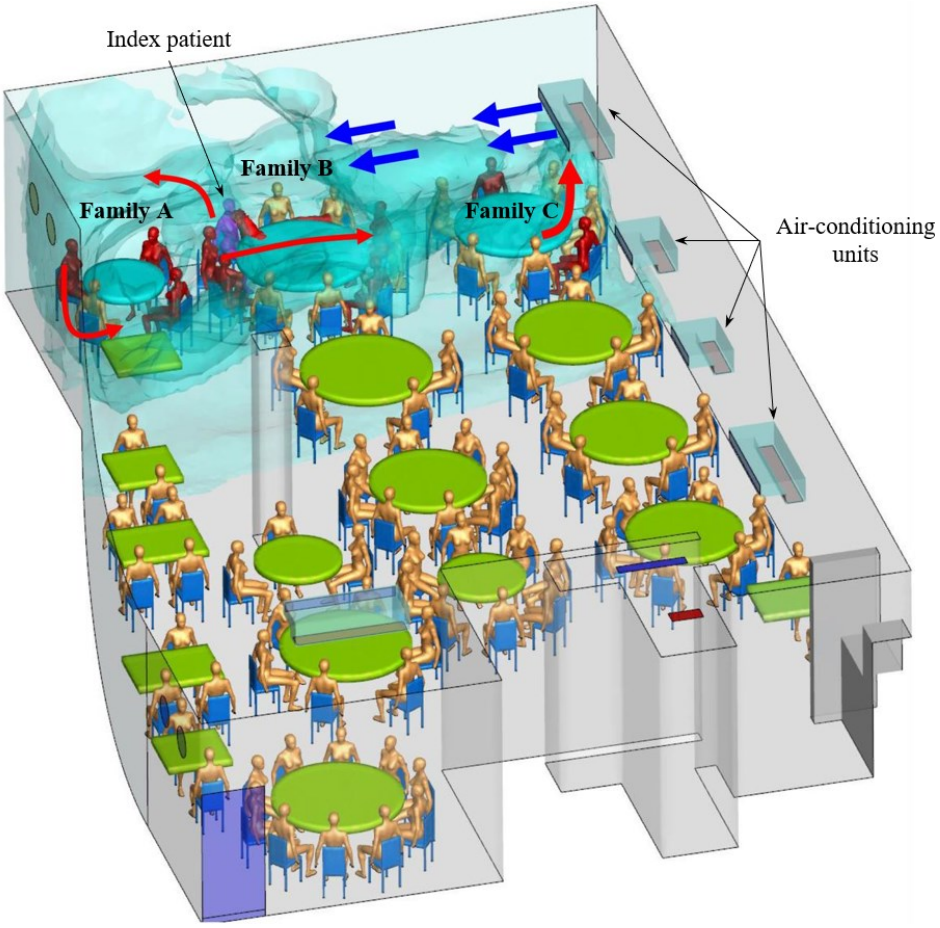

Figure 3.2 - Predicted contaminated cloud envelope involving the tables of the members of three families who have been infected with Sars-CoV-2 virus. In magenta-blue was reported the index patient; while, the infected patients are reported in red and the other non-infected in gold color. With permission from [28].

In the last year, extraordinary efforts were devoted to searching for a vaccine for COVID-19 and starting from the 27 of December Europe-wide vaccination campaign will start. The BNT162b2 mRNA Covid-19 Vaccine [29] will be distributed by the armed forces and will be administrated to individuals over the age of 16 years old. Despite this great step in the treatment of COVID-19, physicists and engineers together with microbiologists have to explore efficient means for preventing the spread. Since ventilation and recirculation systems have been shown to insufficiently reduce the indoor concentration of airborne pathogens or even to increase the risk of aerosol transmission, decontamination of air has become an important area of research with significant impact on several environments including hospitals [27] and other enclosed areas that are prone to microbial contamination. In this perspective, new control technologies capable inactivating aerosolized bacteria and viruses are highly sought after; these new technologies must be economically convenient, should not be responsible for secondary pollution and must be able to effectively inactivate different types of pathogens.[30,31] However, the efficacy of treatments depends on microbes genome structure and their replication machinery;[32] furthermore, new technologies must take into account the possibility that both bacteria and viruses could develop harmful mutagenic outcomes associated with multiple transition mutations across the genome when they are under-exposed or undergo incorrect inactivation treatments.[32,33] In this regard, thanks to CAPs ability of generating many reactive oxygen and nitrogen species (RONS) namely O_3, NO, NO_2, N_2O_5, HNO_2, HNO_3, $ONOO^-$, H_2O_2, ·OH, etc.…, this technology has been increasingly used as a tool for air sterilization and decontamination.[34,35]

3.1.1 CAP devices for the treatment of airborne pathogens

In recent years, DBD plasma sources (characterized by numerous electrodes geometries) were considered suitable devices for air decontamination or sterilization.[33,35–43] DBD sources produce many reactive species with antimicrobial efficacy, including O_3, and short-lived and stabilized species.[44] Gallagher *et al*. [45] used a dielectric barrier grating discharge (DBGD) plasma device to deactivate high concentrations of bacterial bioaerosol in flight at high flow rates in a ventilation system. It is shown that a 1.5 and 5.5 Log Reduction of the airborne *Escherichia coli* were achieved, respectively, after single plasma exposure of 10 s and 2 min. Y. Liang *et al*. reported that non-thermal plasma generated by a wire-to-plate type DBD reactor induces a significant inactivation of bioaerosol containing *Bacillus subtilis* or *Pseudomonas fluorescens*.[35] Park *et al*. used a DBD architecture (with alternately arranged electrodes sandwiched between 0.25 mm thick dielectric) to inactivate *Staphylococcus epidermidis* bioaerosols using a short residence time (0.24 s).[41] Romero-Mangado *et al*. studied the effect of DBD on aerosolized *E. coli* concluding that the cell structure was damaged to varying extent and a severe oxidation of the cell membrane was found, establishing effective inactivation of the bacteria.[33] Moreover, the same authors also demonstrated the possibility of inactivation *S. epidermidis* and *Aspergillus niger*, respectively a Gram-positive bacteria, and fungal spores by means of CAP treatment.[37] The morphology observed using SEM (Scanning Electron Microscope) shows deformations in the cellular structure of both microorganisms. Cell structure damage upon interaction with the DBD suggests leakage of vital cellular materials, which is a key mechanism for microbial inactivation.[37] Nayak *et al*. shows that a volumetric DBD is effective

in inactivating aerosolized PRRS virus in a wind tunnel within a few milliseconds, timescales relevant for typical HVAC conditions (few milliseconds). A 3.5 Log Reduction in the viable porcine reproductive and respiratory syndrome (PRRS) virus titer is achieved and the inactivation effect is independent of the discharge power and the sampling time.[42] Moreover, similar values of Log Reduction were achieved by a packed bed reactor on infective bacteriophage MS2 and PRRS virus, 2.3 Log and 5 Log respectively.[36,43] In this perspective, in the following chapters I will illustrate the design and the development of a direct DBD plasma source suitable for the treatment of bioaerosols.

3.2 Materials and methods

3.2.1 Plasma device and electrical characterization

Figure 3.3a shows the CAP device used for bioaerosol inactivation; it is based on a parallel-plate direct DBD configuration composed of two aluminum electrodes (5 × 150 × 2 mm) encased within two PMMA supports and fixed by epoxy resin. Both the electrodes were covered by 2 mm thick ceramic layers (εr = 6 ÷ 8) and thanks to the presence of two T-section PMMA walls, between the two was maintained a gap of 2 mm (Figure 3.3b).

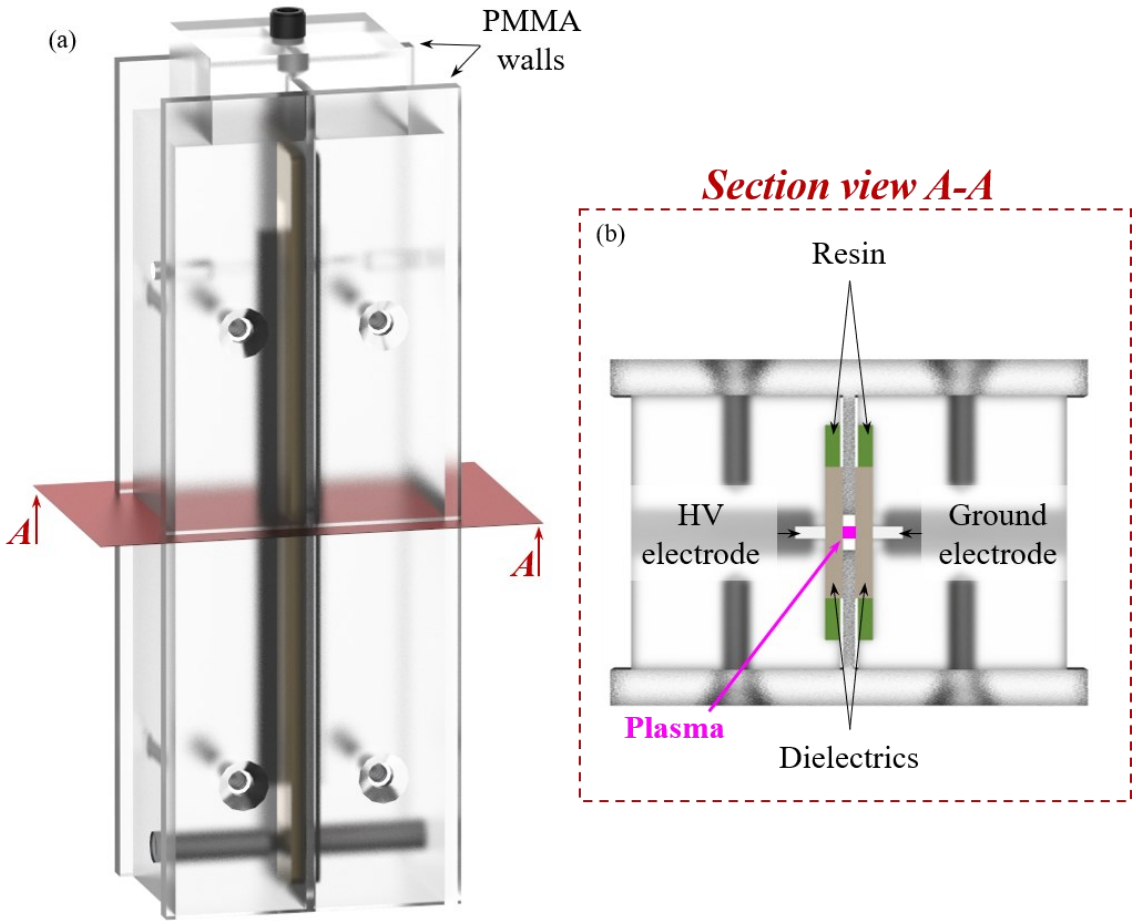

Figure 3.3 – (a) Direct DBD plasma source used for the inactivation of airborne pathogens. As could be seen from the (b) section view, the device is composed of a HV and a ground electrode both covered by dielectric material.

As shown in Figure 3.4, the plasma device was driven by a micropulsed high voltage generator (AlmaPULSE, AlmaPlasma srl, Italy), applying four different operating conditions (Table 3.1). A single jet Blaustein Atomizer (BLAM, CH Technologies – USA), fed with an airflow of 1.2 slpm by a digital mass flow controller (Bronkhorst, EL-FLOW), was used to aerosolize 20 ml of *S. epidermidis* (Gram-positive) suspension contained in a syringe fixed on a syringe pump (Legato®100, kdScientific – USA) delivering a liquid flow rate of 0.852 ml/min; bioaerosol was flown through the interelectrode gap and exposed to the plasma discharge.

The V and the current (I) were measured by means of a high voltage probe (Tektronix P6015A) and a current probe (Pearson 6585), while the charge (Q) was evaluated measuring the voltage across a monitor capacitor of 0.94 nF (connected between the plasma source and the ground) by

means of a low voltage probe (Tektronix P6139A). The corresponding waveforms were recorded using a digital oscilloscope (Tektronix DPO4034, 350 MHz, 2.5 GSa s^{-1}). The average discharge power (P) dissipated over the period (T) was determined from the voltage-charge (Lissajous) plots [46], applying the following formula (1):

$$P = f \oint_T Q(V)dV \tag{1}$$

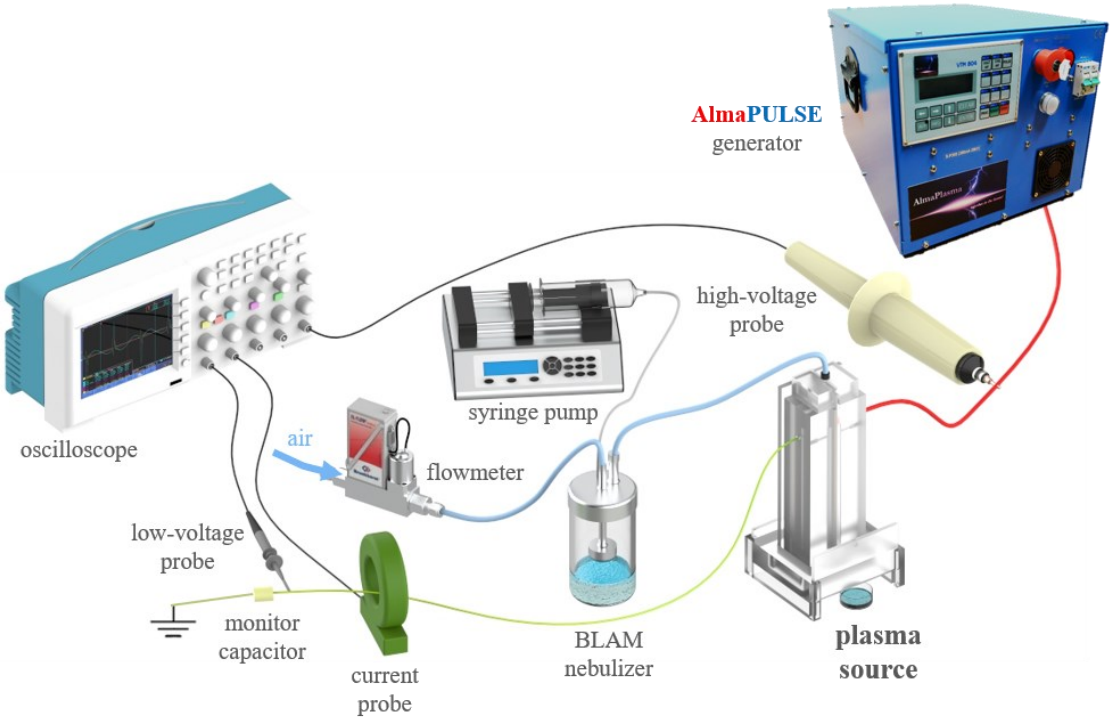

Figure 3.4 – Layout of the setup used for electrical characterization.

Operating condition	Voltage [kV]	Frequency [kHz]	Liquid flow rate [ml/min]	Gas flow rate [slpm]
A	16	4	0.852	1.2
B	20			
C	16	14		
D	20			

Table 3.1 - Operating conditions used for the electrical characterization.

The electrical characterization of the DBD plasma source was performed with the support of Giulia Laghi, a Ph.D. student of the Research Group for Industrial Application of Plasmas (IAP group).

3.2.2 Qualitative monitoring of aerosol behavior by means of low-speed imaging

Figure 3.5 shows the setup used for the qualitative monitoring of the aerosol flowing out the DBD plasma source. During the experiments frequency, voltage, gas flow rate and liquid flow rate were kept constant at 20 kV, 14 kHz, 1.2 slpm and 0.852 ml/min, respectively. Moreover, a

laser pointer (YYLE, 532 nm, 5 mW) was used to illuminate the flow of aerosol at the exit of the plasma source. A low-speed camera (Nikon D800) was operated at 60 fps for the evaluation of the aerosol with plasma off and on.

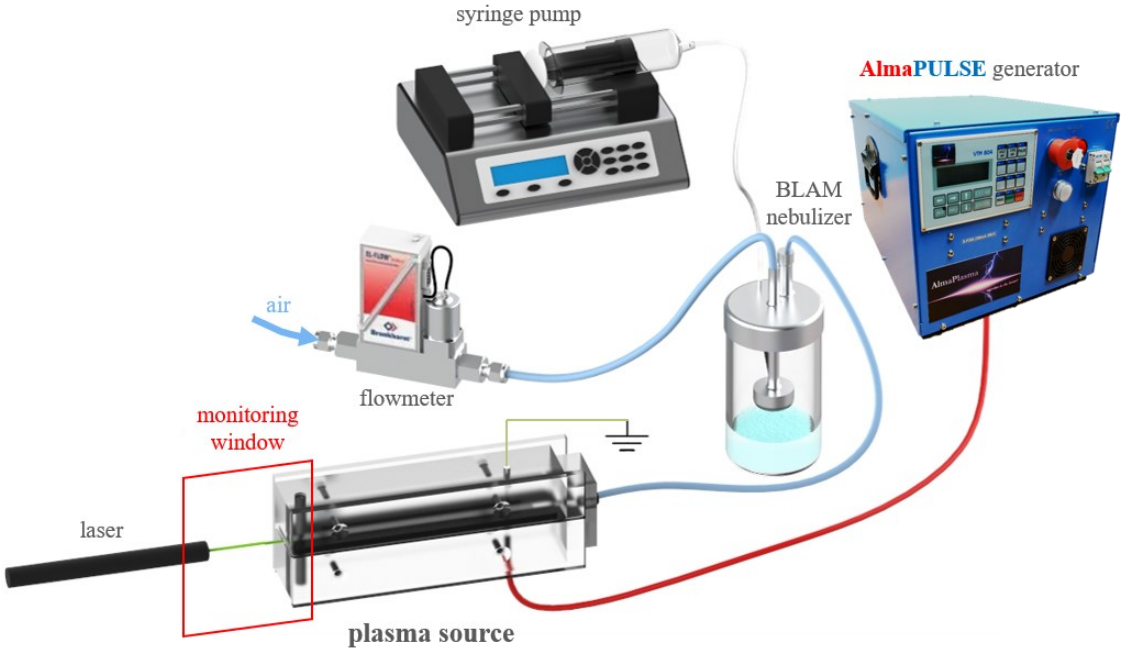

Figure 3.5 – Layout of the setup used for laser monitoring of the aerosol.

3.2.3 Optical Absorption Spectroscopy

The setup used for absorption spectroscopy was reported in Figure 3.6; a deuterium-halogen lamp (characterized by a broad spectrum from UV to NIR radiation) was used as a light source. The light beam emitted by the lamp was focused through an optical fiber and a fused silica lens (50 mm of focus length) into the channel beneath the discharge zone. The outgoing light beam was focused through a second focused silica lens and an optical fiber (Princeton Instruments, fiber optic bundle, 190 – 1100 nm) through the 500 mm spectrometer (Acton SP2500i, Princeton Instruments). For the O_3 measurements (in the wavelength range 253 ± 1.2 nm), the grating resolution was fixed at 150 mm-1 and the width of the inlet and the outlet slit of the spectrometer were fixed at 50 µm and 100 µm, respectively. A photomultiplier tube (PMT-Princeton Instruments PD439) connected to a fast oscilloscope (Tektoronix DPO 4034, 350 MHz, 2.5 GSa s^{-1}) was used as detector and its amplification factor was kept constant (1200) for all acquisitions.

Subsequently, O_3 concentration was calculated using the Lambert – Beer law which correlates the absorbed light with the concentration of the specific molecule (n):

$$n = -\frac{1}{L\sigma} ln\left(\frac{I}{I_0}\right) \quad (2)$$

where I/I_0 is the ratio between the intensity of the lamp emitted (I_0) and the light intensity (I) after the optical path length (L) and σ is the cross-section of the absorbers.

As reported in Table 3.2, the experiments were performed under different operating conditions; more specifically those characterized by the lowest and the highest average power. The aim of this study was to understand the contribution of gas flow rate, the presence of aerosol

and average power on the production of O_3 in the gas phase. Moreover, to avoid any damage of the plasma source, the experiments performed without aerosol inside the volume discharge were performed with the operating condition characterized by the lowest average power.

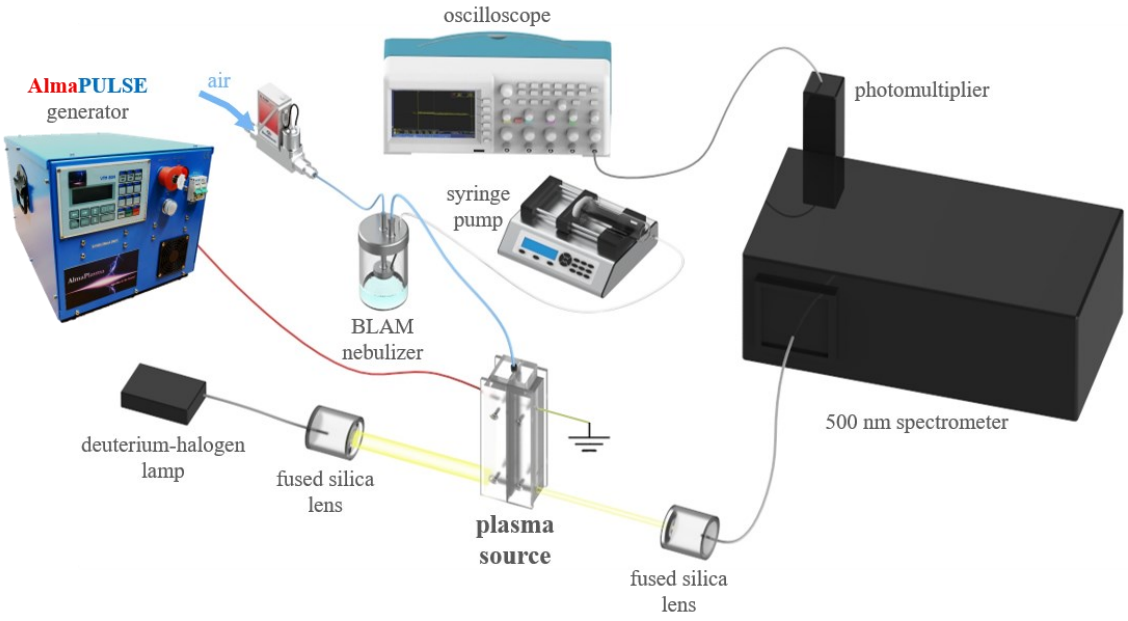

Figure 3.6 - Layout of the setup used for OAS spectroscopy.

Operating condition	Voltage [kV]	Frequency [kHz]	Liquid flow rate [ml/min]	Gas flow rate [slpm]
E	16	4	/	0.3
F				0.6
G				0.9
H				1.2
I	16	4	0.852	1.2
L	20	14		

Table 3.2 – Operating conditions used for the OAS analysis.

3.2.4 *S. epidermidis* culture condition and CAP treatment

S. epidermidis (ATCC 12228) was cultivated on Tryptic Soy Agar (TSA) plates and incubated at 37°C for 24 hours; colonies were used to prepare a standardized suspension in Phosphate Buffered Saline (PBS), a buffered solution commonly used in biological research, at OD_{600nm} = 0.2 (i.e. 10^7–10^8 CFU/ml). To evaluate the CAP anti-bacterial activity on bioaerosol, the syringe was been loaded with 20 ml of standardized suspension and fixed in the syringe pump to deliver inside the nebulizer a liquid flow rate of 0.852 ml/min necessary to produce the bioaerosol. It was flowed through the plasma region for 150 s, collected in 1 ml of a liquid substrate, and plated. Control samples were collected using the same procedure while the plasma discharge was not generated. The liquid substrates for collecting samples were PBS or PBS containing sodium thiosulphate, $Na_2S_2O_3$ (100 mM), as quenching solution for reactive species which dissolve into liquid after plasma exposure, e.g. O_3.[42,47,48]

3.3 Results and discussion

3.3.1 Electrical characterization of the DBD plasma source

The average discharge power values were calculated from the area of voltage-charge plots multiplied by the frequency.[46] As could be seen from Figure 3.7 and in accordance with the work of A.K. Srivastava *et al*. [49], at the fixed voltage the power increases as the frequency increases. Similarly, at the same frequency the power increases as the voltage increases.[49,50]

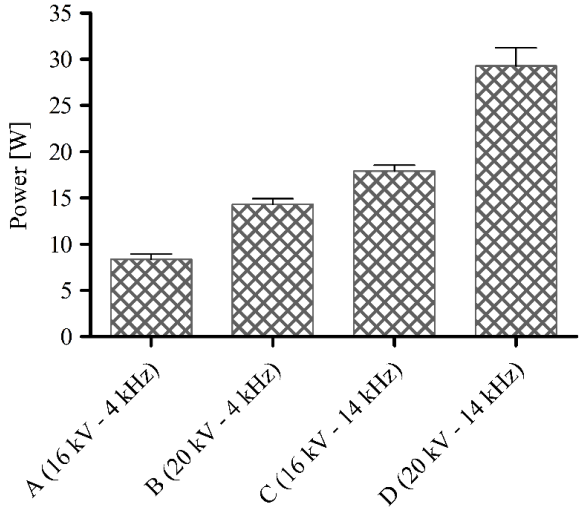

Figure 3.7 – Average discharge power values calculated for four operating conditions.

1.3.2 Qualitative evaluation of the aerosol outgoing from the DBD plasma source

As reported by A. J. Smits and T. T Lim, a laser source could be used to illuminate solid or liquid aerosols for flow visualization.[51] This technique was used in this case to qualitatively visualize the behavior of aerosol flow outgoing from the DBD plasma source with plasma off and at different time points during plasma treatment. Figure 3.8 outlined the presence of laser diffraction when plasma is turned off. In this case a long and homogeneous "tail" of several centimeters could be observed at the outlet of the plasma source. When plasma is turned on, laser diffraction is absent; this phenomenon was probably related to the evaporation of the water droplets inside the discharge zone.[52]

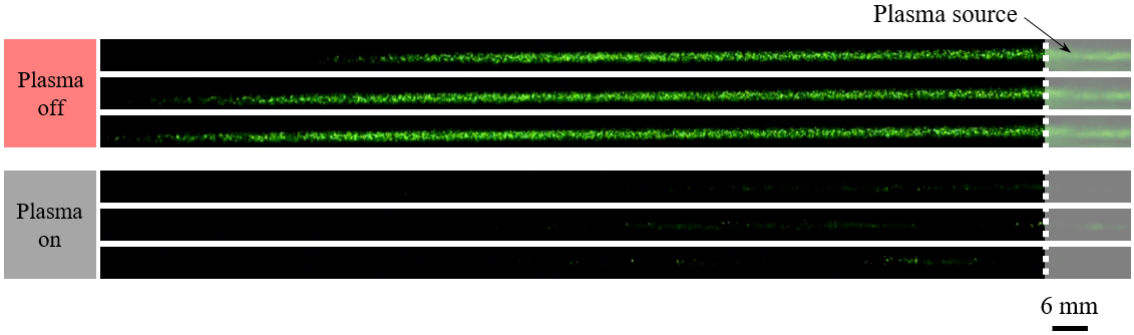

Figure 3.8 - Laser diffraction pictures with plasma off and with plasma on.

1.3.3 Evaluation of RONS concentrations in gas phase

Ozone is well known to have bactericidal properties; moreover, it could spontaneously decompose to oxygen without the emission of toxic compounds. Actually, it is highly used to potabilize water, disinfect swimming pool water or more recently to deactivate airborne microorganisms.[40,53,54] O_3 is generally produced from the dissociation of O_2 molecule resulting from the interaction with electrons (3), followed by the tree body reaction (4), [55,56]:

$$O_2 + e^- \rightarrow 2O + e^- \quad (3)$$

$$O + O_2 + M \rightarrow O_3 + M \quad (2)$$

As reported in Figure 3.9, the ozone concentration was strongly influenced by the gas flow rate. Indeed, by fluxing an airflow through the discharge region, O_3 concentration increases and reaches higher concentrations (about 16000 ppm) compared with the values obtained by S. Patil, *et al*.[57] In this case it is possible to observe a rapid increase of O_3 concentration in the first few seconds of plasma treatment and subsequently a quasi-steady state. In agreement with the study of T. -L. Sung *et al*. [56], an increase of the air flow rate through the discharge zone leads to a reduction of O_3 concentration. The reason is probably related to the residence time of the gas inside the discharge zone; with the increasing of gas flow rate, O_3 production gradually decreases because O atoms produced by (3) are dragged to the outlet of the plasma source.

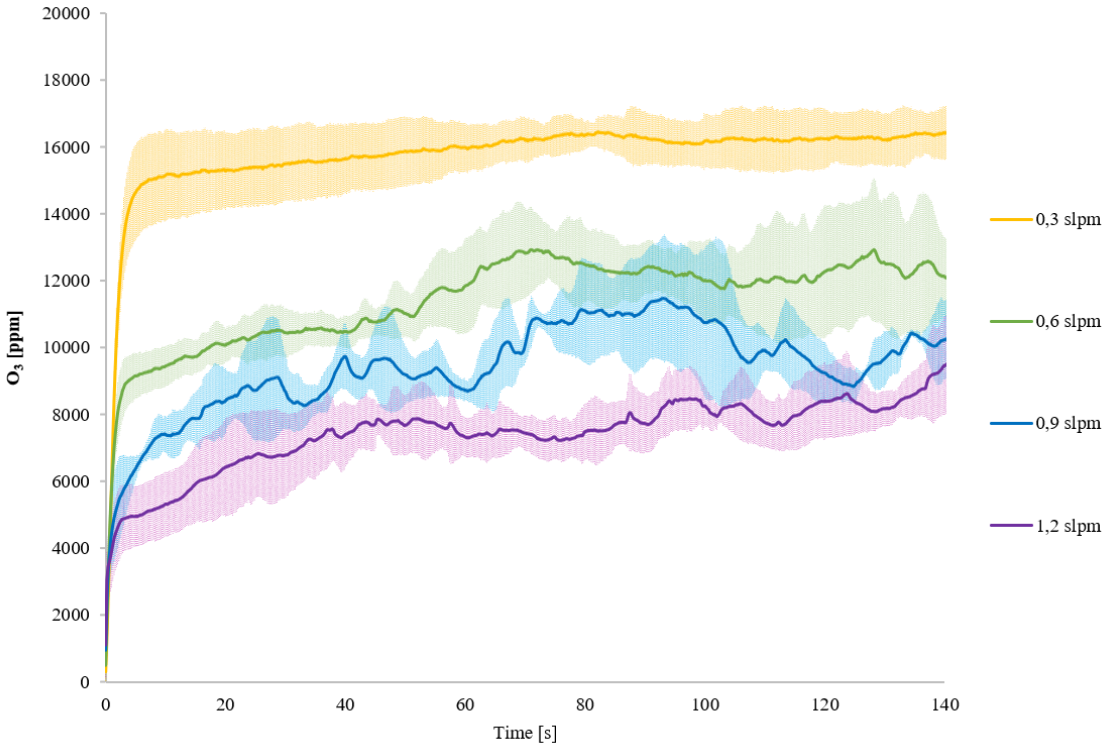

Figure 3.9 – O_3 concertation produced during plasma treatment using different gas flow rates (0 ÷ 1.2 slpm). Data are reported as mean ± SD (n = 3).

As reported in Figure 3.10 and in agreement with X. Zhang *et al*. [58], in addition to the average power, O_3 concentration is strongly influenced also by the presence of water in the discharge zone. In both cases the presence of water inside the plasma zone influenced reaction occurring in the discharge for the formation of O_3. When the discharge gas is dry, all electrons

lead to O atoms formation and subsequently to O_3 production through reaction (3). When water is introduced inside the discharge zone, electron impact reactions lead to the formation of H and OH· which trigger other reaction pathways.

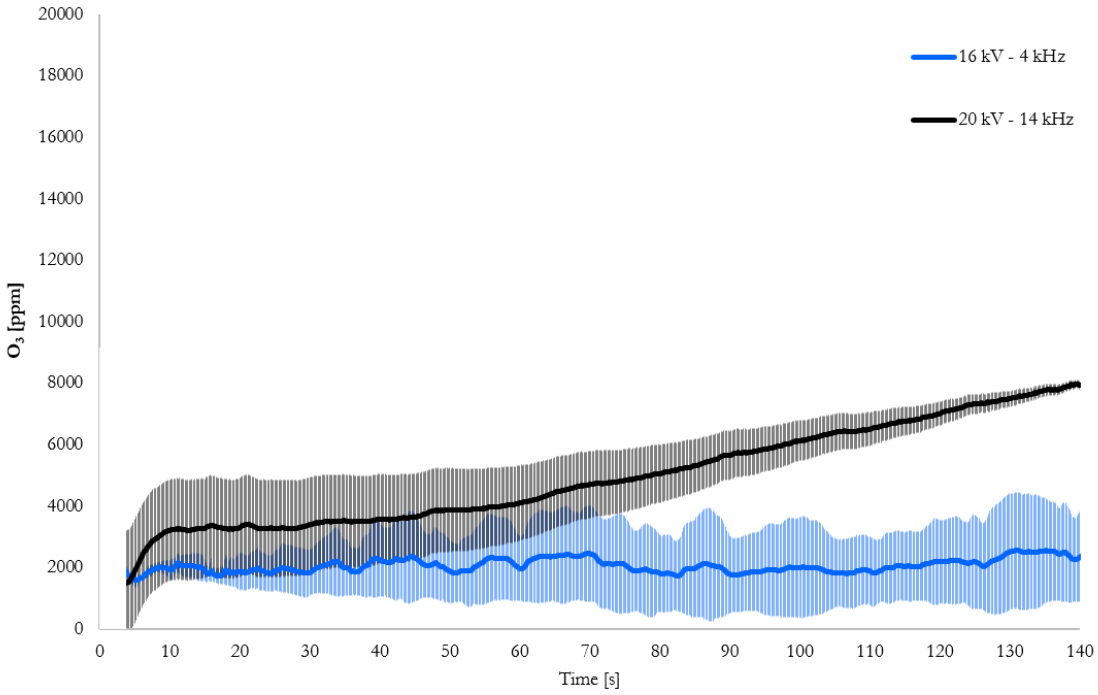

Figure 3.10 – O_3 concertation produced during plasma treatment in presence of aerosol and using two different operating conditions (blue: 16 kV – 4 kHz and black: 20 kV – 14 kHz). Data are reported as mean ± SD (n = 3).

3.3.4 CAP effect on bioaerosol containing S. epidermidis

The anti-bacterial activity of CAP on *S. epidermidis* bioaerosol was investigated using two liquid substrates for collecting samples (i.e. PBS and $Na_2S_2O_3$ in PBS) and four different operating conditions (Table 3.1). As reported in Figure 3.11, CAP exerted an antibacterial activity on bioaerosol; moreover, it depends on both voltage and frequency values. At low frequency (4 kHz) Log R values strongly depends by the voltage values; indeed, an increase of only 4 kV leads to an increase of Log R from 1.31 ± 0.09 to 4.27 ± 0.04. While no significant differences have been detected at higher frequencies (14 kHz). On the contrary, for both 16 kV and 20 kHz, Log R increases with the increase of frequency. The same behaviors were obtain also using PBS containing $Na_2S_2O_3$.

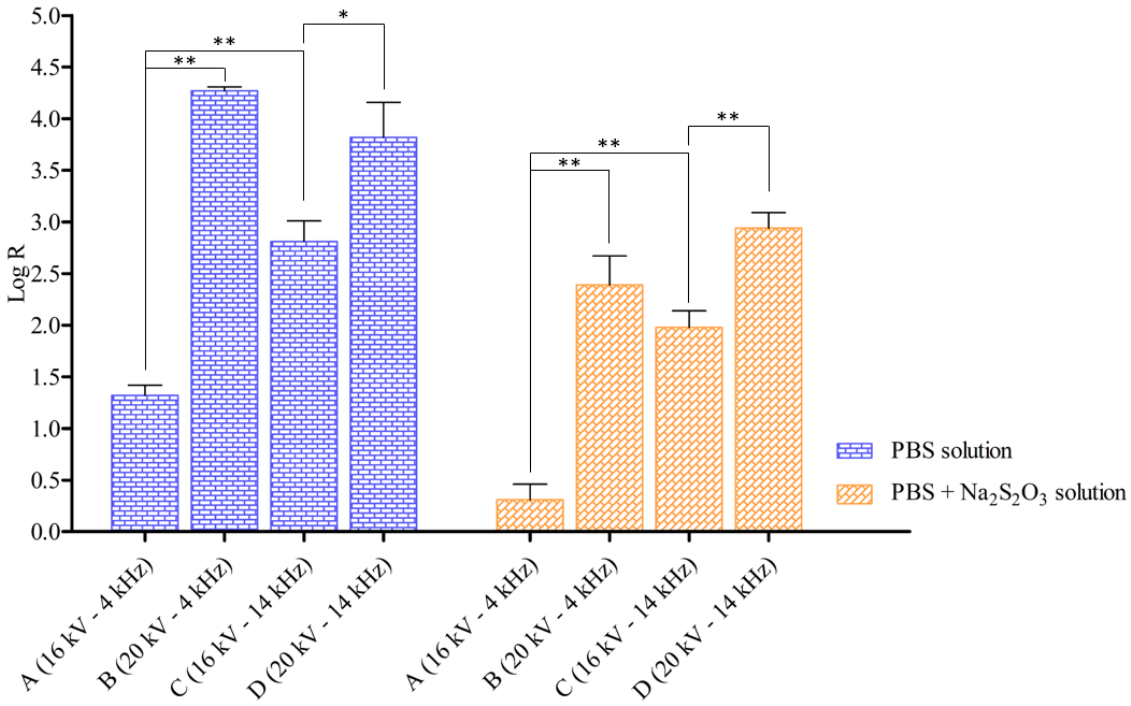

Figure 3.11 - Log Reduction (Log R) of *S. epidermidis* bioaerosol collected in PBS and PBS containing $Na_2S_2O_3$ after CAP treatment for four different operating conditions (Table 3.1). Results are presented as the mean Log R ± SEM of 3 independent experiments (*$p \leq 0.05$, **$p \leq 0.001$ as determined by paired Student t-test).

3.4 Conclusions and future perspectives

The presence of bioaerosol is generally correlated with human activity, particularly in indoor and poorly ventilated spaces, and it has been suspected as one of the causes of spreading diseases. Hence, increasing indoor air quality can play a pivotal role in human health. In this field, there is a need for innovative technology that could inactivate microbes and viruses in a short time. In this regard, a lab-scale flow-through volumetric DBD reactor able to work with different operating conditions was presented. The average discharge power increases with the increase of both voltage and frequency. Moreover, as confirmed by OAS analysis, the plasma source it is able to generate very high concentrations of O_3 whose antimicrobial effects is well known. Actually, plasma technology is explored as a novel approach to inactivate bioaerosol; in this context it was shown the ability of plasma device to inactivate bioaerosol containing *S. epidermidis*. Results show that CAP can induce a Log R reduction which value strongly depend by voltage and frequency values.

This prototype was successfully used for inactivation of aerosol containing purified SARS-CoV-2 RNA.[59] The Figure below shows a picture taken during the experiments.

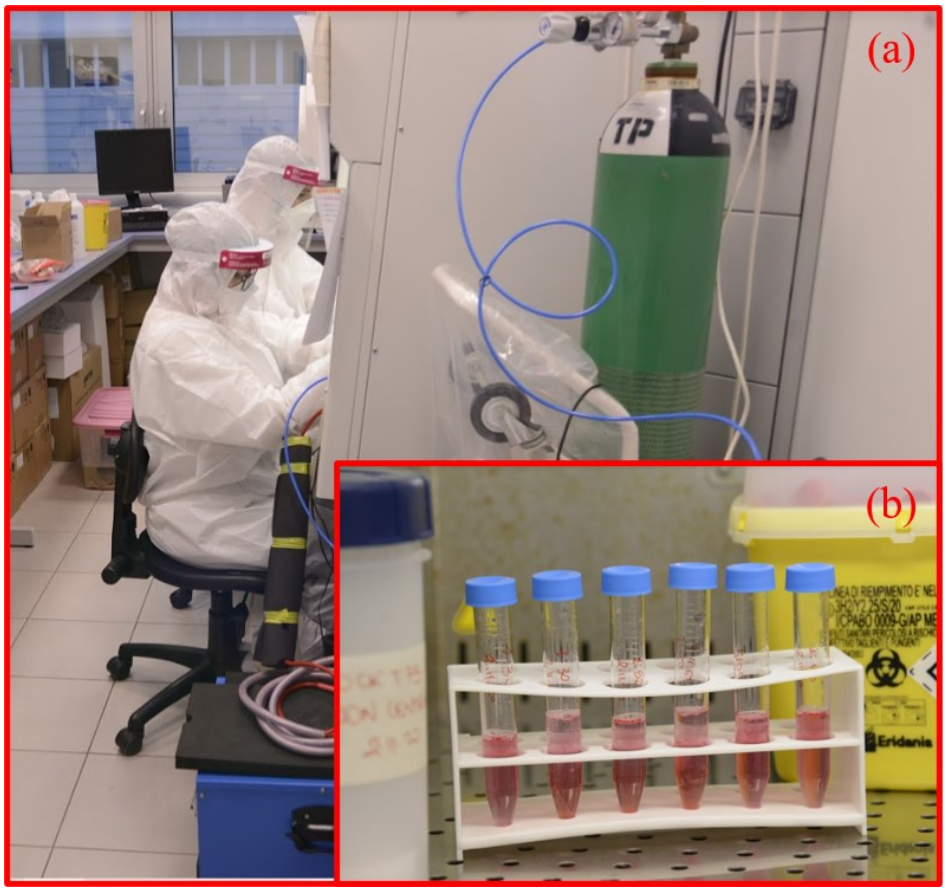

Acknowledgements:

I acknowledge the support of the 2014-2020 European Regional Development Fund Emilia-Romagna Regional Operational Program on industrial research and innovation projects for contrast solutions to the spread of COVID-19 - Project VIKI (VIrus KIller) - Plasma inactivation device to contrast bioaerosol indoor transport.

3.5 References

[1] G.R. Johnson, *et al*., "Modality of human expired aerosol size distributions", *Journal of Aerosol Science*, 42 (12) 839, (**2011**).

[2] J. Douwes, *et al*., "Bioaerosol health effects and exposure assessment: Progress and prospects", *Annals of Occupational Hygiene*, 47 (3) 187, (**2003**).

[3] R. Tellier, "Review of aerosol transmission of influenza A virus", *Emerging Infectious Diseases*, 12 (11) 1657, (**2006**).

[4] S. Mubareka, *et al*., "Bioaerosols and transmission, a diverse and growing community of practice", *Frontiers in Public Health*, 7 (FEB) 23, (**2019**).

[5] J. Wei, *et al*., "Airborne spread of infectious agents in the indoor environment", *American Journal of Infection Control*, 44 (9) S102, (**2016**).

[6] E.Y.C. Shiu, *et al*., "Controversy around airborne versus droplet transmission of respiratory viruses: implication for infection prevention", *Current Opinion in Infectious Diseases*, 32 (4) 372, (**2019**).

[7] M. Abkarian, *et al*., "Stretching and break-up of saliva filaments during speech: A route for pathogen aerosolization and its potential mitigation", *Physical Review Fluids*, 5 (10) 102301, (**2020**).

[8] H. Li, *et al*., "Dispersion of evaporating cough droplets in tropical outdoor environment", *Physics of Fluids*, 32 (11) 113301, (**2020**).

[9] G. Buonanno, *et al*., "Estimation of airborne viral emission: Quanta emission rate of SARS-CoV-2 for infection risk assessment", *Environment International*, 141 (April) 105794, (**2020**).

[10] L. Morawska, *et al*., "It Is Time to Address Airborne Transmission of Coronavirus Disease 2019 (COVID-19)", *Clinical Infectious Diseases*, 2019 (9) 2311, (**2020**).

[11] S.H. Smith, *et al*., "Aerosol persistence in relation to possible transmission of SARS-CoV-2", *Physics of Fluids*, 32 (10) 107108, (**2020**).

[12] X. Xie, *et al*., "How far droplets can move in indoor environments - revisiting the Wells evaporation-falling curve", *Indoor Air*, 17 (3) 211, (**2007**).

[13] M. Jayaweera, et al., "Transmission of COVID-19 virus by droplets and aerosols: A critical review on the unresolved dichotomy", *Environmental Research*, 188 109819, (**2020**).

[14] J. Yan, *et al*., "Infectious virus in exhaled breath of symptomatic seasonal influenza cases from a college community", *Proceedings of the National Academy of Sciences of the United States of America*, 115 (5) 1081, (**2018**).

[15] W.G. Lindsley, *et al*., "Viable influenza a virus in airborne particles from human coughs", *Journal of Occupational and Environmental Hygiene*, 12 (2) 107, (**2015**).

[16] V. Stadnytskyi, *et al*., "The airborne lifetime of small speech droplets and their potential importance in SARS-CoV-2 transmission", *Proceedings of the National Academy of Sciences of the United States of America*, 117 (22) 11875, (**2020**).

[17] N. van Doremalen, *et al*., "Aerosol and Surface Stability of SARS-CoV-2 as Compared with SARS-CoV-1", *New England Journal of Medicine*, 382 (16) 1564, (**2020**).

[18] S. Riddell, *et al*., "The effect of temperature on persistence of SARS-CoV-2 on common surfaces", *Virology Journal*, 17 (1) 1, (**2020**).

[19] S. Verma, *et al*., "Visualizing droplet dispersal for face shields and masks with exhalation valves", *Physics of Fluids*, 32 (9) 091701, (**2020**).

[20] T. Dbouk, *et al*., "On respiratory droplets and face masks", *Physics of Fluids*, 32 (6) 063303, (**2020**).

[21] B. Blocken, *et al*., "Towards aerodynamically equivalent COVID19 1.5 m social distancing for walking and running", *Urban Physics*, (**2020**).

[22] T. Dbouk, *et al*., "On coughing and airborne droplet transmission to humans", *Physics of Fluids*, 32 (5) 053310, (**2020**).

[23] Y. Feng, *et al*., "Influence of wind and relative humidity on the social distancing effectiveness to prevent COVID-19 airborne transmission: A numerical study", *Journal of Aerosol Science*, 147 (April) 105585, (**2020**).

[24] M.R. Pendar, *et al*., "Numerical modeling of the distribution of virus carrying saliva droplets during sneeze and cough", *Physics of Fluids*, 32 (8) 083305, (**2020**).

[25] B. Wang, *et al*., "Transport and fate of human expiratory droplets - A modeling approach", *Physics of Fluids*, 32 (8) 083307, (**2020**).

[26] A.G. Somsen, *et al*., "Small droplet aerosols in poorly ventilated spaces and SARS-CoV-2 transmission", *The Lancet. Respiratory Medicine*, (**2020**).

[27] Y. Liu, *et al*., "Aerodynamic analysis of SARS-CoV-2 in two Wuhan hospitals", *Nature*, 582 (7813) 557, (**2020**).

[28] Y. Li, *et al*., "Evidence for probable aerosol transmission of SARS-CoV-2 in a poorly ventilated restaurant", *MedRxiv*, (**2020**).

[29] F.P. Polack, *et al*., "Safety and Efficacy of the BNT162b2 mRNA Covid-19 Vaccine", *The New England Journal of Medicine*, (**2020**).

[30] Bing-Yuan, *et al*., "Role of viral bioaerosols in nosocomial infections and measures for prevention and control", *Journal of Aerosol Science*, 117 200, (**2018**).

[31] B. Ghosh, *et al*., "Review of bioaerosols in indoor environment with special reference to sampling, analysis and control mechanisms", *Environment International*, 85 254, (**2015**).

[32] K.R. Wigginton, *et al*., "Virus disinfection mechanisms: The role of virus composition, structure, and function", *Current Opinion in Virology*, 2 (1) 84, (**2012**).

[33] J. Romero-Mangado, *et al*., "Morphological and chemical changes of aerosolized *E. coli* treated with a dielectric barrier discharge", *Biointerphases*, 11 (1) 011009, (**2016**).

[34] S. Bekeschus, *et al*., "Gas Plasma Technology — An Asset to Healthcare During Viral Pandemics Such as the COVID-19 Crisis ?", *IEEE Transactions on Radiation and Plasma Medical Sciences*, 4 (4) 391, (**2020**).

[35] Y. Liang, *et al*., "Rapid Inactivation of Biological Species in the Air using Atmospheric Pressure Nonthermal Plasma", *Environmental Science & Technology*, 46 (6) 3360, (**2012**).

[36] T. Xia, *et al*., "Inactivation of airborne porcine reproductive and respiratory syndrome virus (PRRSv) by a packed bed dielectric barrier discharge non-thermal plasma", *Journal of Hazardous Materials*, 393 122266, (**2020**).

[37] J. Romero-Mangado, *et al*., "Efficacy of atmospheric pressure dielectric barrier discharge for inactivating airborne pathogens", *Journal of Vacuum Science & Technology A*, 35 041101, (**2017**).

[38] M. Schmidt, *et al*., "Combined electric wind and non-thermal plasma for gas cleaning", *International Journal of Plasma Environmental Science and Technology*, 11 (2) 133, (**2018**).

[39] E. Timmermann, *et al*., "Indoor air purification by dielectric barrier discharge combined with ionic wind: Physical and microbiological investigations", *Journal of Physics D: Applied Physics*, 51 (16) 164003, (**2018**).

[40] "Determination of the Novaerus NV900 System's Efficacy against Various Bioaerosols", (**2016**).

[41] C.W. Park, *et al*., "Susceptibility constants of airborne bacteria to dielectric barrier discharge for antibacterial performance evaluation", *Journal of Hazardous Materials*, 244 421, (**2013**).

[42] G. Nayak, *et al*., "Rapid inactivation of airborne porcine reproductive and respiratory syndrome virus using an atmospheric pressure air plasma", *Plasma Processes and Polymers*, Dec. 2019 e1900269, (**2020**).

[43] T. Xia, *et al*., "Inactivation of airborne viruses using a packed bed non-thermal plasma reactor", *Journal of Physics D: Applied Physics*, 52 (25) 255201, (**2019**).

[44] A. Moldgy, *et al*., "Inactivation of virus and bacteria using cold atmospheric pressure air plasmas and the role of reactive nitrogen species", *Journal of Physics D: Applied Physics*, 53 (43) 434004, (**2020**).

[45] M. Gallagher, *et al*., "Rapid Inactivation of Airborne Bacteria Using Atmospheric Pressure Dielectric Barrier Grating Discharge", *IEEE Transactions on Plasma Science*, 35 (5) 1501, (**2007**).

[46] A. V. Pipa, *et al*., "The equivalent circuit approach for the electrical diagnostics of dielectric barrier discharges: The classical theory and recent developments", *Atoms*, 7 (1) 14, (**2019**).

[47] V. Agranovski, et al., "Performance evaluation of the UVAPS : influence of physiological age of airborne bacteria and bacterial stress", *Journal of Aerosol Science*, 34 (12) 1711–1727, (**2003**).

[48] K.I.Y. Yoon, *et al*., "Design and application of an inertial impactor in combination with an ATP bioluminescence detector for in situ rapid estimation of the efficacies of air controlling devices on removal of bioaerosols", *Environmental Science & Technology*., 44 (5) 1742–1746, (**2010**).

[49] A.K. Srivastava, *et al*., "Characteristics of parallel-plate and planar-surface dielectric barrier discharge at atmospheric pressure", *Journal of Electrostatics*, 72 (2) 140, (**2014**).

[50] K.G. Kostov, *et al*., "Characteristics of dielectric barrier discharge reactor for material treatment", *Brazilian Journal of Physics*, 39 (2) 322, (**2009**).

[51] A.J. Smit, Flow Visualization - Techniques and Examples, (**2012**).

[52] T. Gallingani, *et al*., "Online ion mobility spectrometry of nanoparticle formation by non-thermal plasma conversion of metal salts in liquid aerosol droplets", *Journal of Aerosol Science*, 150 (August) 105631, (**2020**).

[53] G. Moore, *et al*., "Bactericidal properties of ozone and its potential application as a terminal disinfectant", *Journal of Food Protection*, 63 (8) 1100, (**2000**).

[54] M. Sharma, *et al*., "Ozone gas is an effective and practical antibacterial agent", *American Journal of Infection Control*, 36 (8) 559, (**2008**).

[55] E. Simoncelli, *et al*., "UV-VIS optical spectroscopy investigation on the kinetics of long-lived RONS produced by a surface DBD plasma source", *Plasma Sources Science and Technology*, 28 (9) 095015, (**2019**).

[56] T.L. Sung, *et al*., "Effect of pulse power characteristics and gas flow rate on ozone production in a cylindrical dielectric barrier discharge ozonizer", *Vacuum*, 90 (1) 65, (**2013**).

[57] S. Patil, *et al*., "Influence of high voltage atmospheric cold plasma process parameters and role of relative humidity on inactivation of *Bacillus atrophaeus* spores inside a sealed package", *Journal of Hospital Infection*, 88 (3) 162, (**2014**).

[58] X. Zhang, *et al*., "Ozone production with dielectric barrier discharge: effects of power source and humidity", *IEEE Transactions on Plasma Science*, 44 (10) 2288, (**2016**).

[59] A. Bisag, *et al*., "Cold atmospheric plasma inactivation of aerosolized microdroplets containing bacteria and purified SARS-CoV-2 RNA to contrast airborne indoor transmission", *Plasma Processes and Polymers*, 17 (10) 2000154, (**2020**).

3.6 Appendix

3.6.1 First DBD prototype for the inactivation of airborne pathogens

The parallel-plate direct DBD plasma sources are made up of two electrodes (a high voltage and a ground one) covered by dielectric materials. the first step of this project was realized the plasma device reported in Figure 3.13a. It consists of two electrodes (5 × 150 × 2 mm) fixed inside a PMMA support and covered by 1 mm thick mica layers. Despite the good results in terms of biological inactivation, this prototype was characterized by a very short useful life. Indeed, as reported in Figure 3.12, after few plasma treatments the dielectric detach from the electrodes leading to the formation of undesired electrical discharges (Figure 3.13d/e). In particular, several types of glues have been used to fix the dielectric to the electrodes and PMMA support, but none of them represented a valid solution for increasing the useful live of the plasma device.

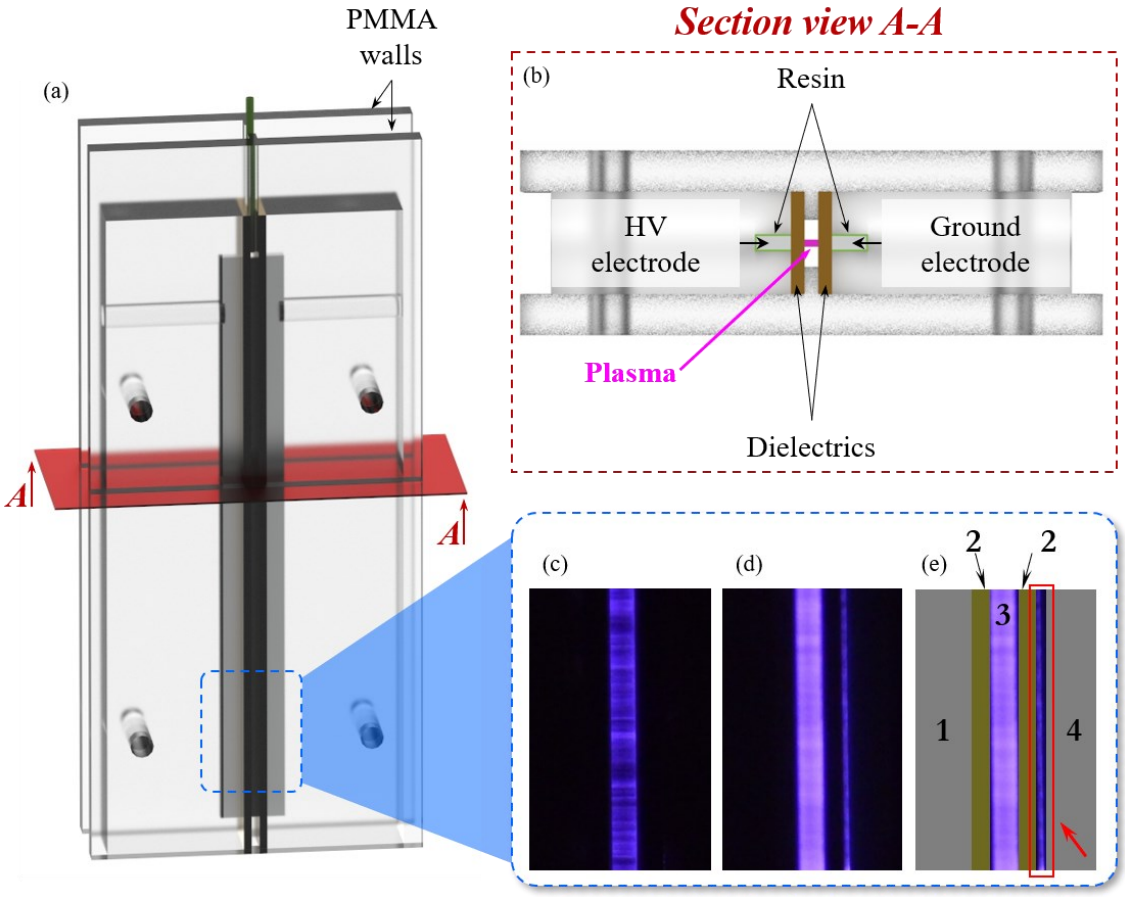

Figure 3.12 – (a) Direct DBD prototype and its (b) section view in which was possible to distinguish the HV and ground electrodes covered by dielectric material and positioned opposite each other. When the power supply was turned on, between the two electrodes was generated a (c) filamentary plasma. After few plasma treatments (d) the appearance of plasma discharge (3) change and established randomly (e) undesired plasma between the HV electrode (1) and dielectric (2) or between the dielectric (2) and the ground electrode (4).

For the reasons outlined above, it was necessary to modify the geometry of PMMA supports in which were encased both the electrodes without changing the dimensions of the electrodes itself and consequently of the plasma behavior.

3.6.2 Second DBD prototype for the inactivation of airborne pathogens

To overcome the problematics related to the detachment of the dielectric due to the small contact surface between electrodes and PMMA supports, their geometry was redesigned (Figure 3.13). In particular, the total footprint has been increased and a rectangular excavation has been made allowing to fix with resin not only the face of the dielectric facing the electrode but also the side wall. Moreover, in order to increase the adhesion, both of dielectric and PMMA inside of which was place the electrode were treated by means of two APPJ devices.

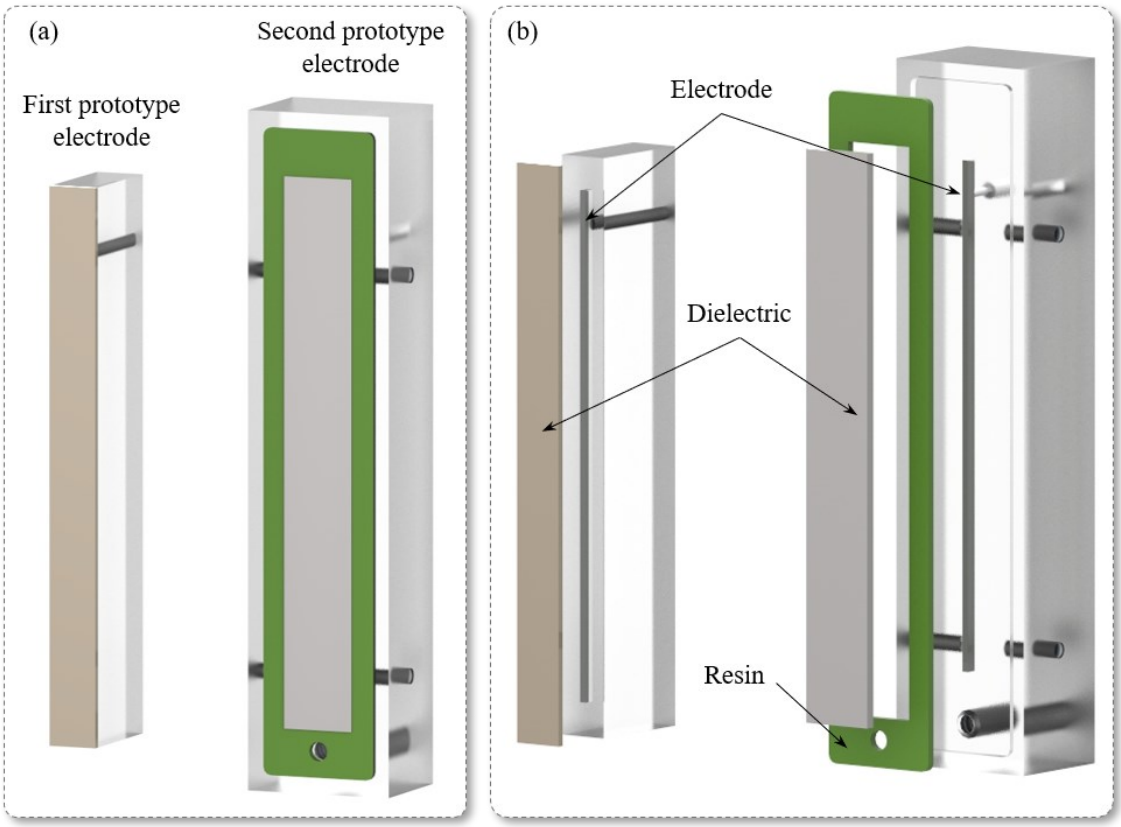

Figure 3.13 - (a) High voltage electrodes of the first and the second prototype. (b) Differently from the first prototype, the electrodes of the second prototype were encase in a bigger PMMA support which presents a rectangular excavation allowing the use of epoxy resin for the fixing of the ceramic dielectric.

1.6.3 Biological experiments required to verify CAP anti-bacterial activity of the first prototype on bioaerosol containing *S. epidermidis*

A bacterial suspension was prepared in physiological saline solution (0.9% NaCl) starting from an overnight culture of *S. epidermidis* (ATCC 12228) on Tryptic Soy Agar (TSA) plates incubated aerobically at 37°C; the suspension was adjusted to approximately $10^7 \div 10^8$ CFU/ml. Ten-fold serial dilutions were prepared and spread on TSA plates to accurately quantify the suspension by colony counting method; subsequently the bacterial suspension was used to produce bioaerosol.[59]

This one was flowed through the plasma region for 150 s, collected on a TSA plate placed in correspondence to the outlet spot of the plasma source. To facilitate colony counting the plate has been handled as reported in Figure 3.14.

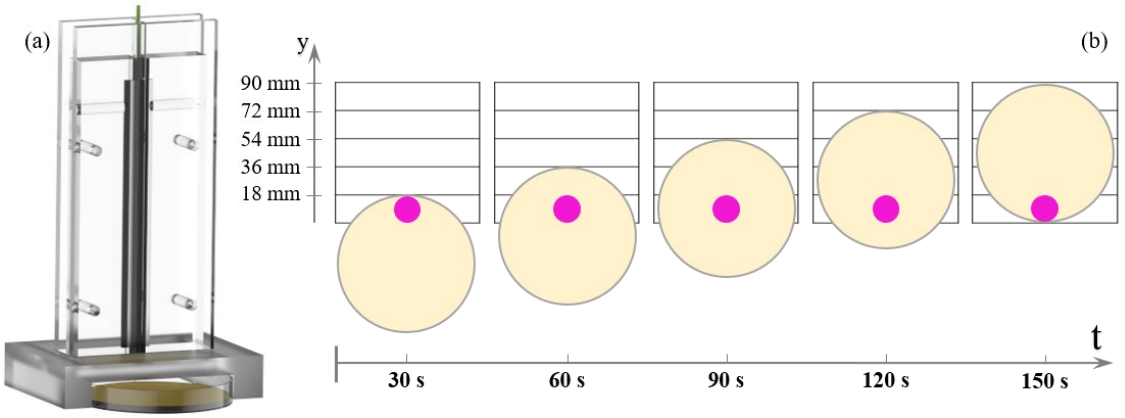

Figure 3.14 – (a) To assess the CAP anti-bacterial activity of the first prototype on bioaerosol containing S. epidermidis a plate was placed under the plasma source and was subsequently (b) handled each 30 s during the entire time of the plasma treatment to facilitate the colony counting after 24 hours of incubation at 37°C.

Figure 3.15 shows the plates with the standardized suspension and after the plasma treatment. On the control plate were counted about 9750 colonies while the total colonies on the treatment plates was 3. These results correspond to a LogR of 3.83 ± 0.16 corresponding to an inactivation of 99.9%.

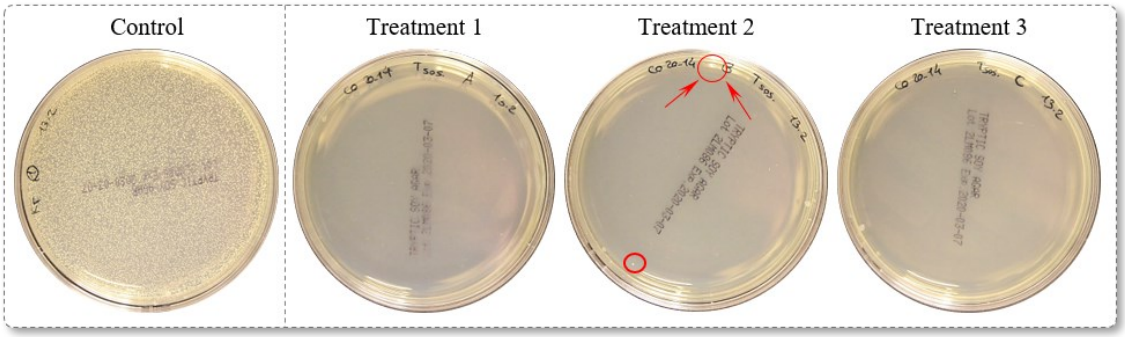

Figure 3.15 - TSA plates of the plated suspension (control) and after the plasma treatment of the bioaerosol.

Acknowledgements

There are many people who deserve my thanks for their support, assistance, and encouragement throughout the last three years.

First, I would like to begin with a sincere and heartfelt thanks to my supervisor Prof. Vittorio Colombo who give me the opportunity to join his wonderful research group of Alma Mater Studiorum – University of Bologna, for encouraging my research, for supporting me and for helping me to grow through life and science. I am very grateful for his enthusiasm and motivation that make him a great mentor. It was a great privilege and honor to be one of his students.

My gratitude is also extended to my co-supervisor Dr. Matteo Gherardi for his support, his suggestions, his teachings and especially for the time spent to read my thesis. Thank you for always giving me a new point of view and for helping me to achieve these results.

A very special thanks to Romolo Laurita for his valuable teachings, for his advice, for his friendship and for his cheerful. He makes special every day spent in the lab. Thanks for helping me with my thesis and for teaching me most of what I learned during these years.

I want to thank Cristiana Bucci, my companion of adventure, for her friendship, for her patience and especially for suffering me every day through all these years. Thank you for your biological support, it was a great pleasure working with you.

Thank you, Filippo Capelli, for your friendship, for making me laugh every day and for all days spent in the university mechanical workshop.

Thank you, Giulia Laghi, for your friendship, great enthusiasm, your enjoyment and especially your ability to lose everything. You make every day much more interesting and adventurous.

Thank you, Pasquale Isabelli, for your friendship, your kindness and your adventurous spirit. I will always remember our Sunday experiments in Pievesestina laboratories.

I would like to thank the past members of our research group: Marco Boselli, Enrico Traldi, Augusto Stancampiano, Tommaso Gallingani and Emanuele Simoncelli. My gratitude goes to all of you.

Thank you, Antonio, for always supporting me and encouraging me.

A special thanks to my parents Simona and Daniel. Words cannot express how grateful I am for all the sacrifices that you have made on my behalf.

Many thanks to Denisa for being the best sister and the best fried into the world.